Multiple weak gauge boson production in high energy hadronic collisions

Hussein, Mohammad Yousif

MULTIPLE WEAK GAUGE BOSON PRODUCTION IN HIGH ENERGY HADRONIC COLLISIONS

Mohammad Yousif Hussein

Department of Physics

University of Durham

A thesis submitted in the University of Durham

for the Degree of Doctor of Philosophy

August 1989

DECLARATION

I declare that no material in this thesis has previously been submitted for a degree at this or any other university.

ACKNOWLEDGEMENTS

There is a number of people to whom I owe a great deal and would like to thank for their contributions towards the completion of this thesis:

I am indebted to my supervisor James Stirling for his continuous support and encouragement, invaluable assistance and true friendship during the time of my research studies. I would also like to thank him for his constructive suggestions in improving the form of this thesis, and also his patience whilst reading the manuscript and correcting my numerous mistakes, both scientific and literary.

Many thanks to past and present members of the High Energy Physics group of the Physics Department: Alan Martin, Peter Collins, Chris Maxwell, Mike Pennington, Mike Whalley, Simon Webb, Yanos Michopoulos, Nick Brown, Mohammad Nobary, Ahmed Bawa, Jenny Nicholls, David Pentney, Peter Harriman, Dominic Walsh, Mike Wade, Neil Shaban, Duncan Curtis and Paul Murphy for their helpful comments and providing a friendly enviroment in which to work.

Last, but not least, I wish to express my gratitude to my family, for their moral encouragement and support: so it is to them that I dedicate this thesis.

ABSTRACT

The electroweak standard model, as well-known, has been remarkably successful in describing a broad spectrum of high energy physics and has also given a satisfactory and consistent theoretical description of all the experimental data which has been obtained so far. The aim of the present work is to investigate some of the most important processes associated with the standard model which involve the charged intermediate bosons $W^{\pm}$, the neutral intermediate boson Z, the pair production of weak gauge bosons and the Higgs boson.

First of all we start with the study of the effect of the strong interaction on the direct production of weak gauge boson production at hadron colliders. We calculate the first order perturbative QCD corrections $O(\alpha_s)$ to the lowest order cross sections for photon and Z pair production at hadron colliders. The calculation contains divergences, represented in dimensional regularisation by poles of order $O(1/\epsilon)$ and $O(1/\epsilon^2)$, where $\epsilon = \frac{4-n}{2}$. The order $O(1/\epsilon^2)$ terms are eliminated when real and virtual corrections are combined, and the remaining $O(1/\epsilon)$ corrections will be absorbed into the quark momentum distribution functions.

We then study the production rate of weak gauge boson pairs for proton-proton and proton-antiproton colliders using single and double parton scattering mechanisms. We extrapolate to the next generation of hadron colliders with centre-of-mass energy E_{cm}= 10-200 TeV. We find comparable values for the single and double scattering cross sections at very high energies. To expand our investigation, we study also the production rate of multiple gauge bosons at hadron supercolliders using the double parton scattering mechanism. These kinds of processes are important and represent a potential significant background for Higgs boson production.

Finally, and for completeness, we study Higgs boson phenomenology, which now forms a substantial part of the physics program at the next generation of high energy colliders. The calculation covers the production rate of single and double Higgs production at hadron colliders via gluon-gluon fusion, their branching ratios and decay widths.

TABLE OF CONTENTS

CHAPTER 1

INTRODUCTION

1.1 Historical Background

The basic rules governing the world require a theory of how the constituent parts of this world exist and interact with each other. Furthermore the understanding of the basic rules of these small particles will give us a clear image of the fundamental laws which govern nature. The problem of understanding the structure and behaviour of matter has attracted the attention of many scientists all over the world for several centuries [1].

At an early time in history, the number of "particles" known in this world had been said to be four, namely earth, wind, fire and water. Eventually, people started to realize one of the most important steps towards more understanding of matter, that is the recognition that all matter is composed of small parts which carry the properties of the matter. These are "MOLECULES". Later on, a hypothesis suggested that the molecules themselves were composed of smaller parts called "ATOMS". The next great step of this history has been largely due to the work of J.J.Thomson and E.Rutherford at the beginning of this century. They revealed that the atoms themselves were composites of still smaller units. The suggestion arose that the mass of the atom is made-up of parts with a net positive charge, called the "NUCLEUS", concentrated in a small region at the centre of the atom with electrons revolving around in closed orbits. Later hypothesis suggested that the nucleus itself consists of smaller entities, namely protons and neutrons.

A large number of attempts have been made to study the properties of these constituents. One important aspect of the modern point of view has been the recognition of the different types of forces governing these particles. To understand how these particles are put together and the way they interact with each

other requires a theory of the basic forces of nature. Four such forces have been identified namely, electromagnetic, weak, strong and gravity. The variety of these forces depends on their strength and range. The electromagnetic force governs the interaction of electrically charged particles, the weak force is responsible for processes of the beta decay type, the strong force holds together the particles in the nucleus and the gravitation force, weakest in strength, determines the behaviour of matter in bulk. One of the major achievements of modern physics is to unify these forces into one theory governing the whole universe.

The first successful attempts to unify two interactions was achieved by J. Maxwell by the middle of the 19th century. That is the unification of electricity and magnetism into electromagnetism theory. The beginning of this century has witnessed the birth of the modern theory of quantum electrodynamics which relates relativity and quantum theory. In the 1930's, Yukawa tried to find a unified explanation for the nuclear and weak nuclear forces. He also noted that the range of any force should be inversely proportional to the mass of the particle transmitted. For this reason he postulated the existence of particles exchanged in the interaction called mesons.

Early in the 1950's, experiments were performed to study the question of the structure of the nucleon. In 1953, the first particle accelerators were built, when for the first time, subatomic particles could be produced and studied in laboratories, independent of cosmic rays. As a result of these experiments, which were performed at high energies, an enormous variety of elementary particles has been discovered. A number of attempts have been made to study the properties of these particles.

Nowadays, high energy physicists are exploring physical phenomena occuring at extraordinary energies. At these energies, particles such as the proton and the electron are accelerated to enormous energy. Subsequently the particles collide

with each other or with other particles, with sophisticated detectors to observe what is happening in these complicated reactions.

1.2 The Quark Model

By the early 1960's a large number of elementary particles had been found in cosmic rays or through particle accelerators. They could be grouped into families according to their spin, parity, strangeness and isospin.

In 1962 Gell-Man and Nee'man [2] used a method of expanding an isospin of the strong force to a higher symmetry representation. Their starting point was the charge independent property of the strong nuclear force which means that particles (such as the protons and the neutrons) are indistinguishable in a world where the strong force is the only interaction.

By using the concept of isospin, the strong interaction can be described in an elegant mathematical way. The charge independence can be expressed as the invariance of the strong interaction under rotation in isospin space. When the strangeness is added to the isospin as a property of the strong interaction, it is clear that the strongly interacting particles are governed now by a symmetry group which is called SU(3). The question is: how can the representation of SU(3) be chosen from other possibilities!

In 1964 the most successful model [2], namely "THE QUARK MODEL ", which describes this composite picture and gives an exact understanding of SU(3) classfication of hadrons, was proposed (independently) by Gell-Mann and Zweig. They postulated the existence of three types of fermions known as quarks, each of different flavour up, down and strange or u, d and s respectively. The u and d quarks formed an s=0, isospin doublet (I=1/2, -1/2 for u and d respectively), with s=-1 and isospin singlet I=0 for s quark.

According to the quark model, baryons are bound states of three quarks (qqq), each quark with baryon number B=1/3 and carrying fractional charge of +2/3

and -1/3, while mesons with baryon number B=0, are considered to be states of a quark-antiquark pair ($q\overline{q}$).

These quarks form the fundamental representation of the symmetry group SU(3). According to the rules of SU(3) algebra, which can be expressed mathematically by combining the representation of the group for the meson,

$$q \otimes \overline{q} = 3 \otimes \overline{3} = 1 \oplus 8,$$

and for the baryon

$$q \otimes q \otimes q = 3 \otimes 3 \otimes 3 = 1 \oplus 8 \oplus 8 \oplus 10$$

The quark model was one of the most successful models for describing the particle picture. Yet despite all its successes, there are still questions to be answered:

1. Why are only combinations of quarks seen, and not free quarks ?
2. Quarks must have spin 1/2 to explain the observed hadrons like Δ^{++}. This leads to a problem, since to make these particles all quarks of the same spin have to be in the same state to form a particle, which is not allowed by Fermi-Draic statistics.

In order to solve some of these problems a further new quantum number was introduced by O. Greenberg in 1964 [2]. Accordingly, each variety comes in three different colour states Red, Blue and Green. The introduction of colour resolves such problems as:

1. The experimental ratio R between the cross sections $e^+e^- \rightarrow hadrons$ and $e^+e^- \rightarrow \mu^+\mu^-$.

$$R = \frac{\sigma(e^+e^- \rightarrow Hadrons)}{\sigma(e^+e^- \rightarrow \mu^+\mu^-)} = \sum e_i^2 \qquad 1.1$$

For three quark flavours, R was found to be a factor of three smaller than the experimental data, but the result comes in good agreement between theory and experiment when the quarks come in three different colours.

2. From the analysis of the hadronic spectrum, there ought to exist precisely three different colours.
3. The colour quantum number solves the problem of Fermi-Dirac statistics, so that we can make particles like Δ^{++}.
4. In the the decay of the neutral pion, the lifetime depends on the number of quark colours. By proposing three quark colours the predicted lifetime is precisely the lifetime observed.

So different phenomena support the existence of colour. The property of colour must be responsible for the confinement of quarks within hadrons. It is natural to say that there must exist an exchanged particle associated with colour, called the "GLUON". Its name leads to the understanding that it glues the quarks together within the hadrons. Unlike the photon, this gluon has to carry the colour charge, which means that there are different coloured gluons corresponding to different possible combinations.

To place this on a mathematical basis, it is expressed as a gauge theory, in analogy with quantum electrodynamics (QED), called quantum chromodynamics (QCD) .

1.3 The Quark-Parton Model

Deep inelastic lepton-nucleon scattering experiments have proved to be the most powerful for the investigation of the substructure of nuclear matter, and also provide one of the most important and fundamental tests of QCD.

In these experiments, an electron collides with a proton, which breaks up and creates a shower of hadronic products. The two particles interact through the exchange of a (high-energy) virtual photon, and the internal structure of the hadronic particles is probed [3].

The process is shown in fig. (1.1), the electron scattering off a proton via one photon exchanged

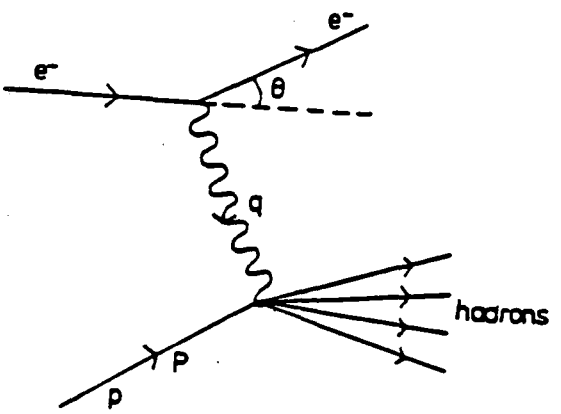

Fig. (1.1) The kinematics of deep inelastic scattering.

Defining the 4-momentum transfered squared by the photon to the proton Q^2 as

$$Q^2 = -q^2 = 4EE' sin^2\theta/2,$$

the energy lost by the electron to the proton ν as

$$\nu = E_i - E_f,$$

and the dimensional variable $x = \frac{Q^2}{2M\nu}$ when $1 > x > 0$. Then the cross-section for the process can be written

$$\frac{d^2\sigma}{dQ^2 d\nu} = \frac{4\pi\alpha^2}{Q^4}\frac{E}{E'}\left(W_2(Q^2,\nu)\cos^2\frac{\theta}{2} + 2W_1(Q^2,\nu)\sin^2\frac{\theta}{2}\right) \qquad 1.2$$

where W_2 and W_1 are the structure functions which correspond to the two possible polarisation states of the exchanged photon .

In general, the structure function depends on two variables, Q^2 and ν. In 1969 the prediction was made by J. Bjorken [3] that when the momentum Q^2 carried by the probe is very large, the structure function will depend on one parameter. This is called Bjorken scaling, i.e.

$$MW_1(x,Q^2) \longrightarrow F_1(x) \qquad 1.3.a$$

$$\nu W_2(x, Q^2) \longrightarrow F_2(x) \qquad 1.3.b$$

Feynman in 1969 [3] had a simple explanation of Bjorken scaling. He assumed that the struck nucleon is made of point-like constituents called "PARTONS". The scaling behaviour of the cross-section was used as an indication of the scattering off point-like partons, which were identified with the quarks of the constituent quark model, as they appeared to have identical quantum properties.

Another surprising result came from experiments indicating that the sum of the quark momentum in a proton is just half the total proton momentum. This suggests the existence of another object besides the quark. In this case, the object must be massless and electrically neutral. These new particles are called "GLUONS" which are responsible for holding the quarks together to form hadrons. The correct picture from deep inelastic experiments shows that

$$PARTONS = QUARKS + GLUONS$$

The theory which describes the interaction of quarks and gluons is called quantum chromodynamics. It is believed to be the theory of strong interaction and is discussed in detail in the next section.

1.4 Quantum Chromodynamics

During the past decade, quantum chromodynamics (QCD) has emerged as a leading candidate for the theory of strong interaction. With its elegant and simple (in principle) properties, it has many of the right properties to give good fits when reliable approximations exist.

QCD acts as a colour gauge theory on the fundamental spin 1/2 quarks and involves the exchange of a spin 1 gauge boson, the gluon.

The mathematical description is essentially the same as that for QED with the complication that a $3 \otimes 3$ unitary matrix appears in QCD due to three colours, in place of U(1) in QED.

This theory has the following properties:

1. Quark carries colour as well as charge.
2. Colour is exchanged by eight coloured gluons.
3. Colour interactions are assumed to be similar to electromagnetic interactions, with the change of $\sqrt{\alpha}$ for QED to $\sqrt{\alpha_s}$ for the strong coupling of QCD.
4. At large momentum transfer (short distances) the coupling is so small that we can use perturbative techniques, like in QED, while at small momentum transfer (long distance) the coupling is so strong that the perturbation technique cannot be used. This is called asymptotic freedom behaviour, and it is a unique property of QCD among other theories [4].

The Lagrangian of QCD is invariant with respect to a local SU(3) gauge transformation. The main idea of QCD is to make the $SU_c(3)$ colour symmetry local rather than global. To put this into effect, one must introduce a suitable vector gauge field $\Psi_i^a(x)$, where a = 1.....8, which transforms as the adjoint reperesentation of SU(3) and the index i refers to the number of flavour. Starting with the Lagrangian density for free quarks

$$\mathcal{L}_0 = \overline{\Psi}(i\gamma^\mu \partial_\mu - m)\Psi \qquad 1.4$$

Herein, only one quark flavour is considered.

To make the physics invariant, we consider the effect on the Lagrangian, if the quark field is transformed under the most general local transformation

$$\Psi(x) \longrightarrow U\Psi(x) = e^{i\alpha_a(x)T_a}\Psi(x) \qquad 1.5.a$$

$$\Psi(x) \simeq (1 + i\alpha_a(x)T_a)\Psi(x) \qquad 1.5.b$$

where U is a special $3 \otimes 3$ matrix, $\alpha_a(x)$ are the group parameters and T_a is the usual 3×3 generator of SU(3). Expanding the last equation by taking its derivative

$$\partial\mu\Psi(x) = (1 + i\alpha_a(x)T_a)\partial_\mu\Psi(x) + iT_a(x)\Psi(x)\partial_\mu\alpha_a(x) \quad 1.6$$

The second term in eqn. (1.6) destroys the invariance of the Lagrangian. Note that if $\alpha_a(x)$ is constant this term is zero which implies that the Lagrangian is invariant under global phase transformations. If we want the Lagrangian to be invariant under local transformations, we should look for a modified Lagrangian. In order to get this, we introduce a gauge field A^a_μ with some transformation property to obtain a covariant derivative such that

$$\partial_\mu \longrightarrow D_\mu = \partial_\mu + igT_aA^a_\mu \quad 1.7$$

where A_μ transform in abelian gauge field (QED) as

$$A^a_\mu \longrightarrow A^a_\mu - \frac{1}{g}\partial_\mu\alpha^a(x) \quad 1.8$$

then the Lagrangian becomes

$$\mathcal{L} = \overline{\Psi}(i\gamma^\mu\partial_\mu - m)\Psi - g(\overline{\Psi}\gamma^\mu T_a\Psi)A^a_\mu \quad 1.9$$

To preserve the invariance of the Lagrangian, it is necessary that the non-abelian gauge field (QCD) A_μ transforms according to

$$A^a_\mu \longrightarrow A^a_\mu - \frac{1}{g}\partial_\mu\alpha^a(x) - f_{abc}\alpha^b(x)A^c_\mu, \quad 1.10$$

where A_μ are regarded as the physical coloured gauge fields.

Thus the complete invariant Lagrangian under the local phase transformation for QCD attains the final form

$$\mathcal{L} = \overline{\Psi}(i\gamma^\mu\partial_\mu - m)\Psi - g(\overline{\Psi}\gamma^\mu T_a\Psi)A^a_\mu - \frac{1}{4}A^a_{\mu\nu}A^{\mu\nu}_a, \quad 1.11$$

where $A^a_{\mu\nu}$, the QCD strength tensor field has the form

$$A^a_{\mu\nu} = \partial_\mu A^a_\nu - \partial\nu A^a_\mu - gA^b_\mu A^c_\nu f_{abc}, \quad 1.12$$

in which f_{abc} the structure constant of SU(3) is defined

$$[T^a, T^b] = i f_{abc} T^c \qquad 1.13$$

where the set a,b,c = 1 . . . N^2 -1 for an SU(N) algebra.

To summarise, we can say that the quarks transform according to the triplet representation and each flavour is a triplet of the colour group, and there are eight gluons transforming as the adjoint representation. Another important note to be made is that the mass term of the form $\frac{m^2}{2} A^\mu A_\mu$ is not allowed in the Lagrangian, hence the local gauge symmetry requires the gluon to be massless like the photon in QED.

1.5 The Way to Unified Weak and Electromagnetic Interactions

In the last section we described QCD which is believed to be the candidate of the strong interaction. We try next to understand the phenomenology of another kind of interaction; that is the weak interaction and the way to unify it with the electromagnetic interaction.

Historically, the first weak interaction to be observed was the nuclear β-decay which involved the emission of electrons and positrons from nuclei. Following up, in 1934 E. Fermi developed a new phenomenology for weak interactions, interpreting nuclear β-decay from the nucleon in a way similar to that of photon emission from an excited atom.

The weak interactions can be divided into two groups:

1. Charge current reactions which change the electric charge

$$n \longrightarrow p + e^- + \overline{\nu}_e \qquad 1.14.a$$

2. Neutral current reactions with no change in electric charge

$$\nu_e + p \longrightarrow \nu_e + p \qquad 1.14.b$$

With the analogy of the current-current form, the Lagrangian of process (1.14.a) appears in the form

$$\mathcal{M} = -\frac{G_F}{\sqrt{2}}(\overline{\Psi}_p O \Psi_n)(\overline{\Psi}_e O \Psi_{\overline{\nu}e}),$$

where G_F is the weak coupling constant and the operator O characterise the coupling, which was found experimentally to be both the vector (V) and the axial-vector (A) type in the weak interactions.

The observation of parity violation in weak interactions is represented in the vector axial (V-A) structure of the coupling. An attempt was made to overcome the fundamental difficulty of four fermion interaction (the interaction is not renormalizable and violates unitarity at high-centre-of mass energy), by introducing a massive charge boson, which mediates the weak interaction and has the following properties:

1. It carries charge $\pm$ 1.
2. It must be rather massive, to reproduce the short range of the weak force.
3. Its parity is indefinite.

The observation of the intermediate vector boson, the mediator of weak interactions, has been a goal of elementary particle physics and it has been a part of the dream to build a unified theory of electromagnetic and weak interactions, since both of them are mediated by spin 1 particles and act with a universal strength, the weak coupling being related to the strength of the e.m. coupling:

$$g = \frac{e}{\sin\theta_W} \qquad 1.15$$

where θ_W is the electroweak mixing angle. This equation implies that the coupling constants of e.m. and weak interactions are connected, which is the direct manifestation of the unified electroweak interaction. Before going into the details of the electroweak theory, we shall start with a brief general discussion of the Higgs mechanism in the following section.

1.6 The Higgs Mechanism

In the last section, we have showed how the weak interacton is mediated by the exchange of a vector massive boson. The phenomenon by which a vector boson requires mass without destroying the gauge invariance of the Lagrangian is known as the Higgs mechanism [5].

The Higgs mechanism is the result of spontaneous symmetry breaking, which paves the way to the generation of mass for the particle. The idea is to include an extra field within the theory. We start with the Lagrangian of the real interacting field

$$\mathcal{L} = (\partial_\mu \Phi)^+ (\partial^\mu \Phi) - \mu^2 \Phi^+ \Phi - \lambda (\Phi^+ \Phi)^2 \qquad 1.16$$

which is invariant under U(1) local gauge transformations $\Phi \longrightarrow \Phi e^{i\alpha(x)}$.

If we consider the case $\lambda > 0$ and $\mu^2 < 0$, then the potential of the Lagrangian has the form

$$V(\Phi) = \mu^2 \Phi^+ \Phi + \lambda (\Phi^+ \Phi)^2, \qquad 1.17$$

which has a minimum at radius $v = \sqrt{\frac{-\mu^2}{\lambda}}$. This corresponds to the ground state.

Now we expand the field Φ about a true ground state field in terms of new fields η and ξ

$$\Phi(x) = 1/2(v + \eta(x) + i\xi(x)), \qquad 1.18$$

and using eqn. (1.18) in the Lagrangian we get

$$\mathcal{L}' = 1/2(\partial_\mu \xi)^2 + 1/2(\partial_\mu \eta)^2 + \mu^2 \eta^2 + \mu^2 \frac{v^2}{2} \qquad 1.19$$

The first term is the kinetic energy of the massless field ξ and the third term is the mass term of the η field.

Our Lagrangian is an example of the Goldstone theorem in which massless scalars occur when a physical system is *spontaneously broken.* In order to study the breaking of the local gauge symmetry, the Lagrangian is invariant under a

U(1) transformation, we expand it to be invariant under an SU(2) transformation as well, which requires ∂_μ to be replaced by the covariant derivative

$$D_\mu = \partial_\mu - ieA_\mu, \tag{1.20}$$

where A_μ is the gauge field which transforms as

$$A_\mu \longrightarrow A_\mu + \frac{1}{e}\partial_\mu \alpha \tag{1.21}$$

The gauge invariant Lagrangian can be written in the form

$$\mathcal{L} = (\partial_\mu + ieA^\mu)\Phi^+(\partial_\mu - ieA_\mu)\Phi - \mu^2\Phi^+\Phi - \lambda(\Phi^+\Phi)^2 - \frac{1}{4}F_{\mu\nu}F^{\mu\nu}, \tag{1.22}$$

where the term $F_{\mu\nu}F^{\mu\nu}$ represents the K.E for the field A_μ. Substituting $\Phi = \sqrt{1/2}(v+\eta+\xi) \simeq \sqrt{1/2}(v+\eta)e^{-i\xi/v}$ in the Lagrangian we get

$$\mathcal{L}' = 1/2(\partial_\mu\xi)^2 + 1/2(\partial_\mu\eta)^2 - v^2\lambda\eta^2 + 1/2e^2v^2A_\mu A^\mu - evA_\mu\partial^\mu\xi - \frac{1}{4}F_{\mu\nu}F^{\mu\nu}, \tag{1.23}$$

where ξ describes a massless Goldstone boson, η a massive scalar and A_μ is the massive vector boson as

$$m_\xi = 0, \quad m_\eta = \sqrt{2\lambda v^2}, \quad m_A = ev$$

We have dynamically generated a mass for the gauge field, but there is still the problem of the occurrence of a massless Goldstone boson. In order to find a gauge transformation which will eliminate the unphysical field from the Lagrangian, we assume

$$\Phi \longrightarrow \sqrt{1/2}(v + h(x))e^{\frac{i\theta(x)}{v}} \tag{1.24.a}$$

$$A_\mu \longrightarrow A_\mu + \frac{1}{ev}\partial_\mu\Phi \tag{1.24.b}$$

Substituting in the Lagrangian we get

$$\mathcal{L}'' = 1/2(\partial_\mu h)^2 - \lambda v^2 h + 1/2e^2v^2A_\mu^2 - \lambda v h^3 - 1/4\lambda h^4 + 1/2e^2A_\mu^2h^2$$

$$+ve^2A_\mu^2h - 1/4F_{\mu\nu}F^{\mu\nu} \qquad 1.25$$

This Lagrangian describes two massive particles, a vector gauge boson A_μ and a massive scalar h , which is called the ' Higgs particle'. Here the vector boson A^μ 'eats' a Goldstone boson and becomes massive. This mechanism is called the Higgs mechanism which is the result of spontaneous symmetry breaking.

1.7 Salam-Weinberg Model

In the previous section we have shown that the Higgs mechanism through spontaneous symmetry breaking gives us a consistent way of introducing the masses of the vector bosons mediating the weak interaction.

One of the most successful new theories establishes a link between weak and electromagnetic interactions, suggesting that they are different manifestation of a single underlying force, the theory which was proposed and established by Salam-Weinberg in 1960's.

Its first prediction was confirmed when experimental neutral current data was obtainned which precisely matched the theoretical predictions. The discovery of the weak bosons W and Z in 1982-1983 at the CERN [6] $p\bar{p}$ collider with masses

$$m_W = 81.0 \pm 2GeV$$

$$m_Z = 92.0 \pm 2GeV,$$

is exactly as predicted by the standard electroweak theory.

The standard $SU(2) \times U(1)$ model was proposed and established to unify the electromagnetic and weak interactions. This model [7] was suggested first by S. Glashow in 1961 and in more detail by S. Weinberg in 1967 and finally, by A. Salam in 1968. They invoked spontaneous symmetry breaking to give a mass to the gauge boson without spoiling the renormalisability of the theory. Herein, the isospin of the scalar meson generates a mass as a result of self interaction. The vector boson is a massive isovector triplet W_μ for SU(2) and a massless isosinglet

B_μ for U(1). As a result of the spontaneous breaking, three bosons W_μ^+, W_μ^- and Z_μ^0 acquire mass and one A_μ the photon remains massless.

In order to do this, we begin with the gauge invariant Lagrangian for the scalar fields

$$\mathcal{L}_2 = (D_\mu\Phi)^\dagger(D^\mu\Phi) - V(\Phi), \qquad 1.26$$

with $D_\mu\Phi = (\partial_\mu - igT.W_\mu - g'\frac{Y}{2}B_\mu)\Phi$, where T and B_μ are the weak hypercharge operator.

To generate gauge boson masses, we use the Higgs potential of eqn. (1.17) with $\mu^2 < 0$ and $\lambda > 0$, so that the complex scalar doublet, at this potential, has the form

$$\Phi_0 = \sqrt{\frac{1}{2}}\begin{pmatrix} 0 \\ v \end{pmatrix}$$

The gauge boson mass are identified by subsituting the vaccum expectation value Φ_0 for $\Phi(x)$ in the Lagrangian. The relevant term for the gauge boson is given by

$$= \frac{1}{8}\left|\begin{pmatrix} gW_\mu^3 + g'B_\mu & g(W_\mu^1 - iW_\mu^2) \\ g(W_\mu^1 + iW_\mu^2) & -gW_\mu^3 + g'B_\mu \end{pmatrix}\begin{pmatrix} 0 \\ v \end{pmatrix}\right|^2$$

$$= (\frac{1}{2}vg)^2 W_\mu^+ W^{-\mu} + \frac{1}{8}v^2(W_\mu^3, B_\mu)\begin{pmatrix} g^2 & -gg' \\ -gg' & g'^2 \end{pmatrix}\begin{pmatrix} W^{3\mu} \\ B^\mu \end{pmatrix}, \qquad 1.27$$

since $W^\pm = \frac{1}{\sqrt{2}}(W^1 \pm iW^2)$. When we compare the first term of eqn. (1.27) with the mass expected for charge boson, $m_W^2 W^+W^-$, we find

$$m_W = \frac{1}{2}gv \qquad 1.28$$

The remaining term is off-diagonal in the W_μ^3 and B_μ basis:

$$\frac{1}{8}v^2[gW_\mu^3 - g'B_\mu]^2 + O[g'W_\mu^3 + gB_\mu]^2,$$

which must be identified with $\frac{1}{2}m_Z^2 Z_\mu^2 + \frac{1}{2}m_A^2 A_\mu^2$.

So on normalising the fields, we get

$$A_\mu = \frac{(g'W_\mu^3 + gB_\mu)}{\sqrt{(g^2 + g'^2)}} \quad with \quad m_A = 0, \qquad 1.29.a$$

$$Z_\mu = \frac{(gW_\mu^3 - g'B_\mu)}{\sqrt{(g^2 + g'^2)}} \quad with \quad m_Z = \frac{1}{2}v\sqrt{(g^2 + g'^2)} \qquad 1.29.a$$

From eqn. (1.15) the coupling strengths are related by

$$\tan\theta = \frac{g'}{g}$$

Using eqn. (1.28) and eqn. (1.29.b), we have the following relation

$$\frac{m_W}{m_Z} = cos\theta_W \qquad 1.30$$

The inequality in masses is due to the mixing between the W_μ^3 and B_μ fields. The mass eigenstates are then a massless photon (A_ν) and a massive Z_μ field.

To summarise, the theory made several predictions and was successfully tested for over more than a decade in many experiments like the observation of the neutral current in 1974, the prediction of the charm quark and more recently the massive bosons W, Z have been observed at CERN $p\bar{p}$ collider with the all right properties and in excellent agreement [6].

In spite of all these successes in which the theory gives a unified description of e.m. and weak interactions with very precise predictions, many parameters in the model had to put in by hand and have to be determined experimentally:

- the e.w. coupling constant e and g and their mixing angle;
- the number of generators;
- the masses of quarks and leptons;
- the mass of Higgs boson;

Because of these large number of free parameters the standard model is probably far from being the ultimate description of particles and their interactions. is The aim nowadays is to find indications for physics beyond the standard model.

1.8 QCD Phenomenology

If quantum chromodynamics, the gauge theory which describes the interaction of coloured quarks and gluons, represents the correct theory of strong interaction, it must describe an enormous range of phenomena in particle physics from the spectrum of hadrons to deep inelastic scattering.

Herein, we are going to review a few of the many qualitatively successful topics in modern phenomenology, which are important in bringing experimentalists and theorists together in order (i) to understand present data (ii) to measure as precisely as possible the fundamental parameters of the theory ($\Lambda_{\overline{MS}}$, the distribution of partons in hadrons, ...) and (iii) to make accurate predictions for the next generation of hadron colliders. The topics which will be covered are [8]:

1. QCD in Deep Inelastic Scattering.
2. Large P_t Hadron Production.
3. W, Z Production and QCD.
4. e^+e^- Annihilation.
5. Higher order QCD Corrections - the K-Factor

1.8.a QCD in Deep Inelastic Scattering

The first deep inelastic scattering experiments started at SLAC in 1968. They involved the scattering of electrons with protons in liquid hydrogen with energies up to 18 GeV, and the scattering happened through exchange of virtual photons.

The observed cross-section gives information about the momentum distribution of the partons inside the proton. In the absence of QCD the distribution structure functions are independent of Q^2, since the partons are assumed to be freely moving pointlike objects. As Q^2 increases, the photon will see the quarks surrounded by gluons. By further increase in Q^2, the photon can resolve the valence quarks into quarks plus gluons and a quark plus $q\overline{q}$ pair.

The cross-section has Bjorken scaling if there are a fixed number of partons

at some distance scale. But in the presence of QCD, the simple parton model is regarded as the zeroth order of the perturbation expansion. The test of perturbative QCD is the breaking of Bjorken scaling in deep inelastic scattering. From all this we can note the following:

1. In the 'naive' parton model the structure functions scale i.e.

$$F(x, Q^2) \to F(x)$$

   in the asymptotic (Bjorken) limit: $Q^2 \to \infty$, x fixed.

2. In QCD this scaling is broken by logarithms of Q.
3. In leading order QCD, the structure function is given by structure function with non-scaling parton densities $q(x, Q^2)$.

Any distribution of a quark q_i can be written as a sum of singlet and non-singlet components. In order to describe the way in which QCD breaks the scaling, it is suitable in this respect to define these singlet and non-singlet distributions:

$$q^{NS} = q_i - q_j$$

$$q^{S} = \sum_i (q_i + \bar{q}_i)$$

In perturbative QCD, because the quarks can radiate gluons, the structure functions varies with Q^2, and these variations with respect to Q^2 are described by the Altarelli-Parisi evolution equations of the form

$$Q^2 \frac{d}{dQ^2} q^{NS} = \frac{\alpha_s(Q^2)}{2\pi} P^{qq} * q^{NS} \qquad 1.31.a$$

$$Q^2 \frac{d}{dQ^2} \begin{pmatrix} q^s \\ g \end{pmatrix} = \frac{\alpha_s(Q^2)}{2\pi} \begin{pmatrix} P^{qq} & P^{qg} \\ P^{gq} & P^{gg} \end{pmatrix} * \begin{pmatrix} q^s \\ g \end{pmatrix}, \qquad 1.31.b$$

where the *splitting function* $P^{ij}(x)$ is defined as the probability of parton j emitting a parton i with momentum fraction ($x < 1$), and * denotes a convolution integral:

$$f * g = \int_x^1 \frac{dy}{y} f(y) g(\frac{x}{y})$$

For massless quarks the splitting function is flavour independent, i.e.

$$P_{q_i q_j}(x) = P_{qq}(x) \quad \delta_{ij}.$$

The explicit form for the splitting function can be written as

$$P^{qq} = \frac{4}{3}\left(\frac{1+x^2}{1-x}\right)_+ \qquad 1.32.a$$

$$P^{qg} = \frac{1}{2}(x^2 + (1-x)^2) \qquad 1.32.b$$

$$P^{gq} = \frac{4}{3}\frac{1+(1-x)^2}{x} \qquad 1.32.c$$

$$P^{gg} = 6\left(\frac{1-x}{x} + \frac{x}{(1-x)_+} + x(1-x)\right) - \frac{\delta(1-x)}{2} - \frac{N_f}{3}\delta(1-x), \qquad 1.32.d$$

where these decay probabilities will determine the structure of a nucleon at a given momentum scale (parton distributions will depend on Q^2).

The precision of present data demands higher order corrections to be included. The actual fits use next to leading order QCD predictions

$$P(x) \rightarrow P^0(x) + \frac{\alpha_s}{2\pi}P^1(x)$$

$$F \rightarrow \sum q \rightarrow F = \sum(1 + O(\alpha))q$$

In spite of the success in using perturbative QCD to study the structure function, there are still some problems to be solved such as the higher twist terms which must be taken into account, and the singlet structure function is sensitive to the gluon distribution at low x. In order to solve these problems, the most recent generation of deep inelastic scattering experiments are trying to achieve the following points:

a. Higher Q^2 so that there is no higher twist.

b. Higher x so that the structure function is just non-singlet part which is not sensitive to gluon distribution.

c. Higher statistics.

1.8.b Large P_t Production

The study of large momentum transfer hadron-hadron scattering has contributed substantially to our understanding of the nature of short distance parton-parton interactions, and provided a fundamental test of QCD. The hard scattering of quarks and gluons can be studied in the production of hadronic jets with large momentum transfer.

In the parton model (lowest order QCD), a high P_t jet is just a single P_t parton and the jet cross-section is the parton cross-section:

$$E\frac{d^3\sigma}{dp_j} = \sum_{a,b,c,d} \int dx_a dx_b G_{a/p}(x_a, Q) G_{b/\overline{p}}(x_b, Q) \delta(\hat{s} + \hat{t} + \hat{u}) \frac{1}{16\pi^2 \hat{s}} \overline{M}^2_{ab \to cd} \quad 1.33$$

The parton distributions are determined by measurements made in deep inelastic lepton-nucleon scattering.

There are various sources of uncertainty in measuring the jet cross-section. These include:

1. The uncertainty in measuring the P_t of the jet which comes from extra soft parton which is needed to conserve colour, electrical charge and energy. The experimental fluctuation of P_t is of the order of 1 GeV.
2. The uncertainty of fixing nucleon structure functions which is due to our limited knowledge of Λ_{QCD} and the gluon distribution function.
3. Higher order QCD corrections to the cross-section which are called 'K-factor'. These must be evaluated and the result must be organised into a form appropriate to the jet cross section.

The leading order QCD calculation for processes like $ab \to cd$ with some scale choice $Q=\frac{P_t}{2}$ gives excellent agreement with experiment over the complete P_t range and provides the cleanest evidence so far for hard parton-parton scattering.

New improved experimental results on high P_t jet production have recently been presented in which multiple parton scattering [9] is expected to occur in single hadronic collison. The cross-section for this process is determined by the product

of two cross-sections and with the appropriate parton momentum distribution $V(x_i, x_j)$

$$d\sigma = \sum_{q/g} \frac{d\hat{\sigma}_{12} d\hat{\sigma}_{34}}{\pi R^2} V(x_1, x_2)\overline{V}(x_3, x_4) \qquad 1.34$$

where πR^2 represents the inelastic cross-section.

Multiple parton interactions are also expected as a potential background for new physics research and for the future of hadron colliders. This will be discussed further in section 4.4.

1.8.c W , Z Production and QCD

The gauge theory of Weinberg-Salam has come to be believed because of the existence and detection of $W^{\mp}$ and Z. Furthermore, the production of gauge bosons provides the most fundamental test of the standard model and gives a useful testing ground for perturbative QCD [10].

In 1983 the weak gauge bosons were discovered at the CERN $p\bar{p}$ collider via the processes:

$$p\bar{p} \rightarrow W^{\pm}X \rightarrow e^{\pm}\nu X$$

$$p\bar{p} \rightarrow ZX \rightarrow e^{+}e^{-}X$$

By studying the momentum distribution of the emitted particles, the mass for the W and Z were measured as:

$$M_W = 81 \pm 2 \quad GeV$$

$$M_Z = 92 \pm 2 \quad GeV$$

The observed cross-section for the production of a W followed by its decay at the collider energy $\sqrt{s} = 540$ GeV is

$$\sigma(p\bar{p} \rightarrow WX \rightarrow e\nu X) = 0.53 \pm 0.08 \quad nb$$

The cross section for Z production and decay into leptons pair is about an order of magnitude smaller than that for W production.

The W and Z production can be calculated using the Drell-Yan mechanism as shown in the fig (1.2).

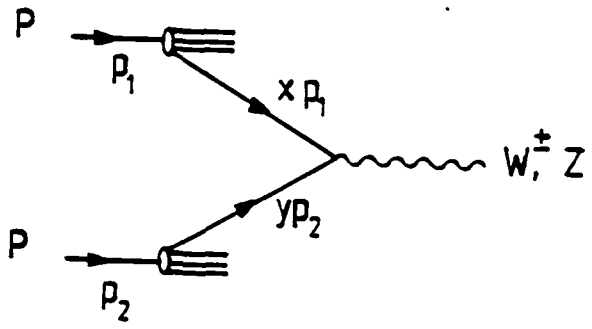

Fig. (1.2) Drell-Yan mechanism for massive gauge boson production.

The total cross-section for W production can be written in the form

$$\sigma(p\bar{p} \to W^{\pm}X) = \sum_{q,\bar{q}} \int_0^1 dx_a \int_0^1 dx_b G_{a/p}(x_a, Q^2) G_{b/\bar{p}}(x_b, Q^2) \hat{\sigma}_{q\bar{q}\to W^{\pm}} \qquad 1.35$$

where $\hat{\sigma}_{qq\to W}$ is the subprocess cross-section

$$\hat{\sigma}_{q\bar{q}\to W^{\pm}} = \frac{4\pi^2\alpha}{3} \frac{1}{4\sin^2(\theta_W)} \delta(x_a x_b s - m_W^2) \qquad 1.36$$

Hard scattering $2 \longrightarrow 2$ process is also produced at the $p\bar{p}$ collider with a large momentum transfer as shown in fig. (1.3).

These events are what is expected from higher $O(\alpha_s)$ subprocesses.

The result of this QCD prediction for the P_t distribution has been compared with the experimental measurement. The agreement is good.

1.8.d e^+e^- Annihilation

Particle-antiparticle beams colliding head-on in collider machines have been a very interesting development in recent years. The class of electron-positron collisions represents one of the most important and fruitful classes of experiments because it gives us a number of important features for creating new particles, besides the fact that the collision is very clean, between which enables us to learn a lot about electroweak and QCD theory.

Fig. (1.4) represents the annihilation process in which both particles annihilate into virtual gauge boson which also convert into particle pairs. The hadronization of this parton pair gives rise to back-to-back jets which represent the lowest order in perturbative QCD.

The total-cross section for the lowest order is given by the formula

$$\sigma_0 = \frac{4\pi^2\alpha}{3s}\sum_q e_q^2 \qquad 1.37$$

To next order, the quark and the antiquark can emit a gluon , which produces an additional jet as shown in fig. (1.5)

Calculating the next order diagrams gives us the correction factor which is clear from the formula

$$1 + \frac{\alpha_s}{\pi} + C_2(\frac{\alpha_s}{\pi})^2$$

Numerically if $N_f = 5$ and $\alpha_s = 0.15$ then the correction factor is

$$1 + 0.048 + 0.0032$$

Now we can write the total cross section obtained by summing over all the quarks in the form

$$\sigma = \sigma_0(3\sum_q e_q^2)\Big(1 + \frac{\alpha_s}{\pi}C_1 + (\frac{\alpha_s}{\pi})^2 C_2 + ...\Big) \qquad 1.38$$

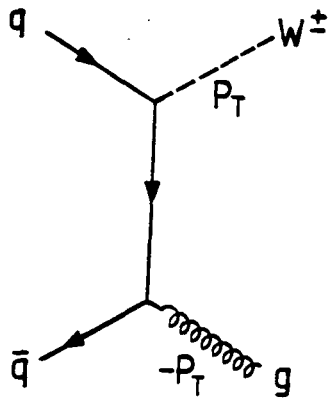

Fig. (1.3) Leading order diagram for direct W production in hadron hadron collisions.

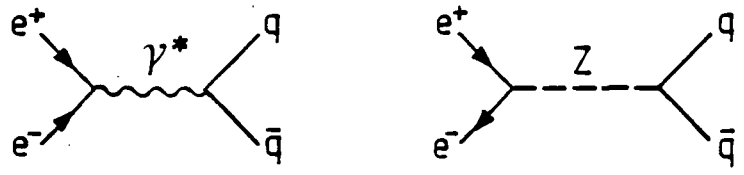

Fig. (1.4) Lowest order contribution to $e^+e^- \rightarrow q\bar{q}$.

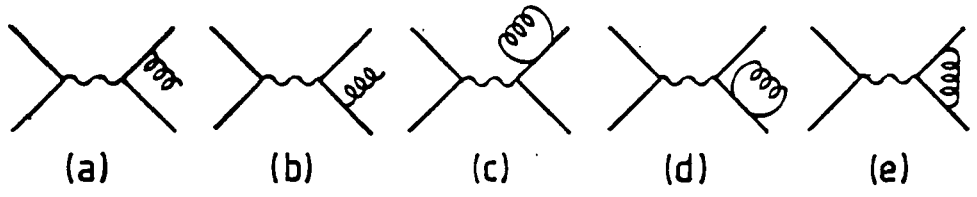

Fig. (1.5) Lowest order contributions to $e^+e^- \rightarrow q\bar{q}g$ (a), (b) and corrections to $e^+e^- \rightarrow q\bar{q}$ (c), (d), (e).

1.8.e Higher Order QCD Corrections - the K-Factor

Most of the calculations and discussions in particle physics up until now have been considered with lowest order calculations. Complete cross-sections for any process in QCD requires the cross-section to all order in α_s, which then brings large number of extra diagrams into consideration. These extra diagrams result in multiplicative corrections called the K-factor, which applied to the leading order cross-section in order to get the complete cross-section [11].

Higher order corrections in QCD as in QED are because of the possibility that the coloured partons radiate gluons. In QED this possibility is small, being proportional to $\alpha = 1/137$, but in QCD this possibility is much greater because it is proportional to α_s which is much greater than α. For this reason one cannot ignore higher order corrections in QCD.

In the past years several important higher order perturbative QCD corrections have been calculated. An approximate calculation [12] for $2 \rightarrow 2$ processes has been calculated by Antoniou et. al., their result can be expressed in the form

$$\frac{d\sigma}{dt} = (1 + \frac{\alpha_s(Q^2)}{2\pi}(C_l + C_b)\pi^2)\frac{d\sigma^0}{dt},$$

where C_l is the correction factor arising from soft gluon loops and C_b from gluon bremsstrahlung.

$O(\alpha_s^3)$ corrections has been calculated to the total cross-sections for $e^+e^- \rightarrow$ *Hadrons* by Gorishny et. al. [13], where the total cross-section has the form

$$\sigma = \sigma_0(3\sum_q e_q^2)\left(1 + \frac{\alpha_s}{\pi}C_1 + (\frac{\alpha_s}{\pi})^2 C_2 + ...\right) \qquad 1.39$$

Recently a complete higher order QCD corrections for all $2 \rightarrow 2$ processes to $O(\alpha_s^3)$ has been found by Ellis and Sexton [14]. They have calculated the cross-section in n-dimensions in order to regulate divergences.

Another phenomenologically important QCD calculation is the $O(\alpha_s^3)$ corrections to the single and two jet inclusive cross-section in hadronic collisions.

An important result is the calculation made by Matsuura et. al. [15] of $O(\alpha_s^2)$ corrections to the Drell-Yan cross section.

1.9 New Physics

The standard $SU(3)\times SU(2)\times U(1)$ model which is known to be a satisfactory and consistent theoretical description of the experimental data has continued to work well, but in recent years a variety of events which are not properly identified have been reported from the CERN $p\overline{p}$ collider. Many physicists believe that some of these events may be inexplicable within the standard model and some of them go beyond it, and may be possible signature for new physics [16].

1.9.a Monojets

In 1984 UA1 at CERN $p\overline{p}$ collider identified a sample of events containing typically one large p_t jet which was not balanced by any other detected particles. In order to understand the missing events, we look at the process

$$p\overline{p} \rightarrow Z + jet + X \rightarrow \nu\overline{\nu} + jet + x$$

the large P_t Z decay into $\nu\overline{\nu}$ pair which is undetectable, so the result is one jet equal and opposite to a missing transverm momemtum .

But the more recent and complete analysis by the UA1 collaboration in 1986 has confirmed that the observed monojet sample with $E > 12$ GeV is consistent with the standard model although we can look for new physics in the limit when $E_T \geq 30GeV$.

1.9.b Higgs Boson Detection

The most exciting experiments with the new accelerators are those which discover new particles with masses up to O(1) TeV. One of the motivations for constructing the superconducting supercollider (SSC) is to detect the missing particle, such as the Higgs boson, predicted by the standard model of electroweak interactions or any corresponding physics [17].

Since the Higgs particle couples weakly to photons, muons, electrons, light quarks and gluons of the beam particles, its detection cross-sections are quite small which makes experimental Higgs searches extremely difficult. Hadron colliders are the most promising possibilities for Higgs production. At hadron colliders, there are again two production mechanisms of W fusion and gluon fusion .

The Higgs boson is detectable through its final state. If the Higgs mass is greater than $2m_W$ or $2m_Z$, its dominant decay is $H \rightarrow W^+W^-$ and $H \rightarrow ZZ$, with branching fraction approximately in the ratio 2 to 1. At multi-TeV hadron colliders it can be produced with a cross section of a few picobarns. For the design luminosity of $10^4(pb)^{-1}$/year of the proposed superconducting super collider (SSC) this gives tens of thousands of Higgs boson events.

At the end we can say that the phenomenological issue of Higgs is extremely important and calling for further study.

1.10 Outline of the Thesis

Having given the introduction as a background of the subject, we outline the topics of this thesis. These are organized as follows:

In chapter 2, we calculate the first order perturbative QCD corrections to photon pair production in hadron colliders. We first derive the lowest order differential cross-section for the process. We then present the calculation of the virtual gluon corrections from self, vertex and box diagrams, as well as the corrections from soft and hard collinear gluon emission. We use the method of dimensional regularisation in order to regulise divergences as a poles of order $O(\frac{1}{\epsilon})$ and $O(\frac{1}{\epsilon^2})$.

In chapter 3, we calculate the first order perturbative QCD corrections to weak gauge boson production in a hadron collider. We start with the derivation of the differential cross-section for the subprocess $q\bar{q} \rightarrow ZZ$. We use exactly the same method of chapter 2 in dealing with corrections from virtual and real gluon emission. As a check on our calculation, we have compared all the calculations for m_Z=0, $g_v = -e_q$ and g_a=0 with the results of chapter 2.

In chapter 4, we calculate the total cross-section for some hard scattering processes in pp and $p\bar{p}$ collisions at $\sqrt{s}$ = 10-200 TeV for the production of single and pair weak gauge bosons . We have compared the total cross-section and the mass invariant distribution of some single scattering processes with same from the double scattering mechanism for the same processes.

In chapter 5, we investigate multiple weak gauge boson production for hadron colliders. We calculate triple and four gauge boson production cross-section in pp collision versus CM energy using the double parton scattering mechanism. We compare our results with triple gauge boson production from single parton scattering.

In chapter 6, we explore our calculation to study Higgs boson production for hadron colliders. We calculate the single pair Higgs production cross-section in pp

collision via gluon fusion, which is suppose to be the dominant mechanism for this process. We also compare the Higgs pair production cross-section, where the main dominant decay of the Higgs boson pair is four gauge bosons, with the production of four gauge bosons from double scattering processes as a background.

Finally, a summary of this thesis, the brief conclusions of our studies, are all the subject of chapter 7.

It should be noted that, a brief introduction and discussion are included at the beginning and end, respectively, of each chapter. Also note that, for reasons of simplicity, equations, figures and references are separately numbered in individual chapters. A list of all references can be found at the end of the thesis.

CHAPTER 2

FIRST ORDER PERTURBATIVE QCD CORRECTIONS TO PHOTON PAIR PRODUCTION IN HADRON COLLISIONS

2.1 Introduction

Quantum chromodynamics has been formulated as a theory of strong interactions. During the last two decades a large amount of sophisticated, theoretical and experimental work has been devoted to testing and predicting this theory [1]. This theory has been used in its perturbative form to explain a variety of hadronic phenomena at high energies and has now met considerable qualitative and quantitative success. Although it has many of the right properties to fit observation and gives correct results where reliable approximations exist, still, no single experiment provide by itself a clear and completely qualitative test [2].

Although testing QCD theory is difficult, at the same time it is particularly important. The difficulty of testing QCD is related to the fact that QCD is the theory of quarks and gluons while real life is made up of hadrons and the perturbation methods, which are unique to QCD, are only applicable in the domain of weak interaction where the coupling is small. This reflects again the fact that no single process provides by itself a definite experimental proof of the theory.

Over the last ten years, there has been a dramatic advance in high energy physics, particularly with the observation of the intermediate gauge bosons and large transverse momentum jets at hadron colliders with CM energy of $\sqrt{s}$=630 GeV. These recent CERN results at the available energy show beautiful agreement with QCD predictions and also give a possible testing ground for various aspects of it.

In this chapter we present the effect of strong interactions on photon pair production in hadron collisions, through the calculation of the first order perturbative

QCD corrections to the basic subprocess $q\overline{q} \rightarrow \gamma\gamma$.

During the last several years there has been a great deal of interest in the perturbative QCD corrections to deep inelastic scattering [3] and the Drell- Yan process [4]. This was followed by the calculation of QCD corrections for single and pair jet production from hadron collisions. The results show that these corrections are very significant, particularly for the Drell-Yan like processes. Moreover, nowadays, at present collider energies, full evaluation of complete and exact QCD corrections to one loop for different processes are needed since the gluons are now playing a prominent role in hadron collisions.

The calculated QCD corrections lead to divergences which arise from the vanishing of the gluon momenta (infrared singularity) and also from the emission of a parallel gluon to massless quarks (mass singularity). These divergences are regularised and represented in dimensional regularisation by poles $O(1/\epsilon)$ and $O(1/\epsilon^2)$, where $\epsilon = \frac{4-n}{2}$ and n is the number of space time dimensions.

In section 2 of this chapter, we calculate the lowest order subprocess for photon pair production in $q\overline{q}$ collisions. This is followed by the virtual gluon corrections, which include the self-energy, vertex and the box diagrams in section 3. Section 4 presents the calculation of the real gluon emission including, the soft, and also hard, real collinear gluon bremsstrahlung. Finally in section 5 we summarise the results with some concluding remarks.

2.2 The Lowest Order Subprocess $q\overline{q} \rightarrow \gamma\gamma$

In order to calculate the higher orders for any process, it is important first to calculate the cross-section at lowest order. To calculate the lowest order for the subprocess $q\overline{q} \rightarrow \gamma\gamma$ [5], we have to consider the two Feynman diagrams of fig. (2.1)

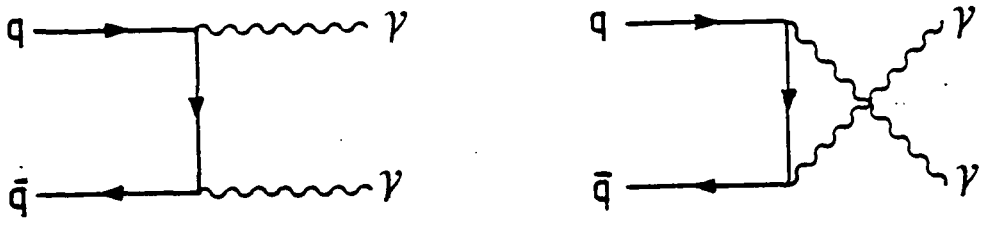

Fig. (2.1) Lowest order Feynman diagrams for $q\bar{q} \to \gamma\gamma$.

The matrix element for this diagram can be written as:

$$\mathcal{M}_1 = \frac{-i}{t} e^2 e_q^2 \overline{u}(k_2) \not{\epsilon}_2 (\not{k}_2 - \not{p}_2) \not{\epsilon}_1 v(k_1)$$

$$\mathcal{M}_2 = \frac{-i}{u} e^2 e_q^2 \overline{u}(k_2) \not{\epsilon}_1 (\not{k}_2 - \not{p}_1) \not{\epsilon}_2 v(k_1), \qquad 2.1$$

where e_q is the quark charge and ϵ_1,ϵ_2 is the polarisation vector of the photons.

To calculate the differential cross section, we only have to calculate

$$\mathcal{F} = \sum [\ \ |\mathcal{M}_1|^2 + \ \ |\mathcal{M}_2|^2 + 2Re\ \ (\mathcal{M}_1^* \mathcal{M}_2)\ \ ], \qquad 2.2$$

where the summation extends over the polarisation states of the photons and the quarks. Using the notation

$$s = (k_1 + k_2)^2 = (p_1 + p_2)^2$$

$$t = (k_1 - p_1)^2 = (k_2 - p_2)^2$$

$$u = (k_1 - p_2)^2 = (k_2 - p_1)^2$$

$$s + t + u = 0 \qquad 2.3$$

In Feynman gauge we have to use $\sum_{\lambda=\pm 1} \epsilon_\mu^\lambda \epsilon_\nu^\lambda = -g_{\mu\nu}$, which leads to the differential cross-section

$$\frac{d\sigma}{d\Omega} = \frac{1}{64\pi^2 s} \quad |\mathcal{F}|$$

$$\frac{d\sigma}{d\Omega} = \frac{\alpha^2}{2s}\frac{1}{3} \quad e_q^4 \quad [\frac{t}{u} + \frac{u}{t}], \tag{2.4}$$

where $\alpha = \frac{e^2}{4\pi}$ and the extra factor $\frac{1}{3}$ arises from the average over the initial q and $\overline{q}$ colour and sum over $q\overline{q}$ combination which can annihilate to form a colourless photon.

The differential cross section for the subprocess $q\overline{q} \rightarrow \gamma\gamma$ can be translated into the following form by introducing further invariants:

$$\frac{d\sigma}{d\Omega} = \frac{\alpha^2}{2s}\frac{e_q^4}{3} \quad 2 \quad \frac{1 + cos^2\theta}{1 - cos^2\theta}, \tag{2.5}$$

where we used the kinematic variables $t = \frac{-s}{2}(1 - cos\theta)$, $u = \frac{-s}{2}(1 + cos\theta)$ and θ is the scattering angle.

2.3 $O(\alpha_s)$ Virtual Gluon Corrections to $q\overline{q} \rightarrow \gamma\gamma$

For the first order virtual gluon corrections to the subprocess $q\overline{q} \rightarrow \gamma\gamma$, there are twelve Feynman diagrams as shown in fig. (2.2). We shall present the calculation in the Feynman gauge, which means that the gluon propagator has the form

$$D_{\mu\nu}^{ab} = -ig_{\mu\nu} \quad \delta_{ab}, \tag{2.6}$$

where μ, ν are the Lorentz indices and a,b the colour indices.

Each of the diagrams contains a loop; the resulting integral over the gluon momentum gives rise to two kinds of divergences (infrared and ultra-violet). There is some cancellation of divergences when all virtual diagrams are added together.

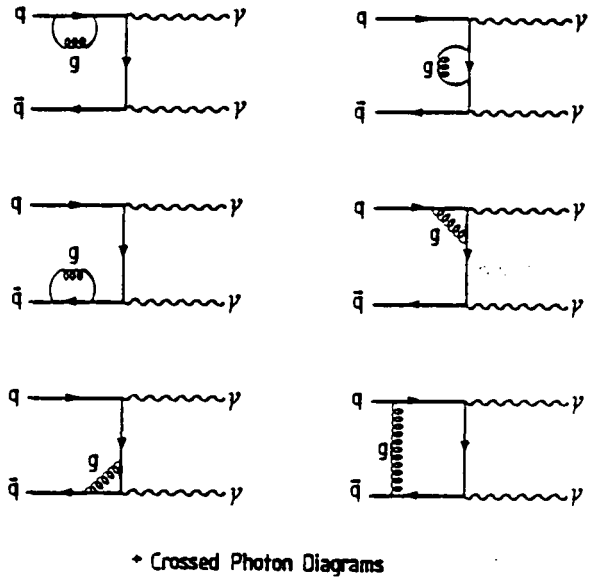

Fig. (2.2) Virtual gluon corrections of order α_s for $q\bar{q} \rightarrow \gamma\gamma$. The solid lines represent quarks, the wavy lines photons and the curly ones gluons.

It is suitable to use the continuous dimension method (dimensional regularisation) to regularise all the divergences [6]. This method provides an elegant framework for (in this case QCD) loop corrections in gauge theories, where the divergences arising from the calculation of the QCD diagrams become poles of order $O(\frac{1}{\epsilon})$ and $O(\frac{1}{\epsilon^2})$ in the final expression of the cross-section. The main motivation for this approach is its relative simplicity compared to the traditional mass regularisation schemes and it preserves gauge invariance [7,8].

The virtual $O(\alpha_s)$ corrections may conveniently be represented by a quantity $\delta_{virtual}$ which is defined as:

$$\frac{d\sigma_{virtual}}{d\Omega} = \frac{d\sigma^0}{d\Omega} \quad \delta_{virtual} \qquad 2.7$$

It is clear from fig. (2.2) that there are in fact three types of virtual corrections namely self-energy diagrams, vertex diagrams and box diagrams. We shall calculate each of them separately.

2.3.a. The Self-Energy Diagrams

These consist of diagrams 1,2 and 3 of fig. (2.2), where two of them (1 and 3) are called external self energy, and diagram 2 is the internal self-energy. The external diagrams give zero contribution to the virtual corrections because of the fact that the momentum squared of on-shell massless quark in dimensional regularisation vanishes which means $(p^2)^\epsilon \rightarrow 0$, so only the internal diagram, represented by fig. (2.3), contributes to the virtual corrections.

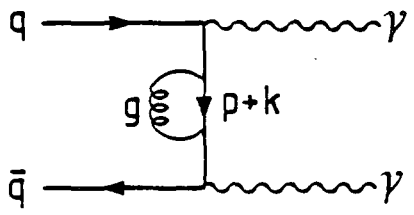

Fig. (2.3) Self-Energy Correction.

The loop integral for the self-energy diagram has the following form:

$$\Sigma = -\frac{i4\pi\alpha_s}{(2\pi)^n}\int d^n k \frac{\gamma_\mu(\not p + \not k)\gamma_\nu}{k^2(p+k)^2} \quad g_{\mu\nu} \tag{2.8}$$

The most important tools for the calculation of these kinds of integrals are the Feynman parametrisation of multiple denominators

$$\frac{1}{A^\alpha B^\beta ....E^\epsilon} = \frac{\Gamma(\alpha+\beta+...+\epsilon)}{\Gamma(\alpha)\Gamma(\beta)...\Gamma(\epsilon)}\int_0^1 dxdy.....dz \quad \delta(1-x-y.....z)$$
$$\frac{x^{\alpha-1}y^{\beta-1}....z^{\epsilon-1}}{(Ax+By+.....Ez)^{\alpha+\beta+...\epsilon}} \tag{2.9}$$

And with the use of the n-dimensional Minkowski space integral [9]

$$\int d^n k \frac{1}{[c-2p.k-k^2]^\alpha} = \frac{i\pi^{n/2}\Gamma(\alpha-n/2)}{(c+p^2)^{\alpha-n/2}\Gamma(\alpha)} \tag{2.10}$$

After applying this in eqn. (2.8) we get:

$$\Sigma = \frac{4\pi\alpha_s}{(2\pi)^n}\pi^{n/2}\Gamma(2-n/2)\int_0^1 dx \frac{\gamma_\mu(\not p(1-x))\gamma_\mu}{[-p^2x(1-x)]^{2-n/2}}, \tag{2.11}$$

where we have used a change of variable of $k = k' + px$. Terms with k' in the numerator vanish upon integration and the rest give:

$$\Sigma = \frac{\alpha_s}{4\pi}(4\pi)^{\epsilon}\Gamma(\epsilon) \quad (-2) \quad (1-\epsilon) \quad [-p^2]^{-\epsilon}\not{p}_{\mu}\int_0^1 dx x^{-\epsilon}(1-x)^{1-\epsilon}, \qquad 2.12$$

where we have used the identity $\gamma_{\mu}\not{p}(1-x)\gamma_{\mu} = -2(1-x)(1-\epsilon)\not{p}_{\mu}$.

Evaluation of eqn. (2.12) is straightforward and by using Γ-function definitions we get:

$$\Sigma = \frac{\alpha_s}{4\pi}(4\pi)^{\epsilon}\not{p}_{\mu}[-\frac{1}{\epsilon} - 1 + \gamma + ln(-t) + ...], \qquad 2.13$$

where $t = p^2 = (k_1 - p_1)^2 = -2k_1.p_1$ and γ_E is Euler's constant.

We get similar form for the crossed photon diagram

$$\Sigma = \frac{\alpha_s}{4\pi}(4\pi)^{\epsilon}\not{p}_{\mu}[-\frac{1}{\epsilon} - 1 + \gamma + ln(-u) + ...], \qquad 2.14$$

Combining eqn. (2.13 and 2.14) with the lowest order amplitude, simplifying and rearranging the terms, we get the following correction due to the self-energy diagrams

$$\delta_{self} = \frac{4\alpha_s}{3\pi} \quad (4\pi)^{\epsilon} \quad [-\frac{1}{2\epsilon} - \frac{1}{2} +$$
$$(t^2+u^2)(\frac{1}{2}u^2(ln(-t)+\gamma) + \frac{1}{2}t^2(ln(-u)+\gamma))] \qquad 2.15$$

Note the inclusion of the colour factor 4/3 in eqn. (2.15).

2.3.b The Vertex Diagram

We calculate, in the Feynman gauge, the virtual gluon corrections to the quark- quark vertex as shown in fig. (2.4)

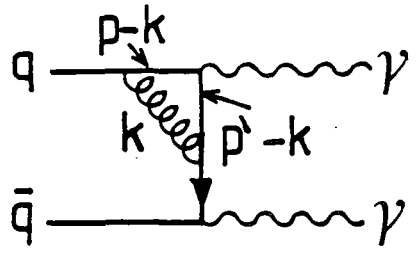

Fig. (2.4) Vertex correction.

For the vertex correction, we have to write the loop integral which has the form:

$$\Lambda_\mu(p,p') = -\frac{i4\pi\alpha_s}{(2\pi)^n}\int d^nk \frac{\gamma^\alpha(\not{p}' - \not{k})\gamma_\mu(\not{p} - \not{k})\gamma^\beta}{k^2(p'-k)^2(p-k)^2} \quad g_{\alpha\beta} \tag{2.16}$$

It is more complicated than the self-energy case. Also we introduce here the Feynman parametrisation as

$$\Lambda_\mu(p,p') = -\frac{i4\pi\alpha_s}{(2\pi)^n}\Gamma(3)\int dxdydz\delta(1-x-y-z)\int d^nk$$

$$\frac{\gamma^\alpha(\not{p}' - \not{k})\gamma_\mu(\not{p} - \not{k})\gamma_\alpha}{[k^2x + (p'-k)^2y + (p-k)^2z]^3} \tag{2.17}$$

Introduce the new integration variable

$$k' = k - p'y - pz,$$

in terms of which eqn. (2.17) becomes

$$\Lambda_\mu(p,p') = -\frac{i4\pi\alpha_s}{(2\pi)^n}\Gamma(3)\int dxdydz\delta(1-x-y-z)\int d^nk'$$

$$\frac{\gamma^\alpha(\not{p}'(1-y) - pz - k')\gamma_\mu(\not{p}(1-z) - \not{p}'y - k')\gamma_\alpha}{[zp^2 - (p'y+pz)^2 + k'^2]^3} \tag{2.18}$$

Note that the photon and one of the quarks are on mass-shell, which simplifies the calculation. For the p'^2=0 case, we have to integrate the following:

$$\Lambda_\mu(p,p') = -\frac{i4\pi\alpha_s}{(2\pi)^n} i\pi^{n/2}\Gamma(1+\epsilon)\int dydz \frac{z(1-z)}{[-zp^2(1-z-y)]^{1+\epsilon}}\gamma^\alpha \not{p}\gamma_\mu \not{p}\gamma_\alpha \tag{2.19}$$

With a suitable change of variable and using the identity

$$\gamma_\mu\gamma_\nu\gamma_\mu = -2(1-\epsilon)\gamma_\nu,$$

where $\epsilon = \frac{4-n}{2}$, which enables us to write

$$\Lambda_\mu(p,p') = \frac{\alpha_s}{4\pi} \quad (4\pi)^\epsilon \quad [-p^2]^{-1-\epsilon} \quad \frac{1}{\epsilon}\frac{\Gamma(1+\epsilon)\Gamma^2(1-\epsilon)}{(1-2\epsilon)\Gamma(1-2\epsilon)}$$

$$(1-\epsilon)p^2(\gamma_\mu - \frac{2p_\mu \not{p}}{p^2}) \tag{2.20}$$

Rearranging eqn. (2.20) we get

$$\Lambda_\mu(p,p') = \frac{\alpha_s}{4\pi}(4\pi)^\epsilon \quad [\frac{1}{\epsilon} - ln(-t) - \gamma + 1] \quad [\gamma_\mu - \frac{2p_\mu \not{p}}{p^2}], \qquad 2.21$$

where γ is Euler's constant. Similarly for $p^2 = 0$ we get

$$\Lambda_\mu(p,p') = \frac{\alpha_s}{4\pi}(4\pi)^\epsilon \quad [\frac{1}{\epsilon} - ln(-t) - \gamma + 1][\gamma_\mu - \frac{2p'_\mu \not{p}'}{p'^2}], \qquad 2.22$$

Taking into account the crossed diagrams, writing the vertex amplitudes and combining them with the lowest order amplitudes, we get the following corrections due to the vertex diagrams:

$$\delta_{vertex} = \frac{4\alpha_s}{3\pi}(4\pi)^\epsilon \quad [\frac{1}{\epsilon} \quad (1 + \frac{4ut}{t^2+u^2}) + 1$$

$$-\frac{1}{t^2+u^2}[u(u+2t)(ln(-t)+\gamma) - 2ut + t \leftrightarrow u]], \qquad 2.23$$

with $t = (p_2 - k_2)^2$ and $u = (p_2 - k_1)^2$.

2.3.c The Box Diagram

For the box diagram we have to work out a four denominator integral. The loop integral of fig. (2.5) can be written in the form:

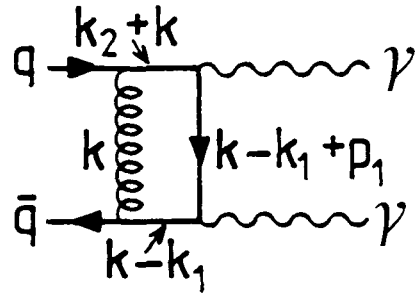

Fig.(2.5) The box diagram

$$\mathcal{M} = \frac{-i4\pi\alpha_s}{(2\pi)^n}\int d^n k \frac{\gamma^\alpha(\not{k}+\not{k}_2)\gamma^{\mu_2}(\not{k}+\not{p}_1-\not{k}_1)\gamma^{\mu_1}(\not{k}-\not{k}_1)\gamma^\beta}{k^2(k+k_2)^2(k-k_1)^2(k+(p_1-k_1))^2} \quad g_{\alpha\beta} \qquad 2.24$$

Here, a double pole $O(1/\epsilon^2)$ term appears as a result of the infrared divergences as well as the mass singularites in the amplitude. Introducing Feynman parametrisation to eqn. (2.24) we get

$$\mathcal{M} = \frac{-i4\pi\alpha_s}{(2\pi)^n}\Gamma(4)\int dxdydzdw \quad \delta(1-x-y-z-w)\int d^nk$$

$$\frac{\gamma^\alpha(\not{k}+\not{k}_2)\gamma^{\mu_2}(\not{k}+\not{p}_1-\not{k}_1)\gamma^{\mu_1}(\not{k}-\not{k}_1)\gamma_\alpha}{[k^2+2k(yk_2-xk_1+z(p_1-k_1))+z(p_1-k_1)^2]^4} \qquad 2.25$$

Introduce the new integration variable

$$k' = k + yk_2 - xk_1 + z(p_1 - k_1)$$

$$k = k' - yk_2 + xk_1 - z(p_1 - k_1),$$

in terms of which eqn. (2.25) becomes

$$\mathcal{M} = \frac{-i4\pi\alpha_s}{(2\pi)^n}\Gamma(4)\int dxdydzdw \quad \delta(1-x-y-z-w)\int d^nk'$$

$$\gamma^\alpha(\not{k}'+k_2(1-y)+\not{k}_1(x+z)-z\not{p}_1)\gamma^{\mu_2}(\not{k}'-\not{k}_1(1-x-z)+\not{p}_1(1-z)-y\not{k}_2)\gamma^{\mu_1}$$

$$\frac{(\not{k}'-\not{k}_1(1-x-z)-y\not{k}_2-z\not{p}_1)\gamma_\alpha}{[k'^2-(yk_2-xk_1+z(p_1-k_1))^2+z(p_1-k_1)^2]^4} \qquad 2.26$$

The calculation of eqn. (2.26) is more lengthly than the previous cases. We made use of the symbolic manipulation program REDUCE [10] to calculate the trace of the numerator interfering with the lowest order. After the trace calculation, we expand the numerator factors, which include factors of 1, x, y, z and w or multiples of such factors. These integrals are calculated and the results are expressed in terms of the invariants, t and s together with functions of ϵ. Here we shall present the non-trivial integration arising from eqn. (2.26) as an example

$$\mathcal{M} = \frac{-i4\pi\alpha_s}{(2\pi)^n}\Gamma(4)\int dxdydzdw \quad \delta(1-x-y-z-w)\int d^nk'$$

$$\frac{1}{[k'^2-(yk_2-xk_1+z(p_1-k_1))^2+z(p_1-k_1)^2]^4} \qquad 2.27$$

Now integrate over $d^n k'$ we get

$$\mathcal{M} = \frac{-i4\pi\alpha_s}{(2\pi)^n} \int dxdydzdw \quad \delta(1-x-y-z-w) i\pi^{n/2}$$

$$\Gamma(4-n/2)[-zt + (yk_2 - xk_1 - zt)^2]^{n/2-4}, \qquad 2.28$$

where $t = (p_1 - k_1)^2$

$$\mathcal{M} = \frac{\alpha_s}{4\pi} \quad (4\pi)^\epsilon \int dxdydzdw \quad \delta(1-x-y-z-w) \frac{1}{t^2}(-t)^{-\epsilon}\Gamma(2+\epsilon)$$

$$[z(1-x-y-z) + xy\frac{s}{t}]^{-2-\epsilon}, \qquad 2.29$$

where $s = (k_1 + k_2)^2$. In order to integrate eqn. (2.29), we have used a suitable change of variables

$$w = \alpha(1-a),$$

$$x = \alpha a,$$

$$y = \beta(1-b),$$

$$z = \beta b, \qquad 2.30$$

so that $w+x+y+z = \alpha+\beta = 1$, $xy = \alpha\beta a(1-b)$ and $z(1-x-y-z) = \alpha\beta b(1-a)$. The Jacobian factor for this transformation is $J = \frac{d(w,x,y,z)}{d(\alpha,\beta,a,b)} = \alpha\beta$.

$$\mathcal{M} = \frac{\alpha_s}{4\pi}(4\pi)^\epsilon \frac{1}{t^2}(-t)^{-\epsilon}\Gamma(2+\epsilon) \int d\alpha d\beta dadb \quad (\alpha\beta) \quad \delta(1-\alpha-\beta)$$

$$[\alpha\beta(1-a)b + \alpha\beta a(1-b)\frac{s}{t}]^{-2-\epsilon} \qquad 2.31$$

$$\mathcal{M} = \frac{\alpha_s}{4\pi}(4\pi)^\epsilon \frac{1}{t^2}(-t)^{-\epsilon}\Gamma(2+\epsilon) \int_0^1 d\alpha d\beta \quad \delta(1-\alpha-\beta) \quad (\alpha\beta)^{-1-\epsilon}$$

$$\int_0^1 dadb \quad [b(1-a) + a(1-b)\frac{s}{t}]^{-2-\epsilon} \qquad 2.32$$

$$\mathcal{M} = \frac{\alpha_s}{4\pi}(4\pi)^\epsilon \frac{1}{t^2}(-t)^{-\epsilon}\Gamma(2+\epsilon)\frac{-2}{\epsilon}\frac{\Gamma^2(1-\epsilon)}{\Gamma(1-2\epsilon)} \quad R, \qquad 2.33$$

with

$$R = \int_0^1 da \int_0^1 db[b(1-a) + a(1-b)\frac{s}{t}]^{-2-\epsilon} \qquad 2.34$$

Evaluation of R is rather lengthy, but with the use of hypergeometrical functions we get [11,12]:

$$R = \frac{-1}{\epsilon(1-\epsilon)}\frac{t}{s}[(-1)^{-\epsilon}(1+\epsilon^2 Li_2(1+\frac{t}{s})+...)+(\frac{-t}{s})^{\epsilon}(1+\epsilon^2 Li_2(1+\frac{s}{t})+...)], \quad 2.35$$

where $Li_2(x) = \sum_{r=1}^{\infty}\frac{x^r}{r^2}$ (Spence function). With the help of the formula

$$Li_2(1-x) + Li_2(1-1/x) = -1/2ln^2(x)$$

The final result for the integration can be written as:

$$\mathcal{M} = \frac{\alpha_s}{4\pi}(4\pi)^{\epsilon}\frac{1}{t^2}(-t)^{-\epsilon}\Gamma(2+\epsilon)\frac{-2}{\epsilon}\frac{\Gamma^2(1-\epsilon)}{\Gamma(1-2\epsilon)}$$

$$[-\frac{1}{\epsilon(1+\epsilon)}\frac{t}{s}(2+\epsilon ln(-t/s) - \frac{\epsilon^2}{2}ln^2(-t/s) - \epsilon^2\frac{\pi^2}{2})] \quad 2.36$$

$$\mathcal{M} = \frac{\alpha_s}{4\pi}(4\pi)^{\epsilon}\frac{1}{ts}(-t)^{-\epsilon}\frac{2}{\epsilon^2}\frac{\Gamma(1+\epsilon)\Gamma^2(1-\epsilon)}{\Gamma(1-2\epsilon)}$$

$$[2+\epsilon ln(-t/s) - \frac{\epsilon^2}{2}ln^2(-t/s) - \epsilon^2\frac{\pi^2}{2} + ...] \quad 2.37$$

All other integrations arising from eqn. (2.26) can be evaluated in a similar way. Due to the large number of terms, we have only concentrated on terms that contain a singularity and we have left finite terms which contain terms of log, dilog and π^2 in. Similar form can be obtain for the crossed photon diagram.

After lengthy calculation we obtain the final form of the corrections from the box diagram as:

$$\delta_{box} = \frac{4\alpha_s}{3\pi} \quad (4\pi)^{\epsilon} \quad [-\frac{1}{\epsilon^2} + \frac{1}{\epsilon}(ln(s) + \gamma - 2 - \frac{4ut}{t^2+u^2})$$

$$+...\text{finite} \quad \text{terms....}], \quad 2.38$$

where the finite terms are terms which are free from singularity.

Note that all results from self, vertex and box diagrams are in full agreement with the result of Berends et. al. [13], in their Feynman gauge calculation of the

corresponding corrections to the subprocess $\gamma\gamma \to q\bar{q}$, which is the inverse of the one considered here.

2.4 $O(\alpha_s)$ Real Gluon Corrections to $q\bar{q} \to \gamma\gamma$.

To calculate the corrections from real gluon emission, we have to calculate the cross-section corresponding to the Feynman diagrams of fig. (2.6)

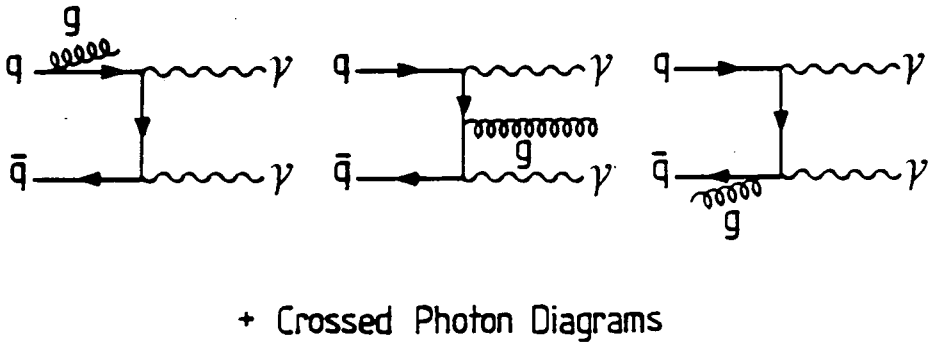

Fig. (2.6) Feynman diagrams for the real gluon emission.

These diagrams contain no loop integrals, but there is an integral over the final 3-body phase space. As in virtual corrections we are facing divergences, generated in the continuous dimension method as poles of order $O(1/\epsilon)$ and $O(1/\epsilon^2)$, in the contribution to the cross-section. These divergences arise from two different limits. First, the soft gluon limit where the gluon energy is very small and second, the collinear limit where the gluon is emitted in a direction which is sufficiently parallel to the quark or the antiquark. In this section we shall calculate the corrections from both regions separately. Finally we shall add the corrections from virtual and real gluons together, in order to get a finite correction value, which should be added to the lowest order cross-section.

2.4.a. Hard Collinear Gluon Emission

The emission of the gluon is in a direction which is sufficiently parallel to the quark or antiquark direction. In this case we have to calculate the cross-

section corresponding to the Feynman diagram of fig. (2.6). The matrix element (omitting colour matrices) for the six Feynman diagrams are:

$$M_1 = \frac{-ie^2g}{4k_1.p_1k.k_2}\overline{u}(k_2)\not{\epsilon}(\not{k}_2 - \not{k})\not{\epsilon}_2(\not{k}_1 - \not{p}_1)\not{\epsilon}_1 v(k_1),$$

$$M_2 = \frac{-ie^2g}{4k_1.p_1k_2.p_2}\overline{u}(k_2)\not{\epsilon}_2(\not{k}_2 - \not{p}_2)\not{\epsilon}(\not{p}_1 - \not{k}_1)\not{\epsilon}_1 v(k_1),$$

$$M_3 = \frac{-ie^2g}{4k_2.p_2k.k_1}\overline{u}(k_2)\not{\epsilon}_2(\not{k}_2 - \not{p}_2)\not{\epsilon}_1(\not{k}_1 - \not{k})\not{\epsilon}_1 v(k_2),$$

$$M_4 = \frac{-ie^2g}{4k_1.p_2k.k_2}\overline{u}(k_2)\not{\epsilon}(\not{k}_2 - \not{k})\not{\epsilon}_1(\not{k}_1 - \not{p}_2)\not{\epsilon}_2 v(k_1),$$

$$M_5 = \frac{-ie^2g}{4k_2.p_1k_1.p_2}\overline{u}(k_2)\not{\epsilon}_1(\not{k}_2 - \not{p}_1)\not{\epsilon}(\not{p}_2 - \not{k}_1)\not{\epsilon}_1 v(k_2),$$

$$M_6 = \frac{-ie^2g}{4k_2.p_1k_1.k}\overline{u}(k_2)\not{\epsilon}_1(\not{k}_2 - \not{p}_1)\not{\epsilon}_2(\not{k}_1 - \not{k})\not{\epsilon} v(k_1), \qquad 2.39$$

where g is the gauge coupling constant ($g^2 = 4\pi\alpha_s$), ϵ is the polarisation vector of the gluon, and ϵ_1 and ϵ_2 are the polarisation vectors of the photons.

For the case when the gluon is parallel to the antiquark k_1, only the diagrams M_3 and M_6 lead to singularities. For the cross-section we have to calculate:

$$F_1 = \sum[|M_3|^2 + 2ReM_3^*(M_1 + M_2 + M_4 + M_5 + M_6) +$$

$$|M_6|^2 + 2ReM_6^*(M_1 + M_2 + M_4 + M_5)], \qquad 2.40$$

where the summation is over the polarisation states of the photons, the gluons, and the quarks.

To calculate the traces we have made use of the symbolic manipulation program (REDUCE) [10]. In our calculation we have used the following

- The gluon has to be treated in n-dimensions.
- The photons and quarks have to be treated in 4-dimensions.
- Because the gluon is almost parallel to the quark k_1, we put $k.k_1$=0 everywhere except in the denominator.

Working the matrix element out we get:

$$F_1 = \frac{2e^4g^2s}{k.k_1k.k_2}[2\frac{t^2+u^2}{t'u'} + (n-4)(\frac{(t-u)^2}{t'u'} + 2 - \frac{t}{u'} - \frac{u}{t'})$$

$$(t \leftrightarrow t', u \leftrightarrow u')], \qquad 2.41$$

where

$$t = (p_1 - k_1)^2, \quad u = (p_1 - k_2)^2, \quad s = (k_1 + k_2)^2,$$

$$t' = (p_2 - k_2)^2, \quad u' = (p_2 - k_1)^2, \quad s' = (p_1 + p_2)^2,$$

As a check to the calculation, we put $t' = t$, $u' = u$ and $s' = s$ in eqn. (2.41) then the form of the lowest order cross-section for the subprocess $q\overline{q} \rightarrow \gamma\gamma$ can be obtained.

For the case when the gluon is emitted parallel to the quark k_2, only the diagrams M_1 and M_4 have singularities. In this case we have to calculate the following:

$$F_2 = \sum[|M_1|^2 + 2ReM_1^*(M_2 + M_3 + M_4 + M_5 + M_6) +$$

$$|M_4|^2 + 2ReM_4^*(M_2 + M_3 + M_5 + M_6)], \qquad 2.42$$

we find a cross-section identical to eqn. (2.41).

In order to get the total corrections due to hard collinear gluon we have to integrate eqn. (2.41) over the gluon phase space.

The total cross-section for a three body final state, after including factors for flux, Bose statistics, colour sum, initial state spin, and final state polarisation, has the form

$$\sigma_{real} = \frac{e_q^4}{3} \quad \frac{\alpha^2}{2s} \quad \frac{4\alpha_s}{3\pi} \quad \frac{(2\pi)^4}{2} \int \frac{d^nk}{(2\pi)^n} \frac{d^4p_1}{(2\pi)^4} \frac{d^4p_2}{(2\pi)^4} \quad (2\pi)^4$$

$$\delta^4(k_1 + k_2 - p_1 - p_2 - k) \quad (2\pi)^3 \quad \delta^+(k^2) \quad \delta^+(p_1^2) \quad \delta^+(p_2^2) \quad |M|^2 \qquad 2.43$$

where $|M|^2$ is the matrix element squared for the hard collinear gluon emission. To integrate eqn. (2.43) we introduce the following

$$1 = \int d^4P\delta^4(P - p_1 - p_2)$$

$$1 = \int_0^\infty dm^2\delta(m^2 - P^2),$$

so that eqn. (2.43) has the following form:

$$\sigma_{real} = \frac{e_q^4}{3} \quad \frac{\alpha^2}{2s} \quad \frac{4\alpha_s}{3\pi} \quad \frac{(2\pi)^4}{2} \quad \frac{1}{(2\pi)^{3-2\epsilon}} \int dm^2 d^4P d^nk \quad \delta^+(P^2 - m^2)$$

$$\delta^+(K - P - k) \quad \delta^+(k^2) \quad \int D2BPS \quad |M|^2, \qquad 2.44$$

where D2BPS is the two body final state phase space integration which has the form:

$$D2BPS = \frac{1}{(2\pi)^2} \int d^4p_1 d^4p_2 \delta^+(p_1^2)\delta^+(p_2^2) \quad \delta^4(k_1 + k_2 - p_1 - p_2) \qquad 2.45$$

Performing the integration over the gluon energy k, and with change of variable $y = \frac{1}{2}(1 + cos\phi)$, we obtain

$$\sigma_{real} = \frac{e_q^4}{3} \quad \frac{\alpha^2}{2s} \quad \frac{4\alpha_s}{3\pi} \quad \frac{(2\pi)^4}{2} \quad \frac{1}{(2\pi)^2} \frac{(4\pi)^\epsilon}{\Gamma(1-\epsilon)} \frac{1}{2}$$

$$\int dx_3(1 - x_3)(1 - x_3)^{-2\epsilon}(s)^{-\epsilon} \int_0^1 dy(y(1 - y))^{-\epsilon}|M|^2 \int D2BPS, \qquad 2.46$$

where we have used the following:

$$\int d^nk\delta^+(k^2) = \int \frac{d^{n-1}k}{2k},$$

$$\int d^{n-1}k = \frac{2\pi\pi^{n/2-2}}{\Gamma(n/2-1)} \int dk k^{n-2} \int_0^\pi d\phi sin^{n-3}\phi,$$

$$dm^2 = sdx_3,$$

the matrix element squared for the process $q\bar{q} \rightarrow \gamma\gamma g$ has the following form:

$$|M|^2 = \frac{2s}{k.k_1 k.k_2} \quad [2\frac{t^2+u^2}{t'u'} + (n-4)(\frac{(t-u)^2}{t'u'} + 2 - \frac{t}{u'} - \frac{u}{t'}) \\ (t \leftrightarrow t', u \leftrightarrow u')], \qquad 2.47$$

using the following collinear kinematics

$$t = -2E^2 x_3(1+cos\theta), \quad t' = -2E^2(1+cos\theta),$$
$$u = -2E^2(1-cos\theta), \quad u' = -2E^2 x_3(1-cos\theta),$$
$$s = 4E^2, \quad s' = 4E^2 x_3 \qquad 2.48$$

By substituting these collinear limits in the matrix element, and with doing more algebra, we find the following form for the corrections from hard collinear gluon emission:

$$\delta_{hardcollinear} = \frac{4\alpha_s}{3\pi} \quad [\int dx_3 \frac{(1+x_3^2)}{(1-x_3)_+} \quad (-\frac{1}{\epsilon} - ln(4\pi) + \gamma) + \frac{1}{\epsilon} ln\varepsilon^2$$
$$-2ln^2\varepsilon + 4\varepsilon ln2\varepsilon E - \varepsilon^2 ln2\varepsilon E - 4\varepsilon - 3ln2E - 4ln\varepsilon ln2E + 4], \qquad 2.49$$

where ε is the fraction of gluon energy and

$$\sigma_{hardcollinear} = \hat{\sigma}_{q\bar{q}\to\gamma\gamma}\delta_{hardcollinear},$$

with

$$\hat{\sigma}_{q\bar{q}\to\gamma\gamma} = \frac{e_q^4}{3} 16\pi^2\alpha^2 \frac{1}{2\hat{s}} \int D2BPS|M|^2_{q\bar{q}\to\gamma\gamma} \qquad 2.50$$

2.4.b Soft Gluon Emission

In this case the gluon energy k is small so that the soft gluon matrix element is proportional to the purely elastic cross section. To order α_s we have to calculate the cross-section of fig. (2.7).

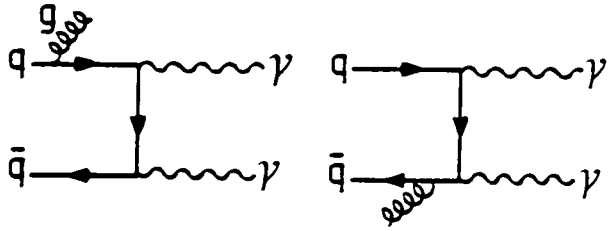

+ Crossed Photon Diagrams

Fig. (2.7) Feynman diagrams for soft gluon corrections.

The correction factor is given by the following form

$$\delta_{soft} = \frac{4\pi\alpha_s}{(2\pi)^n} \quad \frac{4}{3} \quad (2\pi) \quad s\int \frac{d^{n-1}k}{2k} \frac{1}{k.k_1 k.k_2} \qquad 2.51$$

This integral has two fold divergences, with the gluon being soft ($k \rightarrow 0$), and with the quark being massless, we will generate both infrared and mass singularities. Working in the continuous dimension method, we expect a double pole structure in the soft gluon correction. This is the only place where the double pole appears in real gluon emission. Using the following formula

$$\int d^{n-1}k = \frac{2\pi\pi^{\frac{n}{2}-2}}{\Gamma(n/2-1)} \int dk k^{n-2} \int_0^{\pi} d\theta sin^{n-3}\theta, \qquad 2.52$$

We can write the correction factor in the form

$$\delta_{soft} = \frac{2\pi\alpha_s}{(2\pi)^{n-1}} \quad \frac{4}{3} \quad \frac{2\pi\pi^{\frac{n}{2}-2}}{\Gamma(n/2-1)} \int_0^{\pi} d\theta \quad sin^{n-5}\theta \int_0^{2\varepsilon E} dk k^{n-5}, \qquad 2.53$$

where we chose $k.k_1 = Ek(1 - cos\theta)$ and $k.k_2 = Ek(1 + cos\theta)$.

After integrating eqn. (2.52) over the gluon energy and angle we get the following form for the correction

$$\delta_{soft} = \frac{4\alpha_s}{3\pi}(4\pi)^{\epsilon} \quad \frac{\Gamma(1-\epsilon)}{\Gamma(1-2\epsilon)} \frac{1}{\epsilon^2} \quad [4E^2\varepsilon^2]^{-\epsilon} \qquad 2.54$$

Using some gamma function properties like

$$\frac{1}{\Gamma(1-\epsilon)} = 1 - \gamma\epsilon + \frac{\epsilon^2}{2}(\gamma^2 - \frac{\pi^2}{6}) + ...$$

$$\frac{\Gamma^2(1-\epsilon)}{\Gamma(1-2\epsilon)} = (1 - \epsilon^2\frac{\pi^2}{6} + ...), \qquad 2.55$$

the final result for the correction factor from soft gluon emission can be written in the following form:

$$\delta_{soft} = \frac{4\alpha_s}{3\pi}(4\pi)^{\epsilon} \quad [\frac{1}{\epsilon^2} - \frac{1}{\epsilon} \quad (ln(4E^2\varepsilon^2) + \gamma) + \frac{1}{2}(ln(4E^2\varepsilon^2) + \gamma)^2 - \frac{\pi^2}{4}] \qquad 2.56$$

2.5 Results and Discussion

Two photon pair production in hadron collisions gives an important test ground for various aspects of perturbative QCD. Furthermore, the study of the production of photon pairs and weak gauge boson pairs at contemparary hadron colliders, will improve our understanding of some features of the QCD improved parton model.

Two direct photon have been observed in the UA1 experiments [14] at the CERN $p\bar{p}$ collider at centre-of-mass energy $\sqrt{s}$= 630 GeV. They found six candidates with an expectation of 0.9 ± 0.45 events which come from two-jet events or from single-photon events. The integrated cross-section for two photon production has been detected and found to be

$$\sigma_{\gamma\gamma} = 38 \pm 19 \pm 10pb \quad for \quad E_t > 12GeV \quad and \quad |\eta| < 3,$$

where this value is found to be in good agreement and support prediction of QCD theory.

At UA2 experiment [15], they found 4 events with two photon candidates at $p\bar{p}$ collider with CM energy $\sqrt{s}$ = 630 GeV and are expected to be produced at pp collisions also.

In view of the importance of this process, and because it occurs at hadron colliders and observed experimently so it becomes necessary to know the magnitude of the QCD corrections, which arise when gluons are exchanged and emitted from order process $q\bar{q} \rightarrow \gamma\gamma$.

We have calculated the α_s corrections to the $q\bar{q}$ annihilation using the perturbative theory of massless quarks and gluons. The results have been presented for virtual and real gluon emission separately. In order to obtain results which are free from divergences, we add up the corrections due to the virtual and real gluons, the various double and single poles cancel, the leftover $1/\epsilon$ term has the form

$$P_{qq} = \frac{4}{3} \quad (\frac{1+x_3^2}{(1-x_3)_+} + \frac{3}{2}\delta(1-x_3))$$

This term corresponds to a mass singularity which is usually absorbed into the definition of the structure functions beyond the leading order. Since the appearance of this mass singularity in higher order corrections has a universal structure that is independent of the process, it can be removed by standard subtraction procedure. With the $\overline{MS}$ subtraction scheme, the total cross-section can be defined as:

$$d\sigma = d\sigma^0 + d\sigma^1,$$

where $d\sigma^0$ is the Born cross-section, and $d\sigma^1$ denotes the order α_s corrections which appear as large double logarithms or π^2 terms.

Summarising, we can say that QCD corrections arising from virtual and real gluon emission are a sensible addition to the lowest order cross-section. Moreover, it is neccessary to calculate exactly the size of these corrections. We add the reminder here, that our result does not give the complete $O(\alpha_s)$ correction, we have not included the finite terms from the box diagram, because of the large number of integrations required. Besides to that and due to the presence of the ε terms in eqn. (2.49), it is not possible to ask for the numerical value of the QCD

correction. But if we disregard them and calculate the remaining terms, with $\alpha_s \simeq 0.15$, the effect of first order QCD correction is approximately 10% change to the value of lowest order and this is reasonable number for a QCD correction.

In next chapter we are going to calculate the first order QCD corrections to Z boson pair production at hadron colliders. We are going to use the results of two photon pair production to check our calculation, by setting the mass of the Z boson m_Z=0 in the final result.

CHAPTER 3

FIRST ORDER PERTURBATIVE QCD CORRECTIONS TO WEAK BOSON PAIR PRODUCTION IN HADRON COLLISIONS

3.1 Introduction

The nature of the weak interaction and its universal coupling, suggests the existence of vector gauge bosons mediating the interaction, and connecting weak and electromagnetic interactions.

The Higgs mechanism through, spontaneous symmetry breaking of the gauge group allows the vector gauge bosons to become massive, without violating the symmetry.

The application of all these ideas have led to the remarkably successful theory of Glashow, Salam and Weinberg [1] for electroweak interactions, which is part of what is called the standard model. This theory is based on the gauge group of $SU(2) \times U(1)$ and has three massive gauge bosons $W^{\pm}$ and Z in addition to the massless photon.

This success culminated in the discovery of the triplet of gauge boson particles $W^{\pm}$ and Z at CERN in 1983- by far the most massive elementary particles produced within an accelerator up to now. This method of producing massive particles at $p\bar{p}$ collider which tests the Drell-Yan mechanism at new energy regimes, shows that the intermediate boson picture is correct, and gives the most direct verification of the standard model. Any grand unified theory must have a phenomenological structure very similar to the standard model at energies near to 100 GeV.

3.1.a Weak Gauge Boson Production in $p\bar{p}$ Collision

In 1982/1983 the $W^{\pm}$ and Z weak boson were discovered at CERN $p\bar{p}$ collider [2]. Providing there is sufficient energy at the collider, which is assumed to provide

a full source of valence u, d and $\overline{u}$, $\overline{d}$ quarks, hence the dominant mechanisms for $W^{\pm}$ and Z production are

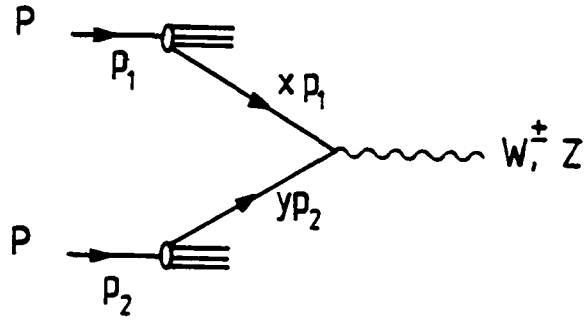

Fig. (3.1) W, Z production at hadron colliders.

Experimentally, it has been found that the rate of production of $W^{\pm}$ and Z at energy $\sqrt{s}$=630 GeV is

$$\sigma^{W^{\pm}} = 4.7 \quad nb, \quad \sigma^{Z} = 1.5 \quad nb,$$

with the luminosity L =$3.5 \times 10^{-4} nb^{-1} s^{-1}$ we can get

$$1 \quad event \quad W^{+} \quad or \quad W^{-} \quad every \quad 10 \quad minutes$$

$$1 \quad event \quad Z \quad every \quad 30 \quad minutes$$

The cleanest signature for detecting the W and Z is through their decay as

$$W \rightarrow e\nu, \qquad W \rightarrow \mu\nu$$

$$Z \rightarrow ee, \qquad Z \rightarrow \mu\mu,$$

because the W and Z are massive bosons, these decay particle pairs will be emitted with very high energies in opposite directions. The electrons are well identified charged particles and they are detectable, while the neutrinos and antineutrinos

are undetectable, and they leave without interacting, although their presence can be detected through momentum conservation.

W and Z masses can be determined through their decay spectrum. The mass m_Z can be determined directly, through the lepton pair mass spectrum, while the prediction of the W mass is more difficult, because the W decays to a charged lepton and missing transverse energy, so the measurement of the lepton p_T gives instead a sharp peak near $m_W/2$.

The theoretical prediction for the W and Z masses depend on one free parameter of the electroweak theory, namely $sin^2\theta_W$. This parameter has been measured in many independent experiments and yield a result of $sin^2\theta_W = 0.230$.

The higher order QCD corrections to W and Z cross sections are very important in order to get good agreement between theoretical prediction and experimental data. Quantitatively, the W and Z cross sections receive about 35% from $O(\alpha_s)$ corrections.

Another important process which lead to a precise determination of gauge boson properties; mass, width and coupling, through the production of gauge boson pair. This also provides us with a good test of the structure of the standard electroweak theory . We are going to discuss in detail gauge boson pair production, through single and double process scattering, in next the chapter.

Finally, we can say that the W and Z do exist with their predicted masses, and their production provides a good test of both electroweak and QCD theories. This will open a very important chapter in the improved understanding of the theories of fundamental forces in nature.

3.1.b This Chapter

In this chapter we calculate the higher order QCD corrections to weak gauge boson pair production at hadron colliders. As we mentioned in the last chapter, gluon effects play an important role at high energies (TeV scales) and the correc-

tions from higher order diagrams provide a significant contribution to the total cross-section. This change to the total cross-section, which results from adding the QCD corrections, will make the comparison of the total cross-section with experimental data much better than that of the lowest order diagrams alone. The most important reason for the calculation of the higher order QCD corrections to weak gauge boson production is related to the investigation of the electroweak symmmetry breaking, which is a primary goal of the proposed Superconducting Super Collider (SSC). The main challenge for the SSC is the detection of the Higgs boson of the standard model. The main dominant decays of the Higgs boson are through $H \rightarrow W^+W^-$ and $H \rightarrow ZZ$ [3], for a Higgs boson mass greater than $2m_W$ or $2m_Z$.

The continuum background for the Higgs boson is mostly expected to be Z boson pair that are produced via $q\overline{q} \rightarrow ZZ$ because both Z's decay leptonically, while the background from W pair is less than expected because W's decay both leptonically and hadronically, the latter is very difficult to distinguish from jets.

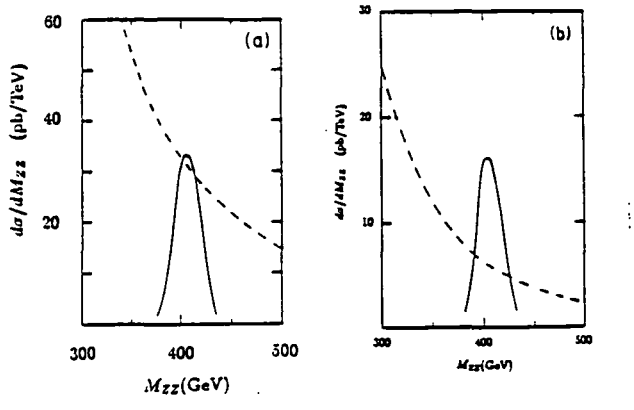

Fig. (3.2) The invariant-mass distribution of Z pairs from Higgs boson decay (solid line) and the continuum background $q\overline{q} \rightarrow ZZ$. The Higgs-boson mass is set at 400 GeV. In (a) no cuts are made. In (b) the outgoing Z's are required to have rapidity $\eta < 1.5$ [3].

Fig. (3.2) shows the invariant mass distribution of Z pairs from Higgs boson decay and the continuum background from $q\bar{q} \rightarrow ZZ$. The encouraging point in the fig. (3.2) is that the background falls sharply with increase of the Higgs mass and the Higgs signal is larger than the background by a factor of two; but on the other hand, the number of events is expected to be small. For this reason it is important to look at an additional signature that can distinguish the Higgs signal from the background. The important processes are the $q\bar{q} \rightarrow ZZg$, $qg \rightarrow ZZq$, and $\bar{q}g \rightarrow ZZ\bar{q}$, where in these processes the produced Z pair will generally receive transverse momentum when the Z pair recoils against the gluon.

Fig. (3.3) shows Monte Carlo results for the transverse momentum distribution of Z pairs. The background here arises from the perturbative QCD processes $q\bar{q} \rightarrow ZZg$, $qg \rightarrow ZZq$, and $\bar{q}g \rightarrow ZZ\bar{q}$.

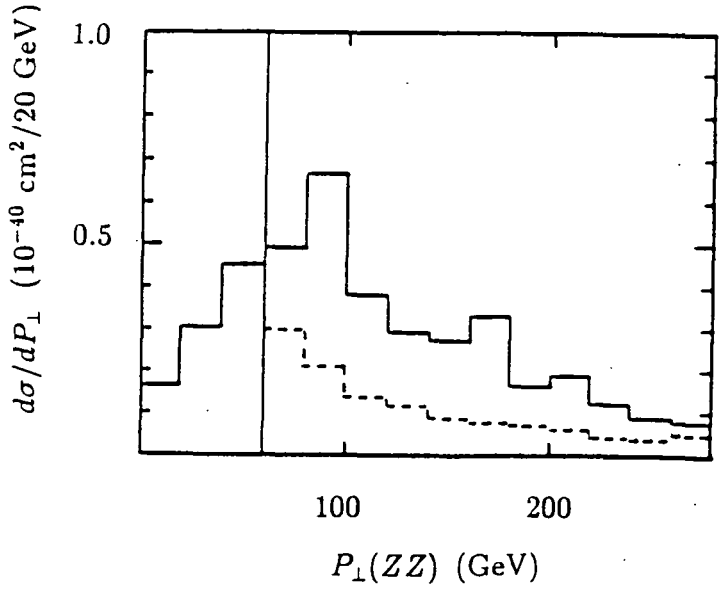

Fig. (3.3) Monte-Carlo results for the transverse-momentum distribution of Z pairs that decay into e^+e^-. The solid line is due to Higgs bosons of mass 400 GeV, while the dotted line indicates the background arising from the perturbative QCD processes $q\bar{q} \rightarrow ZZg, gq \rightarrow ZZq, and \quad g\bar{q} \rightarrow ZZ\bar{q}$.

3.2 The Lowest Order Subprocess $q\bar{q} \to ZZ$

The general amplitude for quark-antiquark annihilation into a weak gauge boson pair ZZ, together with momentum assignments is shown in fig. (3.3) below

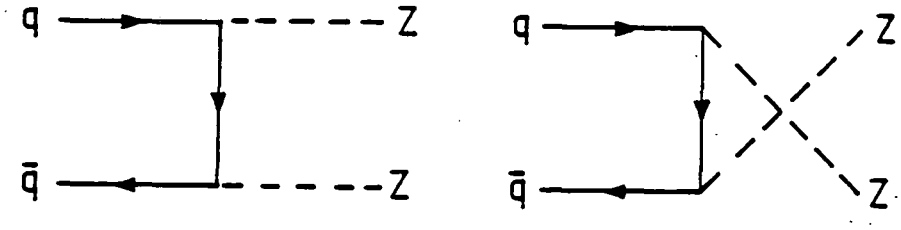

Fig. (3.4) Lowest order Feynman diagrams for $q\bar{q} \to ZZ$.

The matrix element for the process where the Dirac fermion annihilate to produce a boson pair is given by [4]

$$\mathcal{M}_1 = \frac{-i}{t}\bar{u}(k_2)\not{\epsilon}_2(g_v - g_a\gamma_5)(\not{k}_2 - \not{p}_2)\not{\epsilon}_1(g_v - g_a\gamma_5)v(k_1)$$

$$\mathcal{M}_2 = \frac{-i}{u}\bar{u}(k_2)\not{\epsilon}_1(g_v - g_a\gamma_5)(\not{k}_2 - \not{p}_1)\not{\epsilon}_2(g_v - g_a\gamma_5)v(k_1), \qquad 3.1$$

where ϵ_1, ϵ_2 are the polarisation vector of the Z bosons and g_v, g_a are the weak neutral couplings.

To calculate the differential cross-section, we only have to calculate

$$\mathcal{F} = \sum \; [|\mathcal{M}_1|^2 + |\mathcal{M}_2|^2 + 2Re\mathcal{M}_1^*\mathcal{M}_2], \qquad 3.2$$

where the summation is over the polarisation states of the Z bosons and quarks. With the use of the usual variables

$$s = (k_1 + k_2)^2 = (p_1 + p_2)^2$$

$$t = (k_1 - p_1)^2 = (p_2 - k_2)^2$$

$$u = (k_1 - p_2)^2 = (p_1 - k_2)^2$$

$$s + t + u = 2m_Z^2, \qquad 3.3$$

Working the matrix element out by using REDUCE [5], we get the following form for the differential cross section, to lowest order, for the subprocess $q\bar{q} \rightarrow ZZ$ [4]

$$\frac{d\sigma}{d\Omega} = \frac{\alpha^2}{2s} \quad \frac{1}{3} \quad \frac{(g_v^4 + g_a^4 + 6g_v^2 g_a^2)}{e^4} \quad [\frac{t}{u} + \frac{u}{t} + \frac{4m_Z^2 s}{tu} - m_Z^4(\frac{1}{t^2} + \frac{1}{u^2})], \qquad 3.4$$

where the polarization vector is defined so that $\sum \epsilon_\mu \epsilon_\nu = -g_{\mu\nu} + \frac{p_\mu p_\nu}{m_Z^2}$, $\gamma_5^2 = 1$ and $\alpha = \frac{e^2}{4\pi}$

As a check on our calculation, the result for $q\bar{q} \rightarrow ZZ$ for m_Z=0, g_a=0, and $g_v = -e_q$ can be compared with the calculation based on formula of eqn. (2.4) for $q\bar{q} \rightarrow \gamma\gamma$.

3.3 $O(\alpha_s)$ Virtual Gluon Corrections t0 $q\bar{q} \rightarrow ZZ$

To calculate the first order virual gluon corrections to the subprocess $q\bar{q} \rightarrow ZZ$, we have to evaluate all the diagrams of fig. (3.5). We present all the calculation in the Feynman gauge, which means that the gluon propagator has the following form:

$$D_{\mu\nu}^{ab} = -ig_{\mu\nu}\delta_{ab}$$

Each of these diagrams contain a loop, the resulting integral over the gluon momentum leads to ultraviolet and infrared divergence. These divergences occur due to the behaviour of the integrands at high and low virtual momenta (high and low energy behaviour of the loop integrals). The divergences associated with high virtual momentum are called ultraviolet divergences, the other divergences associated with the behaviour of the integrals at low momentum are called infrared divergences. For the integrability of these diagrams, we may either introduce cutoffs or work in a space with dimension $n > 4$. As was done earlier in chapter 2, we are going to use the continuous dimension method (dimensional regularisation), where the divergences arising from the calculation become poles of order $O(1/\epsilon)$ and $O(1/\epsilon^2)$ in the expression for the cross-section.

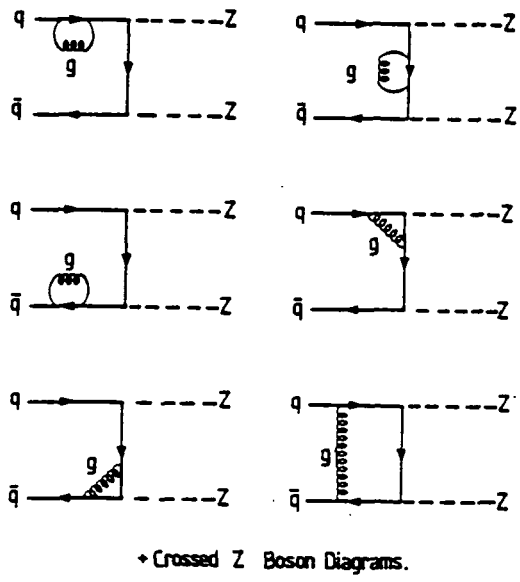

Fig. (3.5) Virtual gluon correction of order α_s for $q\bar{q} \rightarrow ZZ$. The solid lines represent quarks, the dashed lines Z boson, and the curly ones gluons.

It is clear from fig. (3.5) that there are in fact three types of virtual diagrams called self energy, vertex, and box diagrams. We shall calculate each of them separately.

3.3.a. The Self-Energy Diagrams

These consist of diagrams 1, 2 and 3 of fig. (3.5). Only the internal self-energy (diagram 2) gives a contribution to the cross-section, while the external self-energy (diagrams 1 and 3) gives zero contribution to the virtual corrections .

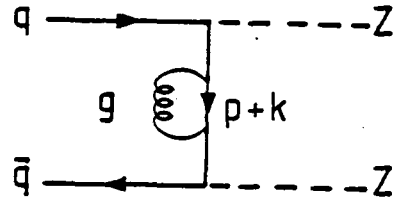

Fig. (3.6) Self-Energy Correction.

The loop integral for the self-energy has the following form:

$$\Sigma = -\frac{i4\pi\alpha_s}{(2\pi)^n}\int d^n k \frac{\gamma_\mu(\not{p}+\not{k})\gamma_\nu}{k^2(p+k)^2} g_{\mu\nu}, \qquad 3.5$$

Using Feynman parametrisation of multiple denominators and with the use of an n-dimensional Minkowski space integral [6], and with a suitable change of variables we get

$$\Sigma = \frac{\alpha_s}{(4\pi)} \quad (4\pi)^\epsilon \quad \not{p}_\mu \quad [-\frac{1}{\epsilon} - 1 + \gamma + ln(-t)], \qquad 3.6$$

where $t = p^2 = (k_1 - p_1)^2 = m_Z^2 - 2k_1.p_1$ and γ_E is Euler's constant.

We get similar form for the crossed Z boson diagram

$$\Sigma = \frac{\alpha_s}{(4\pi)} \quad (4\pi)^\epsilon \quad \not{p}_\mu \quad [-\frac{1}{\epsilon} - 1 + \gamma + ln(-u)], \qquad 3.7$$

Combining eqn. (3.6 and 3.7) with the lowest order amplitude, we get the following correction due to the self-energy diagrams

$$\delta_{self} = \frac{4\alpha_s}{3\pi} \quad (4\pi)^\epsilon \quad [-\frac{1}{2\epsilon} - \frac{1}{2} + \frac{A}{2M_0}(ln(-t)+\gamma) + \frac{B}{2M_0}(ln(-u)+\gamma)], \qquad 3.8$$

where

$$A = 8m_Z^4 tu - 2m_Z^4 u^2 - 4m_Z^2 t^2 u - 4m_Z^2 tu^2 + 2tu^3$$

$$B = -2m_Z^4 t^2 + 8m_Z^4 ut - 4m_Z^2 t^2 u - 4m_Z^2 tu^2 + 2t^3 u,$$

$$M_0 = -2m_Z^4t^2 + 16m_Z^4ut - 2m_Z^4u^2 - 8m_Z^2tu^2 - 8m_Z^2t^2u + 2tu^3 + 2t^3u,$$

where M_0 represents the lowest order for the subprocess $q\bar{q} \to ZZ$

As a check on our calculation for δ_{self}, for m_Z=0, the same result of eqn. (2.23) is obtained.

3.3.b The Vertex Diagram

We calculate in the Feynman gauge, the virtual gluon corrections to the quark-quark vertex as shown in fig. (3.7)

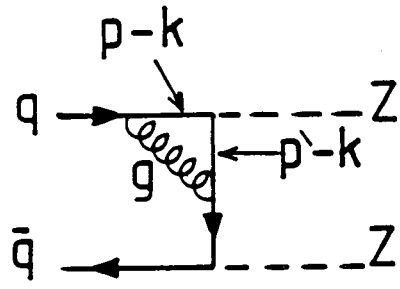

Fig. (3.7) Vertex correction.

For the vertex correction, we have to write the loop integral which has the form:

$$\Lambda_\mu(p,p') = -\frac{i4\pi\alpha_s}{(2\pi)^n}\int d^nk \frac{\gamma^\alpha(\not{p}' - \not{k})\gamma_\mu(\not{p} - \not{k})\gamma^\beta}{k^2(p'-k)^2(p-k)^2} \quad g_{\alpha\beta} \qquad 3.9$$

It is more complicated than the self-energy case. Also we introduce here Feynman parametrisation as

$$\Lambda_\mu(p,p') = -\frac{i4\pi\alpha_s}{(2\pi)^n}\Gamma(3)\int dxdydz\delta(1-x-y-z)\int d^nk$$
$$\frac{\gamma^\alpha(\not{p}' - \not{k})\gamma_\mu(\not{p} - \not{k})\gamma_\alpha}{[k^2x + (p'-k)^2y + (p-k)^2z]^3} \qquad 3.10$$

We introduce the new integration variable

$$k' = k - p'y - pz,$$

in terms of which eqn. (3.10) becomes

$$\Lambda_\mu(p,p') = -\frac{i4\pi\alpha_s}{(2\pi)^n}\Gamma(3)\int dxdydz\delta(1-x-y-z)\int d^nk'$$

$$\frac{\gamma^\alpha(\not{p}'(1-y)-pz-k')\gamma_\mu(\not{p}(1-z)-\not{p}'y-k')\gamma_\alpha}{[zp^2-(p'y+pz)^2+k'^2]^3} \qquad 3.11$$

Note that one of the quarks are on mass-shell, which simplifies the calculation. For the p'^2=0 case, we have to integrate the following:

$$\Lambda_\mu(p,p') = -\frac{i4\pi\alpha_s}{(2\pi)^n} i\pi^{n/2}\Gamma(1+\epsilon)\int dydz \frac{z(1-z)}{[-zp^2(1-z-y)-m_Z^2yz]^{1+\epsilon}}\gamma^\alpha \not{p}\gamma_\mu\not{p}\gamma_\alpha \qquad 3.12$$

With a suitable change of variable, and using the identity

$$\gamma_\mu\gamma_\nu\gamma_\mu = -2(1-\epsilon)\gamma_\nu,$$

where $\epsilon = \frac{4-n}{2}$, we can write

$$\Lambda_\mu(p,p') = \frac{\alpha_s}{4\pi}(4\pi)^\epsilon[m_Z^2-t]^{-1-\epsilon} \quad \frac{1}{\epsilon}\frac{\Gamma(1+\epsilon)\Gamma^2(1-\epsilon)}{(1-2\epsilon)\Gamma(1-2\epsilon)}(1-\epsilon)(m_Z^2-t)(\gamma_\mu - \frac{2p_\mu\not{p}}{p^2}) \qquad 3.13$$

Rearranging eqn. (3.13) we get

$$\Lambda_\mu(p,p') = \frac{\alpha_s}{4\pi}(4\pi)^\epsilon \quad [\frac{1}{\epsilon} - ln(m_Z-t) - \gamma + 1] \quad [\gamma_\mu - \frac{2p_\mu\not{p}}{p^2}], \qquad 3.14$$

where γ is Euler's constant and $p^2 = t$. Similarly for $p^2 = 0$ we get

$$\Lambda_\mu(p,p') = \frac{\alpha_s}{4\pi}(4\pi)^\epsilon \quad [\frac{1}{\epsilon} - ln(m_Z-t) - \gamma + 1][\gamma_\mu - \frac{2p'_\mu\not{p}'}{p'^2}] \qquad 3.15$$

Taking into account the crossed diagrams, writing the vertex amplitudes and combining them with the lowest order amplitudes, we get the following corrections due to the vertex diagrams:

$$\delta_{vertex} = \frac{4\alpha_s}{3\pi} \quad (4\pi)^\epsilon \quad [\frac{1}{\epsilon}(1+\frac{8}{M_0}) + 1$$

$$-\frac{1}{M_0}[(A+4)(ln(m_Z^2-t)+\gamma) - 4 + t \leftrightarrow u]], \qquad 3.16$$

where

$$A = 2(-m_Z^4u^2 + 4m_Z^4tu - 2m^2tu^2 - 2m_Z^2ut^2 + tu^3)/t^2u^2$$

$$M_0 = 2(-m_Z^4 t^2 + 8m_Z^4 tu - m_Z^4 u^2 - 4m_Z^2 tu^2 - 4m_Z^2 ut^2 + tu^3 + ut^3)/t^2u^2$$

3.3.c The Box Diagram

For the box diagram we have to work out a four denominator integral. The loop integral of fig. (3.8) can be written in the form:

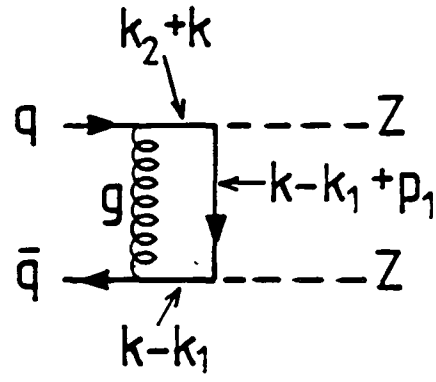

Fig.(3.8) The box diagram

$$\mathcal{M} = \frac{-i4\pi\alpha_s}{(2\pi)^n}\int d^n k \frac{\gamma^\alpha(\not{k}+\not{k}_2)\gamma^{\mu_2}(\not{k}+\not{p}_1-\not{k}_1)\gamma^{\mu_1}(\not{k}-\not{k}_1)\gamma^\beta}{k^2(k+k_2)^2(k-k_1)^2(k+(p_1-k_1))^2} \quad g_{\alpha\beta} \qquad 3.17$$

Here, a double pole $O(1/\epsilon^2)$ term appears as a result of the infrared divergences as well as the mass singularities in the amplitude. Introducing Feynman parametrisation into eqn. (3.17) we get

$$\mathcal{M} = \frac{-i4\pi\alpha_s}{(2\pi)^n}\Gamma(4)\int dxdydzdw \quad \delta(1-x-y-z-w)\int d^n k$$

$$\frac{\gamma^\alpha(\not{k}+\not{k}_2)\gamma^{\mu_2}(\not{k}+\not{p}_1-\not{k}_1)\gamma^{\mu_1}(\not{k}-\not{k}_1)\gamma_\alpha}{[k^2+2k(yk_2-xk_1+z(p_1-k_1))+z(p_1-k_1)^2]^4} \qquad 3.18$$

We introduce the new integration variable

$$k' = k + yk_2 - xk_1 + z(p_1 - k_1)$$

$$k = k' - yk_2 + xk_1 - z(p_1 - k_1),$$

in terms of which eqn. (3.18) becomes

$$\mathcal{M} = \frac{-i4\pi\alpha_s}{(2\pi)^n}\Gamma(4)\int dxdydzdw \quad \delta(1-x-y-z-w)\int d^nk'$$

$$\gamma^\alpha(\not{k}' + k_2(1-y) + \not{k}_1(x+z) - z\not{p}_1)\gamma^{\mu_2}(\not{k}' - \not{k}_1(1-x-z) + \not{p}_1(1-z) - y\not{k}_2)\gamma^{\mu_1}$$

$$\frac{(\not{k}' - \not{k}_1(1-x-z) - y\not{k}_2 - z\not{p}_1)\gamma_\alpha}{[k'^2 - (yk_2 - xk_1 + z(p_1-k_1))^2 + z(p_1-k_1)^2]^4} \qquad 3.19$$

The calculation of eqn. (3.19) is more lengthy than the previous cases. We made use of the symbolic manipulation program REDUCE [5] to calculate the trace of the numerator interfering with the lowest order. After the trace calculation, we expand the numerator factors, which include factors of 1, x, y, z and w or multiples of such factors. These integrals were calculated and the results are expressed in terms of the invariants, t and s together with functions of ϵ. Here we shall present the non-trivial integration arising from eqn. (3.19) as an example

$$\mathcal{M} = \frac{-i4\pi\alpha_s}{(2\pi)^n}\Gamma(4)\int dxdydzdw \quad \delta(1-x-y-z-w)\int d^nk'$$

$$\frac{1}{[k'^2 - (yk_2 - xk_1 + z(p_1-k_1))^2 + z(p_1-k_1)^2]^4} \qquad 3.20$$

Now integrating over d^nk' we get

$$\mathcal{M} = \frac{-i4\pi\alpha_s}{(2\pi)^n} \quad \frac{(-t)^{-\epsilon}}{t^2} \quad \int dxdydzdw \quad \delta(1-x-y-z-w)i\pi^{n/2}$$

$$\Gamma(4-n/2)[\frac{m_Z^2}{t}z(x+y) + z(1-x-y-z) + xy\frac{s}{t}]^{-2-\epsilon} \qquad 3.21$$

where $t = (p_1 - k_1)^2$ and $s = (k_1 + k_2)^2$.

Evaluation of eqn. (3.21) is rather lengthy, but straightforward, with the use of some mathematical reference books [7,8,9]. The final result for the integration has the form:

$$\mathcal{M} = \frac{\alpha_s}{4\pi}(4\pi)^\epsilon \quad \frac{1}{ts} \quad \frac{\Gamma^2(1-\epsilon)\Gamma(1+\epsilon)}{\Gamma(1-2\epsilon)}$$

$$[\frac{1}{\epsilon^2} + \frac{1}{\epsilon}ln(-t/s) - \frac{2}{\epsilon}ln(m_Z^2 - t) + ln^2(-t/s) - \frac{\pi^2}{2} + ...], \qquad 3.22$$

where we have dropped all positive powers of ϵ in the calculation. All other integrations arising from eqn. (3.19) evaluated in similar way. Taking into account the crossed Z diagram, the final form of the correction from the box diagrams has the form:

$$\delta_{box} = \frac{4\alpha_s}{3\pi} \quad (4\pi)^{\epsilon} \quad [\frac{-1}{\epsilon^2} + \frac{1}{\epsilon}(ln(s) + \gamma - 2 - \frac{8}{M_0}) \\ + \quad finite \quad terms], \qquad 3.23$$

where M_0 is the lowest order cross-section for the subprocess $q\bar{q} \rightarrow ZZ$. We also remind that we have only concentrated on terms that contain a singularity.

3.4 $O(\alpha_s)$ Real Correction to $q\bar{q} \rightarrow ZZ$

Not only the emission of virtual gluon leads to an expermental degeneracy, but also the emission of real gluons.

In order to calculate the corrections from real gluon emission, we have to calculate the cross-section corresponding to the Feynman diagrams of Fig. (3.8) .

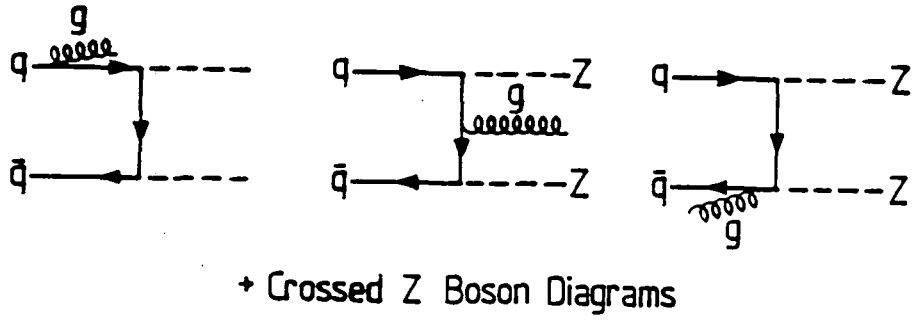

Fig. (3.9) Feynman diagrams for the real gluon emission.

As is clear from Fig. (3.9), these diagrams contain no loop integrals, but there is an integral over the final 3-body phase space. We again face divergences, generated in the continuous dimension method as poles in the contribution to the cross-section. These divergences arise from two limits: First, when the gluon is emitted in a direction parallel to either the quark or antiquark, this is called the collinear limit, and second, when the gluon is emitted with very small energy, we have what is called soft gluon emission. We shall calculate each of them separately.

3.4.a. Hard Collinear Gluon Emission

In this case the emission of the gluon is in a direction sufficiently parallel to quark or antiquark direction, which means that the angle between the gluon and the quark is very small.

In order to regulate the divergences we have to work out the cross-section corresponding to the Feynman diagram of Fig. (3.9)

The matrix element for the six Feynman diagrams are:

$$M_1 = \frac{-igG}{4k_1.p_1 k.k_2}\overline{u}(k_2)\not{\epsilon}(\not{k}_2 - \not{k})\not{\epsilon}_2(\not{k}_1 - \not{p}_1)\not{\epsilon}_1 v(k_1),$$

$$M_2 = \frac{-igG}{4k_1.p_1 k_2.p_2}\overline{u}(k_2)\not{\epsilon}_2(\not{k}_2 - \not{p}_2)\not{\epsilon}(\not{p}_1 - \not{k}_1)\not{\epsilon}_1 v(k_1),$$

$$M_3 = \frac{-igG}{4k_2.p_2 k.k_1}\overline{u}(k_2)\not{\epsilon}_2(\not{k}_2 - \not{p}_2)\not{\epsilon}_1(\not{k}_1 - \not{k})\not{\epsilon}_1 v(k_2),$$

$$M_4 = \frac{-igG}{4k_1.p_2 k.k_2}\overline{u}(k_2)\not{\epsilon}(\not{k}_2 - \not{k})\not{\epsilon}_1(\not{k}_1 - \not{p}_2)\not{\epsilon}_2 v(k_1),$$

$$M_5 = \frac{-igG}{4k_2.p_1 k_1.p_2}\overline{u}(k_2)\not{\epsilon}_1(\not{k}_2 - \not{p}_1)\not{\epsilon}(\not{p}_2 - \not{k}_1)\not{\epsilon}_1 v(k_2),$$

$$M_6 = \frac{-igG}{4k_2.p_1 k_1.k}\overline{u}(k_2)\not{\epsilon}_1(\not{k}_2 - \not{p}_1)\not{\epsilon}_2(\not{k}_1 - \not{k})\not{\epsilon} v(k_1), \qquad 3.24$$

where g is the gauge coupling constant ($g^2 = 4\pi\alpha_s$), $G = (g_v^2 + g_a^2 - 2g_v g_a\gamma_5)$, ϵ is the polarisation vector of the gluon, and ϵ_1, ϵ_2 are the polarisation vectors of the Z pair boson.

For the case when the gluon is parallel to the antiquark k_1, only the diagrams M_3 and M_6 lead to singularities. For the cross-section we have to calculate:

$$F_1 = \sum[|M_3|^2 + 2ReM_3^*(M_1 + M_2 + M_4 + M_5 + M_6) +$$

$$|M_6|^2 + 2ReM_6^*(M_1 + M_2 + M_4 + M_5)], \qquad 3.25$$

where the summation is over the polarisation states of the photons, the gluons, and the quarks.

To calculate the traces we have made use of the symbolic manipulation program (REDUCE) [5]. In our calculation we have used the following

- The gluon has to be treated in n-dimensions.

- The Z bosons and quarks have to be treated in 4-dimensions.

- Because the gluon is almost parallel to the quark k_1, we put $k.k_1$=0 everywhere, except in the denominator.

Working the matrix element out we get:

$$F_1 = \frac{2g^2(g_v^4+g_a^4+6g_v^2g_a^2)s}{k.k_1 k.k_2}\Big[2 \quad [(\frac{t^2+u^2}{t'u'}+\frac{t'^2+u'^2}{tu})$$

$$+4m_Z^2 s'(\frac{1}{tu'}+\frac{1}{t'u})-m_Z^4(\frac{t}{t'uu'}+\frac{u}{u'tt'}+\frac{t'}{tuu'}+\frac{u'}{utt'})]$$

$$+(n-4)\quad (\frac{(t-u)^2}{t'u'}+\frac{(t'-u')^2}{tu}+4-\frac{t}{u'}-\frac{u}{t'}-\frac{t'}{u}-\frac{u'}{t}+f(m_Z^2,u,t))\Big], \quad 3.26$$

where

$$f(m_Z^2,u,t)=\frac{m_Z^2}{s}(8t^4ut'-16t^3u^3t'-8t^3u^2u'-16t^3ut'^2+32t^3ut'u'+8t^2u^3t'+8t^2u^3u'$$

$$+16t^2u^2t'^2-40t^2u^2t'u'-8t^2u^2u'^2+8t^2ut'^3-40t^2ut'^2u'+48t^2ut'u'^2$$

$$-8t^2t'^2u'^2-8tu^3t'^2+8tu^3t'u'+48tu^2t'^2u'-40tut'u'^2+8tuu't'^3-40tut'^2u'^2$$

$$+32tut'u'^3+8tt'^3u'^2-8tt'^2u'^3+8u^3t'u'^2-8u^2t'^3u'+16u^2t'^2u'^2$$

$$-16u^2t'u'^3+8ut'^3u'^2+8ut'u'^4)/(tu^2u't'^2),$$

$$t=(p_1-k_1)^2, \quad u=(p_1-k_2)^2, \quad s=(k_1+k_2)^2,$$

$$t'=(p_2-k_2)^2, \quad u'=(p_2-k_1)^2, \quad s'=(p_1+p_2)^2,$$

We can check eqn. (3.26) in two ways. First, if we put $t'=t$, $u'=u$ and $s'=s$ in eqn. (3.26), then the form of the lowest order cross-section for the subprocess $q\bar{q}\rightarrow ZZ$ is be obtained, and second, if we put the mass of Z boson $m_Z=0$ we get the same form as eqn. (2.41) for the two photon case [10].

For the case when the gluon is emitted parallel to the quark k_2, only the diagrams M_1 and M_4 have singularities. In this case we have to calculate the following:

$$F_2 = \sum[|M_1|^2 + 2ReM_1^*(M_2 + M_3 + M_4 + M_5 + M_6) + |M_4|^2 + 2ReM_4^*(M_2 + M_3 + M_5 + M_6)], \quad 3.27$$

we find a cross section identical to eqn. (3.26).

In order to get the total corrections due to hard collinear gluon we have to integrate eqno. (3.26) over the gluon phase space.

The total cross-section for a three body final state, after including factors for flux, Bose statistics, colour sum, initial state spin, and final state polarization has the form

$$\sigma_{real} = \frac{(g_v^4 + g_a^4 + 6g_v^2 g_a^2)}{3} \quad \frac{\alpha^2}{2s} \quad \frac{4\alpha_s}{3\pi} \quad \frac{(2\pi)^4}{2} \int \frac{d^n k}{(2\pi)^n} \frac{d^4 p_1}{(2\pi)^4} \frac{d^4 p_2}{(2\pi)^4} \quad (2\pi)^4$$
$$\delta^4(k_1 + k_2 - p_1 - p_2 - k) \quad (2\pi)^3 \quad \delta^+(k^2) \quad \delta^+(p_1^2 - m_Z^2) \quad \delta^+(p_2^2 - m_Z^2) \quad |M|^2 \quad 3.28$$

where $|M|^2$ is the matrix element squared for hard collinear gluon emission from the subprocess $q\bar{q} \rightarrow ZZ$. To integrate eqn. (3.28) we introduce the following

$$1 = \int d^4 P \delta^4(P - p_1 - p_2)$$
$$1 = \int_0^\infty dm^2 \delta(m^2 - P^2),$$

so that eqn. (2.43) has the following form:

$$\sigma_{real} = \frac{(g_v^4 + g_a^4 + 6g_v^2 g_a^2)}{3} \quad \frac{\alpha^2}{2s} \quad \frac{4\alpha_s}{3\pi} \quad \frac{(2\pi)^4}{2} \quad \frac{1}{(2\pi)^{3-2\epsilon}}$$
$$\int dm^2 d^4 P d^n k \quad \delta^+(P^2 - m^2) \quad \delta^+(K - P - k) \quad \delta^+(k^2) \quad \int D2BPS \quad |M|^2, \quad 3.29$$

where D2BPS is the two body final state phase space integration which, has the form:

$$D2BPS = \frac{1}{(2\pi)^2} \int d^4 p_1 d^4 p_2 \quad \delta^+(p_1^2 - m_Z^2) \quad \delta^+(p_2^2 - m_Z^2) \quad \delta^4(k_1 + k_2 - p_1 - p_2) \quad 3.30$$

Performing the integration over the gluon energy k, and with the change of variable $y = \frac{1}{2}(1 + cos\phi)$, we obtain

$$\sigma_{real} = \frac{(g_v^4 + g_a^4 + 6g_v^2 g_a^2)}{3} \quad \frac{\alpha^2}{2s} \quad \frac{4\alpha_s}{3\pi} \quad \frac{(2\pi)^4}{2} \quad \frac{1}{(2\pi)^2} \frac{(4\pi)^\epsilon}{\Gamma(1-\epsilon)} \frac{1}{2}$$

$$\int dx_3(1-x_3)(1-x_3)^{-2\epsilon}(s)^{-\epsilon} \int_0^1 dy(y(1-y))^{-\epsilon}|M|^2 \int D2BPS, \qquad 3.31$$

where we have used the following:

$$\int d^n k \delta^+(k^2) = \int \frac{d^{n-1}k}{2k},$$

$$\int d^{n-1}k = \frac{2\pi\pi^{n/2-2}}{\Gamma(n/2-1)} \int dk k^{n-2} \int_0^\pi d\phi sin^{n-3}\phi,$$

$$dm^2 = s dx_3,$$

now we subsitute the matrix element squared for the process $q\bar{q} \to ZZg$ which has the form of eqn. (3.26) in eqn. (3.31). Using the following collinear kinematics

$$t = m_Z^2 - 2E^2 x_3(1 + \beta cos\theta), \quad t' = m_Z^2 - 2E^2(1 + \beta cos\theta),$$

$$u = m_Z^2 - 2E^2(1 - \beta cos\theta), \quad u' = m_Z^2 - 2E^2 x_3(1 - \beta cos\theta),$$

$$s = 4E^2, \quad s' = 4E^2 x_3, \qquad 3.32$$

where $\beta = \sqrt{1 - \frac{m_Z^2}{E^2}}$.

By subsituting these collinear limit expressions in the matrix element, and with more algebraic work, we find the following form for the corrections from hard collinear gluon emission:

$$\delta_{hardcollinear} = \frac{4\alpha_s}{3\pi} \quad [\int dx_3 \frac{(1+x_3^2)}{(1-x_3)_+} \quad (-\frac{1}{\epsilon} - ln(4\pi) + \gamma) + \frac{1}{\epsilon} ln\varepsilon^2$$

$$-2ln^2\varepsilon + 4\varepsilon ln2\varepsilon E - \varepsilon^2 ln2\varepsilon E - 4\varepsilon - 3ln2E - 4ln\varepsilon ln2E + 4 + .. \quad finite \quad terms...], \qquad 3.33$$

where

$$\sigma_{hardcollinear} = \hat{\sigma}_{q\bar{q}\to ZZ} \delta_{hardcollinear},$$

and the lowest order subprocess for Z pair production has the form:

$$\hat{\sigma}_{q\bar{q}\to ZZ} = \frac{(g_v^4 + g_a^4 + 6g_v^2 g_a^2)}{3} 16\pi^2\alpha^2 \frac{1}{2\hat{s}} \int D2BPS \quad |M|^2_{q\bar{q}\to ZZ}$$

3.4.b Soft Gluon Emission

In this case the gluon energy k is small so that the soft gluon matrix element is proportional to the purely elastic cross section. To order α_s we have to calculate the cross section of fig. (3.10)

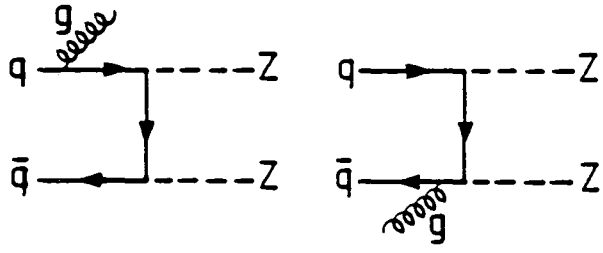

Fig. (3.10) Feynman diagrams for soft gluon corrections.

The correction factor is given by the following form

$$\delta_{soft} = \frac{4\pi\alpha_s}{(2\pi)^n} \quad \frac{4}{3} \quad (2\pi) \quad s \int \frac{d^{n-1}k}{2k} \frac{1}{k.k_1 k.k_2} \qquad 3.34$$

This integral has two fold divergences; with the gluon being soft ($k \to 0$), and with the quark being massless, we will generate both infrared and mass singularities. Working in the continuous dimension method, we expect a double pole structure in the soft gluon correction. This is the only place where the double pole appears in real gluon emission. Using the following formula

$$\int d^{n-1}k = \frac{2\pi\pi^{\frac{n}{2}-2}}{\Gamma(n/2-1)} \int dk k^{n-2} \int_0^\pi d\theta sin^{n-3}\theta, \qquad 3.35$$

We can write the correction factor in the form

$$\delta_{soft} = \frac{2\pi\alpha_s}{(2\pi)^{n-1}} \quad \frac{4}{3} \quad \frac{2\pi\pi^{\frac{n}{2}-2}}{\Gamma(n/2-1)} \int_0^\pi d\theta \quad sin^{n-5}\theta \int_0^{2\varepsilon E} dk k^{n-5}, \qquad 3.36$$

where we have chosen $k.k_1 = Ek(1 - cos\theta)$ and $k.k_2 = Ek(1 + cos\theta)$.

After integrating eqn. (3.36) over the gluon energy and angle we get the following form for the correction

$$\delta_{soft} = \frac{4\alpha_s}{3\pi}(4\pi)^{\epsilon} \quad \frac{\Gamma(1-\epsilon)}{\Gamma(1-2\epsilon)}\frac{1}{\epsilon^2} \quad [4E^2\varepsilon^2]^{-\epsilon} \tag{3.37}$$

Using some gamma function properties like

$$\frac{1}{\Gamma(1-\epsilon)} = 1 - \gamma\epsilon + \frac{\epsilon^2}{2}(\gamma^2 - \frac{\pi^2}{6}) + ...$$

$$\frac{\Gamma^2(1-\epsilon)}{\Gamma(1-2\epsilon)} = (1 - \epsilon^2\frac{\pi^2}{6} + ...), \tag{3.38}$$

the final result for the correction factor from soft gluon emission can be written in the following form:

$$\delta_{soft} = \frac{4\alpha_s}{3\pi}(4\pi)^{\epsilon} \quad [\frac{1}{\epsilon^2} - \frac{1}{\epsilon} \quad (ln(4E^2\varepsilon^2) + \gamma) + \frac{1}{2}(ln(4E^2\varepsilon^2) + \gamma)^2 - \frac{\pi^2}{4}] \tag{3.39}$$

3.5 Results and Discussion

Weak gauge boson pair production in hadron collisions provides an important testing ground for various aspects of perturbative QCD. Furthermore, a remarkable test of the structure of the electroweak interaction may be achieved in measurements of the cross sections for the production of pairs of gauge bosons $(W^+W^-, W^\pm Z, ZZ)$. In addition, the gauge boson pairs may give a significant background to the detection of the Higgs boson, and possibly for new degree of freedom.

In this chapter, we have calculated the differential cross-secton for the lowest order subprocess $q\bar{q} \to ZZ$. In view of the importance of this process, and because it occurs at hadron colliders, it becomes necessary to calculate the magnitude of the QCD corrections which arise when gluons are exchanged and emitted from the lowest order subprocess $q\bar{q} \to ZZ$. We have used the perturbative theory of massless quarks and gluons. Our results have been presented for virtual and real gluon emission separately. In order to obtain results which are free from divergences, we add up the corrections due to the virtual and real gluons; the various double and single poles cancel, and the leftover $1/\epsilon$ terms have the form:

$$P_{qq} = \frac{4}{3} \quad (\frac{1+x_3^2}{(1-x_3)_+} + \frac{3}{2}\delta(1-x_3)) \qquad 3.40$$

This term corresponds to a mass singularity which is usually absorbed into the structure functions beyond the leading order. Since the appearance of the mass singularities in higher order corrections have universal structure, process independent and they can be factorise according to a fundamental property of factorisation theorem which tells that the bare cross-section can be factorised into universal factors containing the singularity which can be removed by subtraction procedure, and a well defined finite short distance cross-section, which is free from mass singularites. Thus the total cross-section can be defined as:

$$d\sigma = d\sigma^0 + d\sigma^1, \qquad 3.41$$

where $d\sigma^0$ is the Born cross-section, and $d\sigma^1$ denotes the order α_s corrections which appear as large double logarithms and π^2 terms.

The physical cross-section, next to leading order in α_s is obtained by using the following form

$$d\sigma(p\overline{p} \rightarrow ZZX) = \sum \int_0^1 dx_a dx_b q(x_a, Q^2)\overline{q}(x_b, Q^2)\sigma_{q\overline{q}\rightarrow ZZ} \qquad 3.42$$

where $\sigma_{q\overline{q}\rightarrow ZZ}$ is the total cross section for the subprocess and has the following form (up to order $O(\alpha_s)$)

$$\sigma_{q\overline{q}\rightarrow ZZ} = \hat{\sigma}_{q\overline{q}\rightarrow ZZ} \quad (\delta(1-x) + \frac{\alpha_s}{\pi}\Delta(x) + ...),$$

where $\Delta(x)$ is the complete first order QCD correction to the process $q\overline{q} \rightarrow ZZ$.

CHAPTER 4

HARD SCATTERING PROCESSES

4.1 Introduction

With a new energy regime, the $p\bar{p}$ collider programme at CERN in 1981 has opened a new chapter in high energy physics. After five years of very successful operation during 1981 to 1985 the collider has been undergoing an important upgrading programme. The collision energy has been increased from 540 GeV during the years (1981-1983) to 630 GeV for the most recent running periods, also the two large experiments UA1 and UA2 have received just less than 1 pb^{-1} of integrated luminosity in the period up to 1985.

The CERN $p\bar{p}$ collider and its experiments have played a very important role in particle physics in particular the discovery of the Intermediate Vector Bosons (IVBs) at the UA1 and UA2 experiments and the study of hard parton scattering in jet phenomena [1].

In the recent years, the CERN S$p\bar{p}$S collider has provided some remarkable evidence in support of the "standard model" of strong, weak and electromagnetic interactions. Besides from the discovery of W and Z bosons, there have been evidence for hard scattering of quarks and gluons in the production of large transverse momentum, the accumulation of large sample of b quark events and stringent limits on a wide variety of new particles and interactions.

So the standard model i.e. the $SU(3)\times SU(2)\times U(1)$ gauge theory of the strong and electroweak interactions was successfuly tested over more than a decade and has continued to work well. All of the $p\bar{p}$ collider data is in beautiful agreement with the model both with the study of jet physics which provides a qualitative confirmation of QCD theory and the production of electroweak W and Z gauge bosons which forms the basis of the electroweak sector. Also high energy e^+e^-

experiments provide precise and complementary evidence in favour of the strong and electroweak standard model.

It is important to continue in order to test the standard model, where over the next decade, the experimental programs at accelerators now operating or under construction will subject it to more precise testing. In recent years a variety of events have been reported from the CERN collider, and it has been believed that some of these events may be inexplicable within the standard model and at least one or more of them may lead beyond it [2].

Section 2 of this chapter contains more description of the electroweak phenomena and of our present understanding of the IVB production mechansims. Section 3 contains a description of the pair gauge boson productions in hadronic colliders which gives a test to the standard model over the 100 GeV scale. Section 4 covers the theory of double scattering parton mechansim in producing pair of gauge bosons in pp and $p\bar{p}$ scattering. Like-charge W pair production has also been studied in section 5. A comparison with single parton scattering for the same processes has been made. Finally a brief discussion and summary for the chapter is given in section 6.

4.2 Electroweak Phenomena

In this section we discuss the processes which are associated with the standard electroweak interactions. As we mentioned earlier with gauge symmetry breaking, the particles associated with the electroweak interactions are the charged intermediate bosons $W^{\pm}$, the neutral intermediate boson Z and an elementary Higgs scalar H.

The standard model topics which will be covered with multi-TeV hadron colliders are [3]:

1. The rate of $W^{\pm}$ and Z production, investigation of the production mechanism of the intermediate boson with more basic measurements of the cross-section, mass

and width.

2. The cross-section for pair gauge production which is understood as potential background to the observation of Higgs bosons.

3. The Higgs boson itself is the only boson remaining to be found in the standard model.

4.2.a The Production Mechanism for W and Z at Hadron Colliders

Massive particles can be produced directly in e^+e^-, lepton-hadron and hadron-hadron collision provided the avaliable energy in the collision is sufficient.

The W and Z production cross-section can be calculated using the Drell-Yan mechanism. As well known this mechanism was used first to describe the lepton pair production in hadron hadron collisions in the framework of the quark- parton model [4] as shown in fig. (4.1)

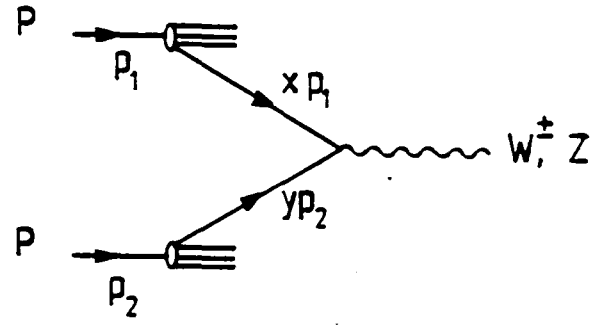

Fig. (4.1) Production of W and Z by Drell-Yan quark-antiquark annihilation.

The distribution of the fractional momenta of quarks in hadrons is described by the structure functions which were obtained from lepton-nucleon scattering experiments [5].

In $p\overline{p}$ collisions at the CERN collider with a CM energy of $\sqrt{s}$=630 GeV, valence quarks annihilate with a typical CM energy of $\sqrt{\hat{s}} = \sqrt{x_a x_b s} = 100$

GeV, where x_a and x_b are the momentum fraction of the quark and antiquark, respictively. This is sufficient to produce an object of corresponding mass, such as the $W^{\pm}$ or Z.

The $p\overline{p}$ collider provides the source of valence $\overline{u}$, $\overline{d}$ and u, d quarks. The basic subprocesses for forming a W and Z in $p\overline{p}$ collision are

$$u + \overline{d} \rightarrow W^+, \quad d + \overline{u} \rightarrow W^-$$

$$u + \overline{s} \rightarrow W^+, \quad s + \overline{u} \rightarrow W^-$$

$$u + \overline{u} \rightarrow Z, \quad d + \overline{d} \rightarrow Z, \quad s + \overline{s} \rightarrow Z, \qquad 4.1$$

where in eqn. (4.1) s-quarks are sea quarks only.

The production cross-section depends on three factors:

- The probability that a q and $\overline{q}$ having fractional momenta so to obtain CM energy equal to m_W or m_Z.
- The probability that a quark and antiquark form a colour neutral system.
- The electroweak coupling strength

The total production cross-section for W, Z can be written in the form

$$\sigma(p\overline{p} \rightarrow V + X) = \sum_{q,\overline{q}} \int_0^1 dx_a \int_0^1 dx_b G_{a/p}(x_a, Q^2) G_{b/\overline{p}}(x_b, Q^2) \hat{\sigma}_{q\overline{q} \rightarrow V}|_{\hat{s}=x_a x_b s} \qquad 4.2$$

where V=$W^{\pm}$ or Z, and $\hat{\sigma}_{qq \rightarrow V}$ is the subprocess cross-section, which has the following form (for W boson)

$$\hat{\sigma}_{q\overline{q} \rightarrow W} = \frac{4\pi^2 \alpha}{3} \frac{1}{4 \sin^2 \theta_W} \delta(x_a x_b s - m_W^2) \qquad 4.3$$

The inclusive cross-section is obtained by summing over all quark-antiquark combinations possible for that process as shown

$$\sigma(p\overline{p} \rightarrow W^{\pm} + X) = \sum_{q,\overline{q}} \int_0^1 dx_a \int_0^1 dx_b W(x_a, x_b) \hat{\sigma}_{q\overline{q} \rightarrow W^{\pm}}$$

$$\sigma(p\bar{p} \to W^{\pm} + X) = \frac{4\pi^2\alpha}{3}\frac{1}{4\sin^2\theta_W}\frac{1}{s}\int_{\tau}^{1}\frac{dx_a}{x_a}W(x_a, \frac{\tau}{x_b}), \tag{4.4}$$

where $\tau = \frac{m_W^2}{s}$, the factor 3 accounts for the colour degree of freedom and $W(x_a, x_b)$ has the form

$$W(x_a, x_b) = [U(x_a)D(x_b) + D(x_a)U(x_b)]\cos^2\theta_c +$$

$$[U(x_a)S(x_b) + S(x_a)U(x_b)]\sin^2\theta_c \tag{4.5}$$

U,D and S are the probabilities of finding u,d and s quarks (antiquarks) in the proton (antiproton) with a momentum fraction x and the parameter θ_c, the quark mixing angle known as the Cabibbo angle, the corresponding value to this angle $\theta_c = 13^0$.

Likewise, the cross-section for Z production is given by

$$\hat{\sigma}_{q\bar{q}\to Z} = \frac{4\pi^2\alpha}{3}\frac{(V_q^2 + A_q^2)}{16\sin^2\theta_W\cos^2\theta_W}\delta(x_a x_b s - m_Z^2) \tag{4.6}$$

The total cross-section is obtained as

$$\sigma_{p\bar{p}\to Z+X} = \frac{4\pi^2\alpha}{3}\frac{1}{\sin^2\theta_W}\frac{1}{s}\int_{\tau}^{1}\frac{dx_a}{x_a}Z(x_a, \frac{\tau}{x_b}), \tag{4.7}$$

where $\tau = \frac{m_Z^2}{s}$, and

$$Z(x_a, x_b) = 2[U(x_a)U(x_b)(\frac{1}{4} - \frac{2}{3}\sin^2\theta_W + \frac{8}{9}\sin^4\theta_W)$$

$$+(D(x_a)D(x_b) + S(x_a)S(x_b))(\frac{1}{4} - \frac{1}{3}\sin^2\theta_W + \frac{2}{9}\sin^4\theta_W)] \tag{4.8}$$

4.2.b The Results

On the basis of eqns. (4.2 to 4.8), we get the total cross-section for weak gauge bosons $W^{\pm}$ and Z respectively. Fig (4.2) shows the total cross-section as a function of the CM energy.

Comparing cross-sections for pp with $p\bar{p}$ collsion, the value of the cross-section for pp is smaller than the cross-section for $p\bar{p}$ at small energy, since in pp collsion the antiquarks are only from the sea quarks which carry, on the average, smaller fractional momentum at this range of energy.

Both UA1 and UA2 collabration have measured the production cross-section for both $\sigma(p\bar{p} \rightarrow W)B(W \rightarrow l\nu)$ and $\sigma(p\bar{p} \rightarrow Z)B(Z \rightarrow l^{+}l^{-})$. The uncertainties in the calculation are not only from the uncertainties in the parton distribution , but also from the unknown $O(\alpha_s^2)$ QCD corrections and the unknown mass of the top quark which enters into the branching ratios.

Although the general agreement between theory and experiments from UA1, UA2 at $\sqrt{s}$= 630 GeV and from CDF [6] at $\sqrt{s}$= 1.8 TeV is remarkably good, but there is no information yet on the top quark mass. With more increase in an experimental statistics in the next few years, and with complete calculation of higher order corrections to W and Z production the agreement will become better. It has been mentioned that the total W and Z cross-sections receive a large next-to-leading order perturbative QCD correction of order 30%. Also higher order QCD processes, for example $q\bar{q} \rightarrow W(Z) + ng$ give rise to a multijet production with W and Z, which represents another important background for many 'new physics' processes and provides a good quantitative explanation of the data.

In all these calculation we used the structure functions of ref [7], set 1 with Λ_{QCD} =.107 GeV .

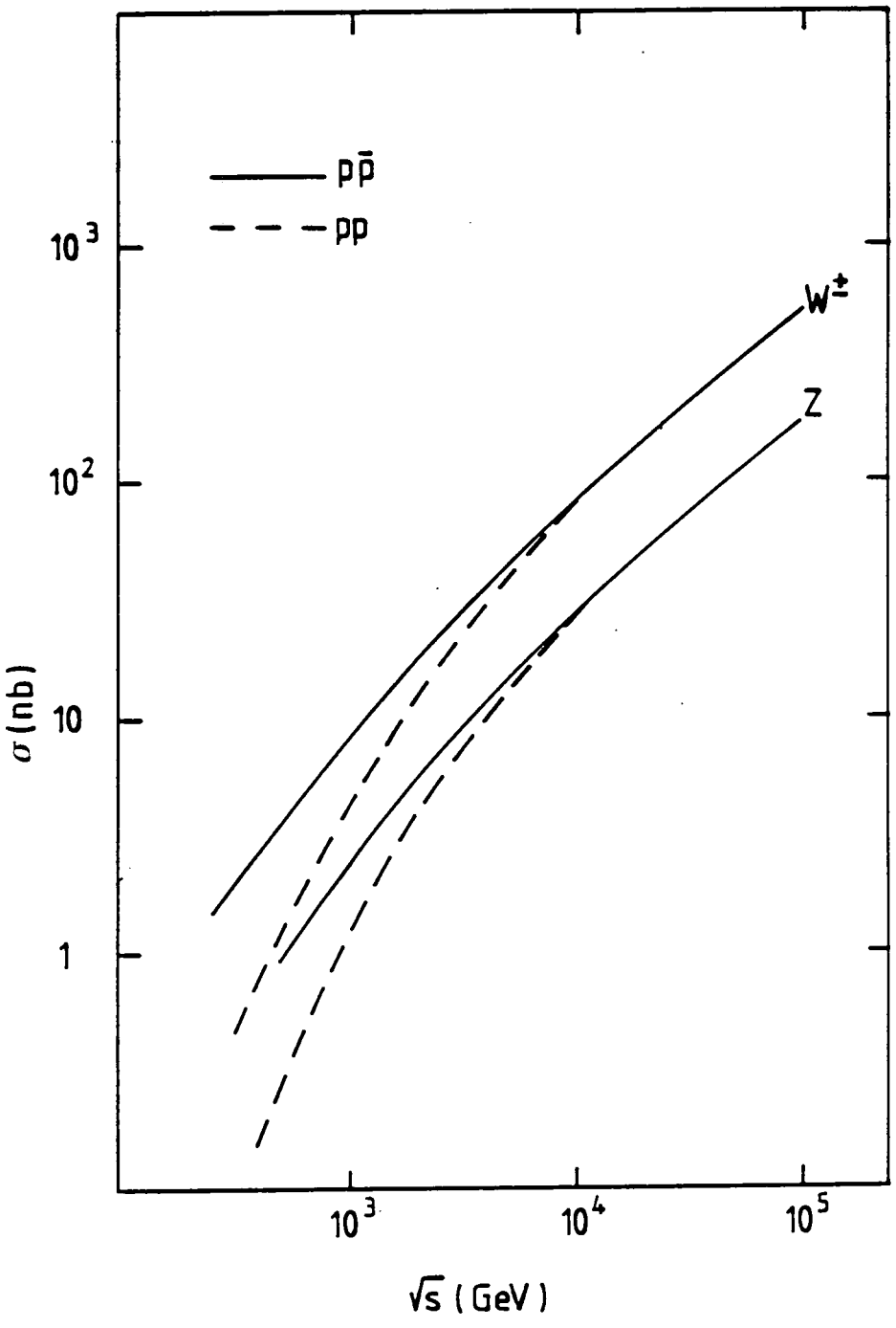

Fig. (4.2) Total cross-section for $W^{\pm}$ and Z production as a function of $\sqrt{s}$.

4.3 Gauge Boson Pair Production at Hadron Colliders

The standard electroweak model has been successful in describing physics below the 100 GeV scale. However this model contains too many undetermined parameters to be considered as a fundamental theory, so it is interesting and important to search and test this theory.

The potential studies of the electroweak gauge boson pair production was recognized along times ago [8]. Pair production of gauge bosons is important for various reasons. Firstly, it will provide us with another important test of the structure of the standard electroweak theory at high energy range. It also tests the cancellations which are expected in the theory as an indication of the renormalisability of gauge theories. Finally, the W^+ W^- and Z Z final state is considered as the most promising channel and may give a significant background for the detection of Higgs boson and for possible new degrees of freedom.

This production has been recognised at high energy hadron-hadron and e^+e^- colliders [8]. The cross-sections are not particularly large at a realisable range of energies. In this section we will focus on W^+W^- and Z Z pair production rate at pp and $p\bar{p}$ collisions.

4.3.a W^+W^- Pair Production at Hadron Colliders

The Feynman for the process $q_i\overline{q}_i \rightarrow W^+W^-$ are shown in fig. (4.3)

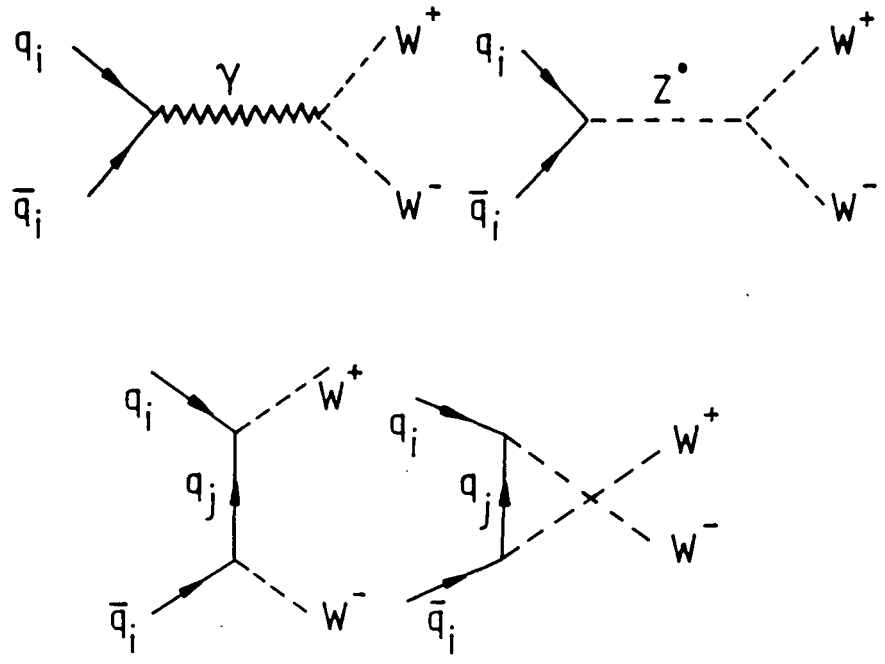

Fig. (4.3) Lowest order Feynman diagrams for $q\overline{q} \rightarrow W^+W^-$

where the Dirac point fermions here are quarks which annihilate to produce boson pairs.

The amplitude for this process can be calculated from the lowest order and has the form

$$T_{\mu\nu} = i(Q_i\frac{e^2}{s} + e_Z\frac{g_v^i + g_a^i\gamma_5}{s - m_Z^2})[g_{\mu\nu}(\not{p}_1 - \not{p}_2) + \gamma_\mu(2p_2 + p_1)_\nu - \gamma_\nu(2p_1 + p_2)_\mu]$$

$$-2i(1+\gamma_5)\sum_j G_{v-a}^2[\theta(-Q_i)\frac{(\gamma_\mu \not{k}_1 \gamma_\nu)}{t} + \theta(Q_i)\frac{(\gamma_\nu \not{k}_2 \gamma_\mu)}{u}], \qquad 4.9$$

where the usual variables in eqn (4.9) are defined

$$s = (k_1 + k_2)^2 = (p_1 + p_2)^2$$

$$t = l_1^2 = (k_1 - p_1)^2 = (p_2 - k_2)^2$$

$$u = l_2^2 = (k_1 - p_2)^2 = (p_1 - k_2)^2$$

$$s + t + u = 2m_W^2, \tag{4.10}$$

and the weak coupling defined as

$$g_v^i = 2^{1/4} \frac{m_W}{\cos\theta_W} \sqrt{G_F} a_i, \tag{4.11}$$

$$g_a^i = 2^{1/4} \frac{m_W}{\cos\theta_W} \sqrt{G_F} b_i \tag{4.12}$$

with

$$a_u = a_c = \frac{1}{2} - \frac{4}{3}\sin^2\theta_W, \quad a_d = a_s = -\frac{1}{2} + \frac{2}{3}\sin^2\theta_W,$$

$$b_d = b_s = -\frac{1}{2}, \quad b_u = b_c = \frac{1}{2} \tag{4.13}$$

The total differential cross-section for the process (from Brown and Mikaelian (1979) [8]) has the form

$$\frac{d\sigma}{dt} = \frac{2\pi\alpha^2}{s^2}[[(Q_i) + \frac{e_Z g_v^i}{e^2}\frac{s}{s - m_Z^2})^2 + (\frac{e_Z g_a^i}{e^2}\frac{s}{(s - m_z^2)})^2]A(s,t,u)$$

$$+4[Q_i + \frac{e_Z(g_v^i + g_a^i)}{e^2}\frac{s}{s - m_Z^2}]\sum_j (G^{ij}_{(v-a)/e})^2[\theta(-Q_i)I(s,t,u) - \theta(Q_i)I(s,u,t)]$$

$$+8[\sum_j (G^{ij}_{(v-a)/e})^2]^2[\theta(-Q_i)E(s,t,u) + \theta(Q_i)E(s,u,t)]], \tag{4.14}$$

where

$$A(s,t,u) = (\frac{ut}{m_W^4} - 1)(\frac{1}{4} - \frac{m_W^2}{s} + 3\frac{m_W^4}{s^2}) + \frac{s}{m_W^2} - 4,$$

$$I(s,t,u) = (\frac{ut}{m_W^4} - 1)(\frac{1}{4} - \frac{1}{2}\frac{m_W^2}{s} - \frac{m_W^4}{st}) + \frac{s}{m_W^2} - 2 + 2\frac{m_W^2}{t},$$

$$E(s,t,u) = (\frac{ut}{m_W^4} - 1)(\frac{1}{4} + \frac{m_W^4}{t^2}) + \frac{s}{m_W^2} \tag{4.15}$$

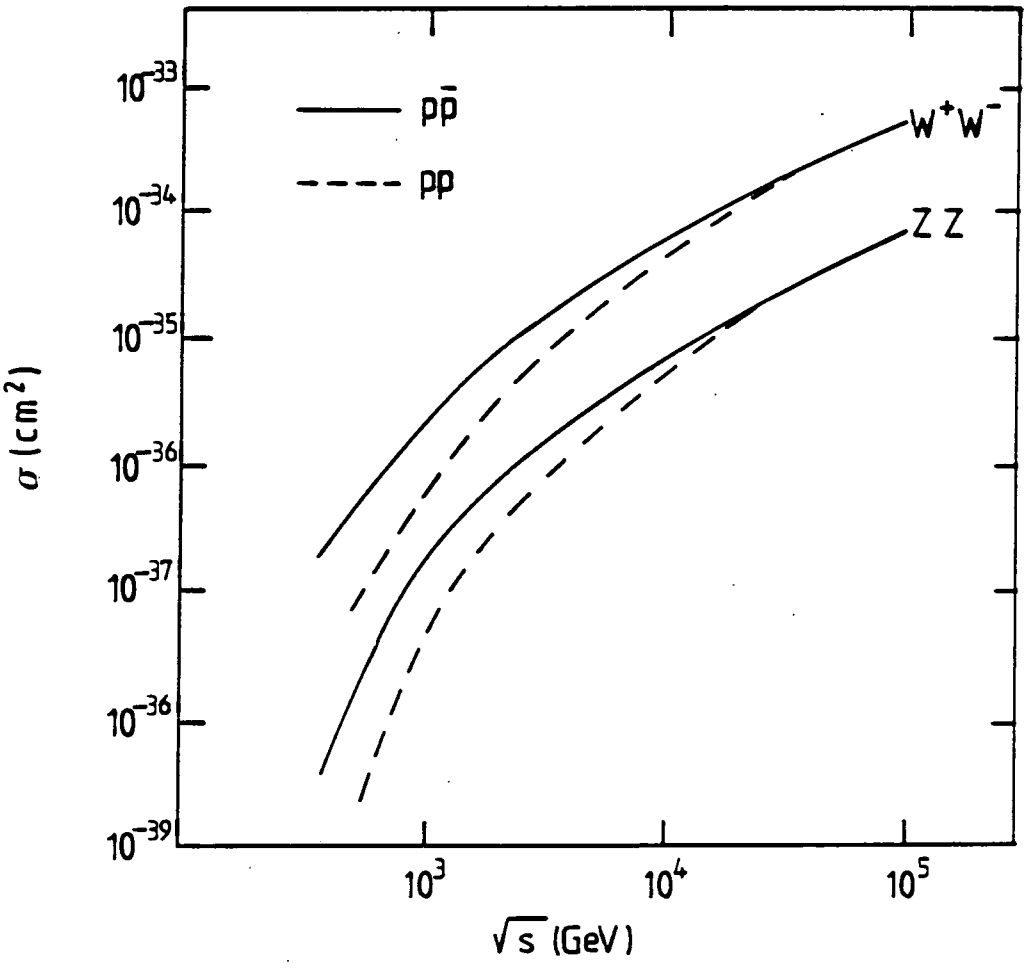

Fig. (4.4) The integrated cross-section for the two parton scattering of a gauge boson pair production as a function of energy $\sqrt{s}$.

The total cross-section for $W^{\pm}$ pair production can be calculated from

$$d\sigma = \frac{1}{flux}\frac{1}{2}\sum_{q=u,d,c,s}|F|^2 dLIPS, \qquad 4.16$$

where the two body phase space final state is given by

$$dLIPS = (2\pi)^4\delta^4(p_1 + p_2 - k_1 - k_2)\frac{d^3p_1}{2E_1(2\pi)^3}\frac{d^3p_2}{2E_2(2\pi)^3},$$

finally, the total cross-section to produce a W^+W^- is given by

$$\sigma(p\bar{p} \rightarrow W^+W^-X) = \frac{1}{3}\sum\int_0^1 dx_a dx_b[f_i(x_a,Q)f_{\bar{i}}(x_b,Q) + f_{\bar{i}}(x_a,Q)f_i(x_b,Q)]$$

$$\sigma(q\bar{q} \rightarrow W^+W^-) \qquad 4.17$$

Integrating eqn. (4.17), we get the total cross-section σ at CM energy. The distributions $f_i(x,Q)$ are summed over colour, the factor 1/3 is needed since $q_i\bar{q}_i$ annihilate to form a colour singlet.

Fig. (4.4) shows the total cross-section for W^+W^- pair as a function of CM energy for pp (solid line) and $p\bar{p}$ (dashed line) collisions. Comparing pair production with single intermediate gauge boson production, it is clear that the cross-section for pair production is smaller by three orders of magnitude than single gauge boson production.

Also figs. (4.13,4.14,4.15) show the invariant mass distribution for W^+W^- production. The calculations have been done for three types of collider energy, SSC (40 TeV) , LHC (17 TeV) and the ELOISATRON (200 TeV).

4.3.b Z Z Pair Production at Hadron Colliders

The Feynman diagrams for the process

$$q\bar{q} \rightarrow ZZ$$

are shown in fig. (4.5)

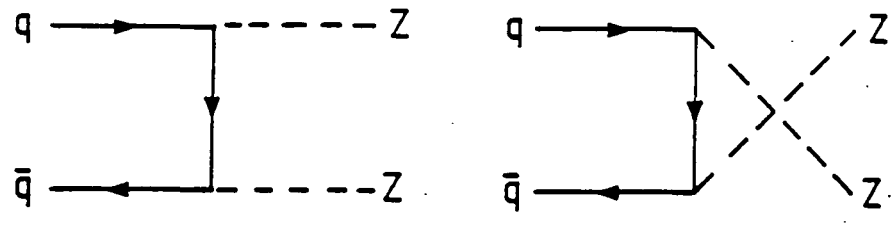

Fig. (4.5) Lowest order Feynman diagrams for $q\bar{q} \rightarrow ZZ$

As we mentioned earlier in the section, this process is very important and it could be the promissing background to the production and detection of Higgs bosons.

The matrix element for the lowest order of fig. (4.4) is given by

$$T_{\mu\nu} = -i(g_v^2 + g_a^2 + 2g_v g_a \gamma_5)(\gamma_\mu \frac{1}{\not{l}_1} \gamma_\nu + \gamma_\nu \frac{1}{\not{l}_2} \gamma_\mu), \qquad 4.18$$

and the differential cross section is given by [8]

$$\frac{d\sigma}{dt} = \frac{2\pi\alpha^2}{s^2} \frac{(g_v^4 + g_a^4 + 6g_v^2 g_a^2)}{e^4} [\frac{t}{u} + \frac{u}{t} + \frac{4m_Z^2 s}{tu} - m_Z^4 (\frac{1}{t^2} + \frac{1}{u^2})] \qquad 4.19$$

On the basis of eqns. (4.16, 4.17, 4.19), we get the quark-antiquark total cross-section σ at CM energy. The distributions $f_i(x, Q)$ are summed over colour, the factor 1/3 is needed since $q_i\bar{q}_i$ must have zero colour. Here we include a statistical symmetry factor of 1/2 because of the identical particles in the final state.

Fig (4.4) shows the total cross-section for Z^+Z^- pair as a function of CM energy for pp (solid line) and $p\bar{p}$ (dashed line) collisions. In all these calculations we used the set 1 structure functions from ref. [7].

4.4 Double Parton Scattering Mechanism

The Drell-Yan mechanism, which describes the production of large mass lepton pairs in hadron collider interactions due to the annihilation of single quarks, has played an important role in determining of the structure functions and testing the ideas of the parton model and later the quantum chromodynamics.

In addition to the single subprocess hard scattering mechanism, there can also be events featuring two hard parton-parton collisions [9,10] in parallel.

Fig (4.6) shows the two mechanisms which are responsible for producing gauge boson pair in hadron collision.

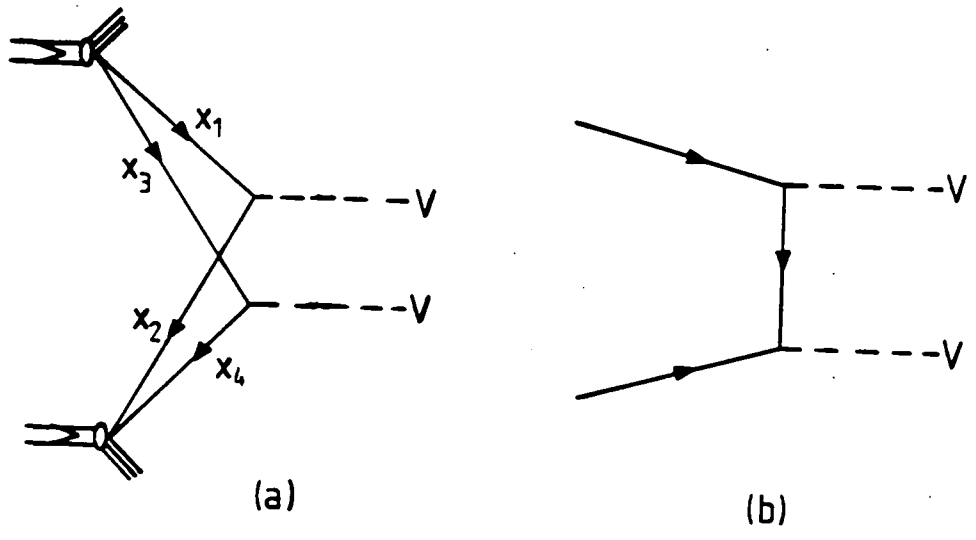

Fig. (4.6) Production of two gauge bosons by (a) double and (b) single quark-antiquark annihilation.

The first mechanism produces the gauge pairs through two Drell-Yan annihilations, while the second mechanism produces the gauge pairs through single Drell-Yan annihilation.

The double scattering mechanism is important because it could provide some significant background to new particle searches, and also the multiple production of weak bosons via double parton scattering can be considered as a potential

background for the detection and production of Higgs boson in future hadron colliders.

Recently, the AFS collaboration at the CERN ISR have claimed evidence for double scattering in proton-proton collisions [11]. Such events could not be accounted for in standard QCD $2 \rightarrow 4$ hard scattering subprocesses, but the UA1 and UA2 experiments failed to observe multiple parton interactions at $\sqrt{s}$=630 GeV.

The total cross-section for four jet events from the double disconnected scattering, which represents the alternative source of four jets, can be estimated (neglecting any correlation between quarks/gluons inside the nucleon) as

$$\sigma^{DS} = \frac{\sigma^{2\rightarrow 2}\sigma^{2\rightarrow 2}}{\sigma_{eff}}, \qquad 4.20$$

where $\sigma^{2\rightarrow 2}$ is the two jet total cross section. Thus, the size of $\sigma^{2\rightarrow 2}$ determines the importance of σ_{DS}.

The explicit expression for the double parton scattering cross-section (when the nucleon constituents, however, are correlated) has been worked out [10]. The cross-section is determined as a product of two parton cross-sections $d\sigma_{ij}$, with the appropriate two parton momentum distributions $q(x_k, x_l)$ as

$$d\sigma = \frac{1}{\sigma_{eff}} \int dx_1 dx_2 dx_3 dx_4 \sum_{i,j,k,l} q_{ij}(x_1, x_3) q_{kl}(x_2, x_4) d\sigma_{12} d\sigma_{34}, \qquad 4.21$$

where the factor σ_{eff} in eqns. (1.20,1.21) represents the hadronic cross-section which estimates the size of a hadron [12]. The reason for this is that because the probability of a second interaction process is proportional to the flux factor accompanying quarks and their flux is thus inversely proportional to the area of a hadron.

A more accurate value for σ_{eff} requires more detailed information on the hadron structure. In all our analysis we choose: $\sigma_{eff} = \pi R^2$= 2.5 mb, where this

is the value presented by the AFS collabration [11] who gave evidence for double parton scattering at the CERN ISR. Good agreement was obtained by including a double parton scattering component of this value.

The sum $\sum_{i,j,k,l}$ is taken over all quark combinations.

In eqn. (4.20) $q(x_1, x_3)$ represents the joint probability of finding quarks with momentum fraction x_1, x_3 inside the hadron, which has a quasi-factorised form and sufficiently represented by

$$q(x_1, x_3) = q(x_1)q(x_3)(1 - x_1 - x_3), \tag{4.22}$$

where $q(x_1), q(x_3)$ represents the single quark momentum distribution and the factor $(1 - x_1 - x_3)$ is required by phase space considerations.

The joint probabilities in, for example, a proton have the form

$$q^p_{uu}(x_1, x_3) = \frac{1}{4}u_v(x_1)u_v(x_3) + u_v(x_1)sea(x_3) + sea(x_1)u_v(x_3) + sea(x_1)sea(x_3)$$

$$q^p_{dd}(x_1, x_3) = d_v(x_1)sea(x_3) + sea(x_1)d_v(x_3) + sea(x_1)sea(x_3)$$

$$q^p_{ud}(x_1, x_3) = u_v(x_1)d_v(x_3) + u_v(x_1)sea(x_3) + sea(x_1)d_v(x_3) + sea(x_1)sea(x_3)$$

. 4.23

There are many other such quark pairs in each hadron, which have to be considered in the calculation.

With the above framework we have carried out our analysis for the processes

$$q(x_1)q(x_3) + \overline{q}(x_2)\overline{q}(x_4) \rightarrow W^+W^-, ZZ \tag{4.24}$$

We have evaluated the total cross-section for the process (4.24), by integrating over eqn. (4.21), where the summation is over all pairs of quarks and antiquarks in both hadrons, which can give rise to a pair of $W^{\pm}$ and a Z using the structure functions from Ref [7].

In figs. (4.7,4.8) we present the total cross-sections for W^+ W^-, ZZ pair as a function of CM energy, where in each figure we show the total cross-sections from single scattering processes as well. It is clear that the cross-sections from single scattering process are larger than from double scattering mechanism especially at low values of energy, where as at high energies the double scattering cross-sections are rising faster with energy and it become smaller only by a factor of 3-4 for W^+ W^- and 6-7 for Z Z.

If Higgs mass is greater than $2m_W$ then the dominant decay of the Higgs are into W^+ W^- and Z Z. The dominant physics background comes from the single process $q\overline{q} \rightarrow W^+W^-$ or Z Z and from the double scattering process $qq + \overline{qq} \rightarrow W^+W^- or Z^0Z^0$.

Higgs bosons can be produced in two significant production mechanisms [13]. The first is through the gluon fusion mechanism in which two gluons couple to a heavy fermion loop. The second is through WW fusion mechanism in which the incident quarks emit a virtual W which subsequently collides to form a Higgs boson.

At high energies the first mechanism is important because the gluon-gluon luminosity is much higher than the quark-quark luminosity. We shall discuss and calculate this further in chapter 6 .

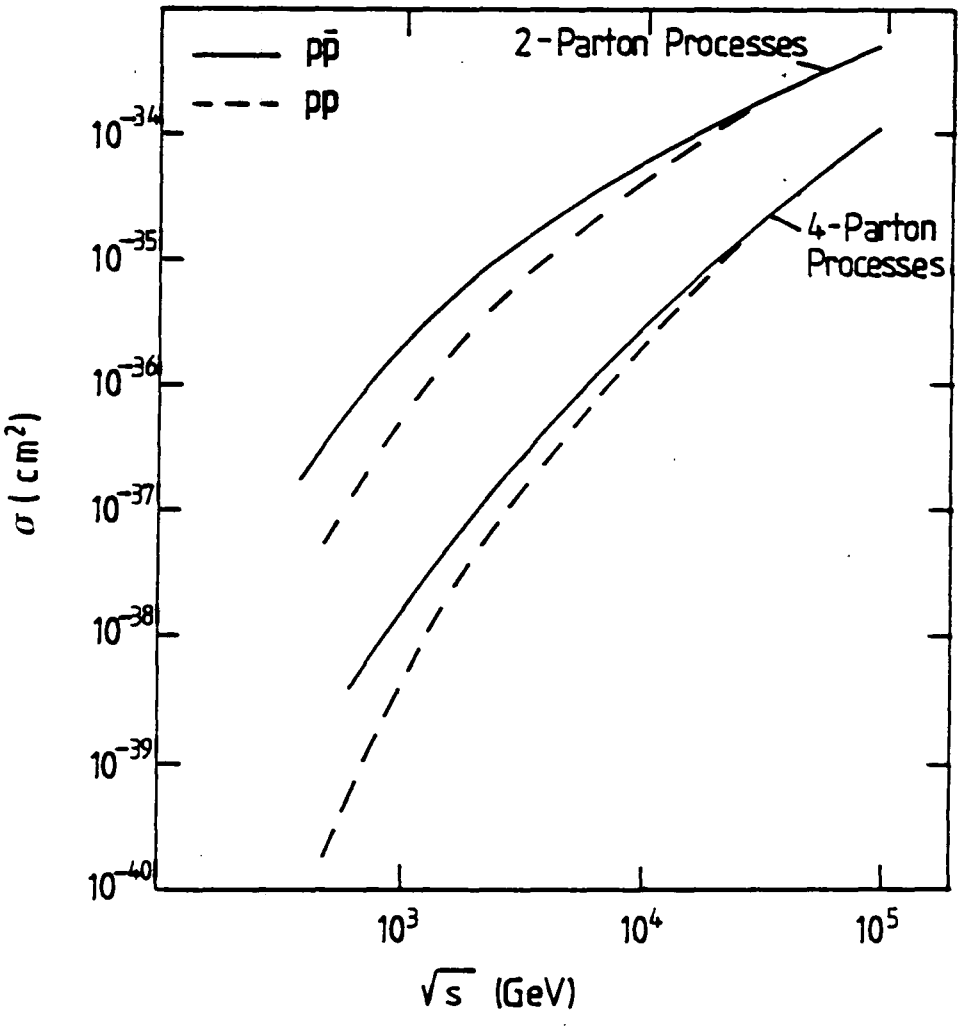

Fig. (4.7) The integrated cross-section for two and four parton scattering of W^+W^- pair production as a function of CM energy.

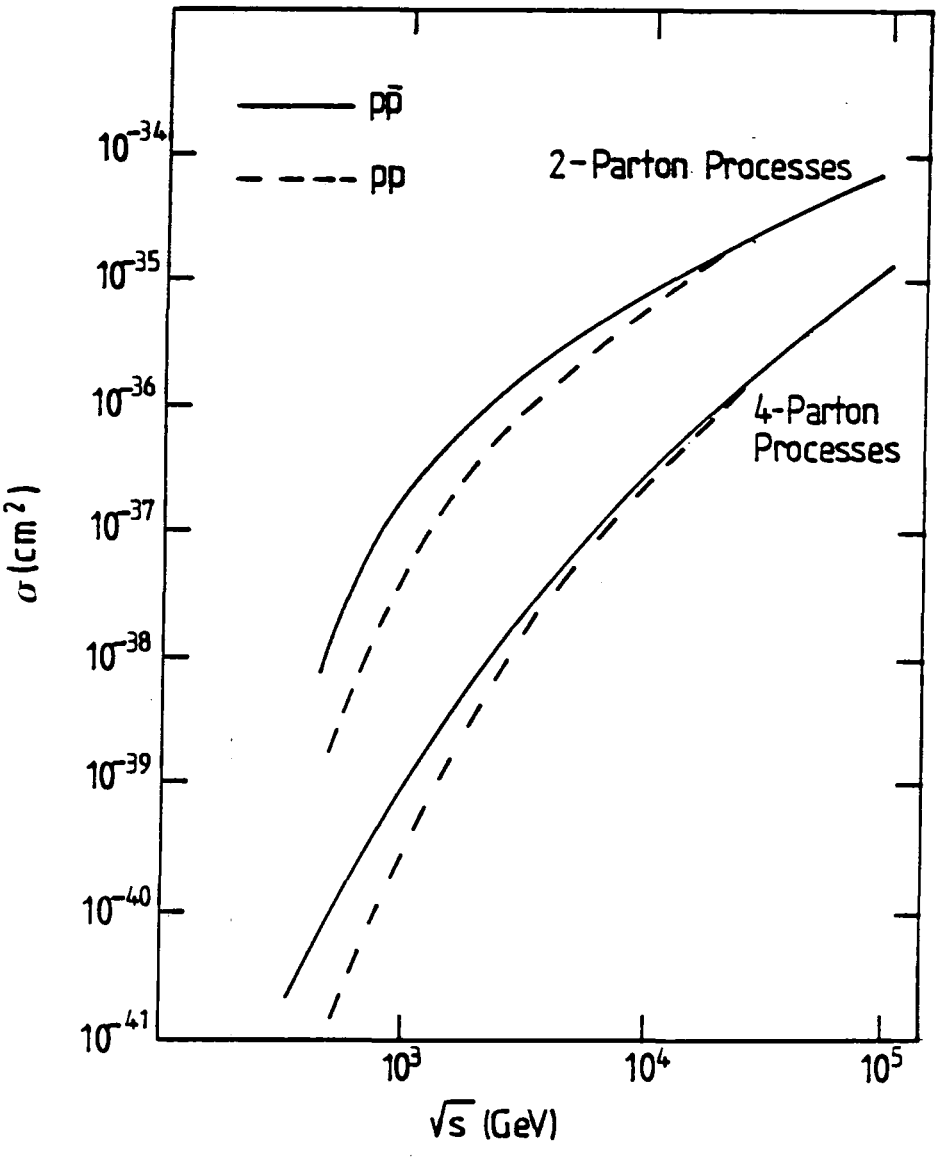

Fig. (4.8) The integrated cross-section for two and four parton scattering of ZZ pair production as a function of CM energy.

4.5 Like-Charge W Pair Production in Single and Double Parton Scattering Mechanisms

In this section we shall discuss the possibility of the production of like charged W^+W^+ and W^-W^- at pp colliders in single and double parton scattering mechanism.

Recently Gunion et.al. [14], and Dicus and Vega [15] have calculated the invariant mass distribution for the electroweak strong processes $pp \rightarrow W^+W^+ + X$ via gluon exchange for both SSC and LHC energies, where the complete set of single scattering is represented in fig. (4.9)

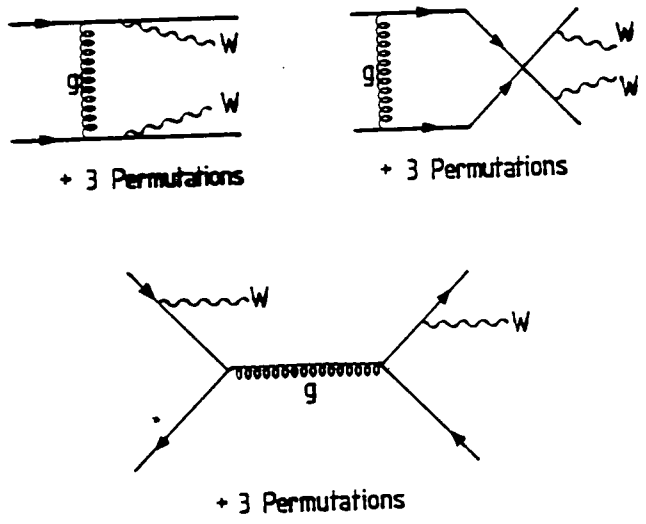

Fig. (4.9) Complete set of diagrams for the process $pp \rightarrow W^+W^+ + X$.

This calculation is of great interest since the gluon exchange mechanism is considered to be the dominant production mechanism for like-charged W pairs at high energies like that of at SSC and this is considered as the promising background to Higgs boson production. Another interesting reason is that this process provide the dominant background for the production of doubly charged Higgs which is produced via WW fusion.

In this section we are calculating the total cross-section for like-charged W

pair production using double scattering parton mechanism. We also compare the mass invariant distribution of single and double scattering processes.

As we discussed earlier in section (4.4), the total scattering cross-section for double scattering process is determined by the product of two single parton cross-section, with an appropriate two parton momentum distribution as in the form

$$d\sigma = \frac{1}{\sigma_{eff}} \int dx_1 dx_2 dx_3 dx_4 \sum_{i,j,k,l} q_{ij}(x_1, x_3) q_{kl}(x_2, x_4) d\sigma_{12} d\sigma_{34}, \qquad 4.25$$

where all the kinematics is as defined in the last section except the summation is over all quark and atiquark pairs in both hadrons, which can give rise to a pair of $W^+ W^+$ and $W^- W^-$.

In fig. (4.10), we show the total like charged W production cross-section for $p\bar{p}$ collision versus CM energy in double scattering process. The total W^+W^- production cross section from single scattering is present.

The invariant mass distribution of like W pair production for pp collision at $\sqrt{s} = 40$ TeV is shown in fig (4.11). We used set 1 of the Q^2 dependent gluon distribution of MRS [7] with $\Lambda_{QCD} = 0.107$ GeV. The invariant mass falls sharply with increasing W pair mass which means that the background from W^+W^+ and W^-W^- to Higgs boson detection is small as $m_H >> 2m_W$. For completeness the invariant mass distribution of W^+W^- for pp collision from the lowest order contribution is also present. We obtained similar results for LHC (17 TeV) and ELOISATRON (200 TeV) energies in figs. (4.12,4.13) respectively.

In figs. (4.14),(4.15), we try to compare the mass invariant distribution of like charged W pair production for pp collision from double scattering process with single scattering via gluon exchange. Curves are shown for double scattering (solid line) and for single scattering via gluon exchange (dashed lines) as given in Ref. [15].

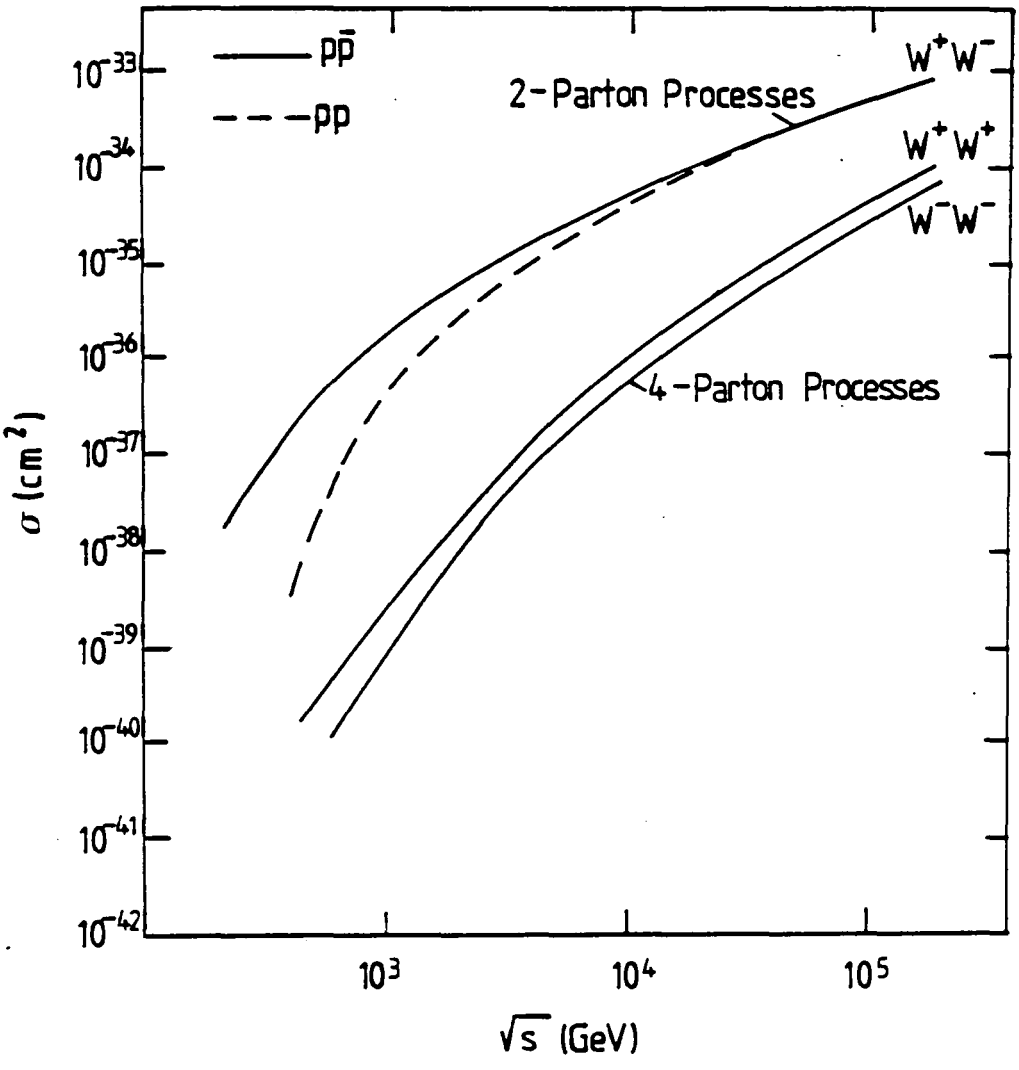

Fig. (4.10) The total cross-section for the production of W^+W^+ and W^-W^- pair production. The total cross-section for W^+W^- is also present.

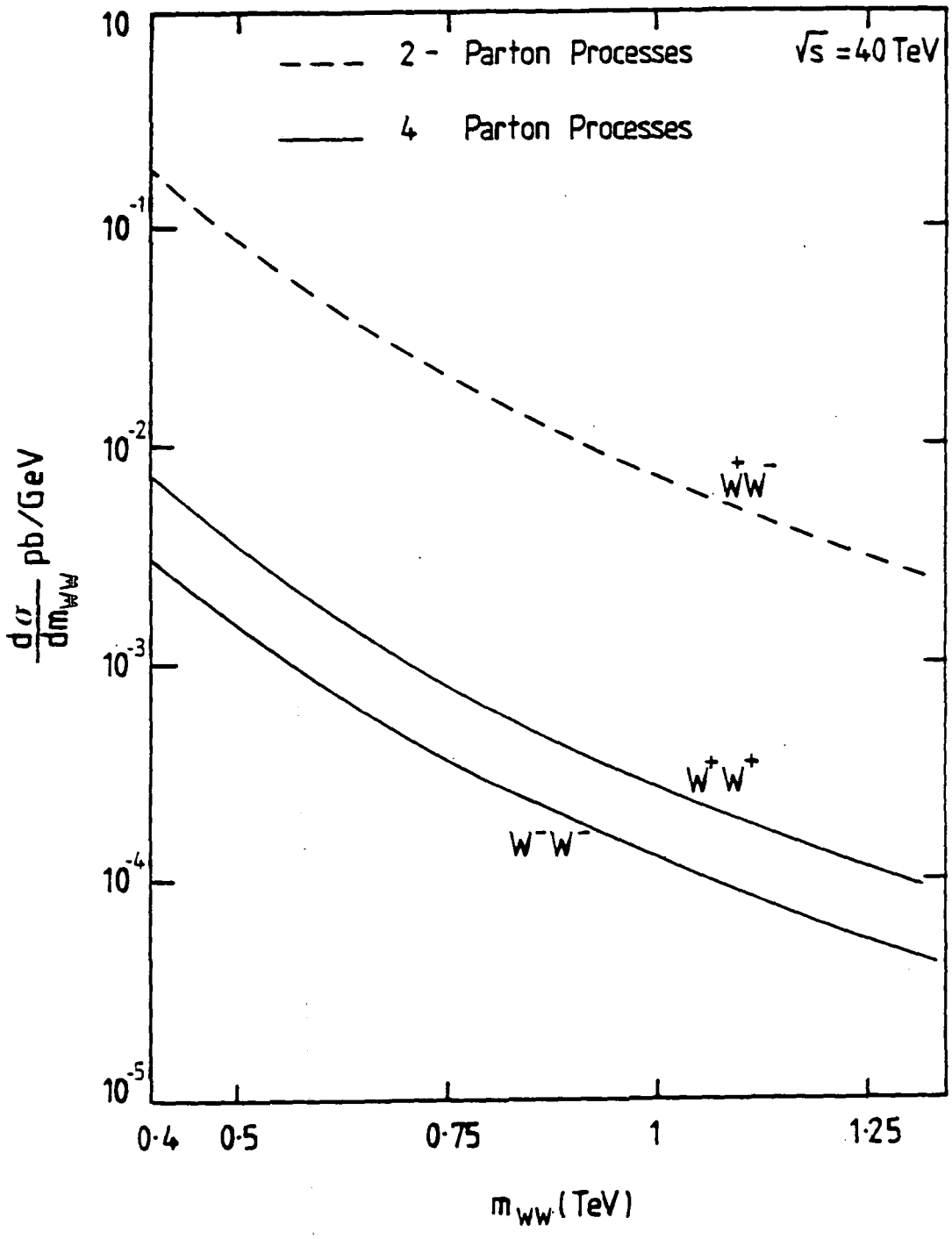

Fig. (4.11) The invariant mass distribution for $p\bar{p} \to W^+W^+ + X$, $pp \to W^-W^- + X$ and $pp \to W^+W^- + X$ in pb/GeV. Results shown are for no rapidity cuts. $\sqrt{s}$ is 40 GeV.

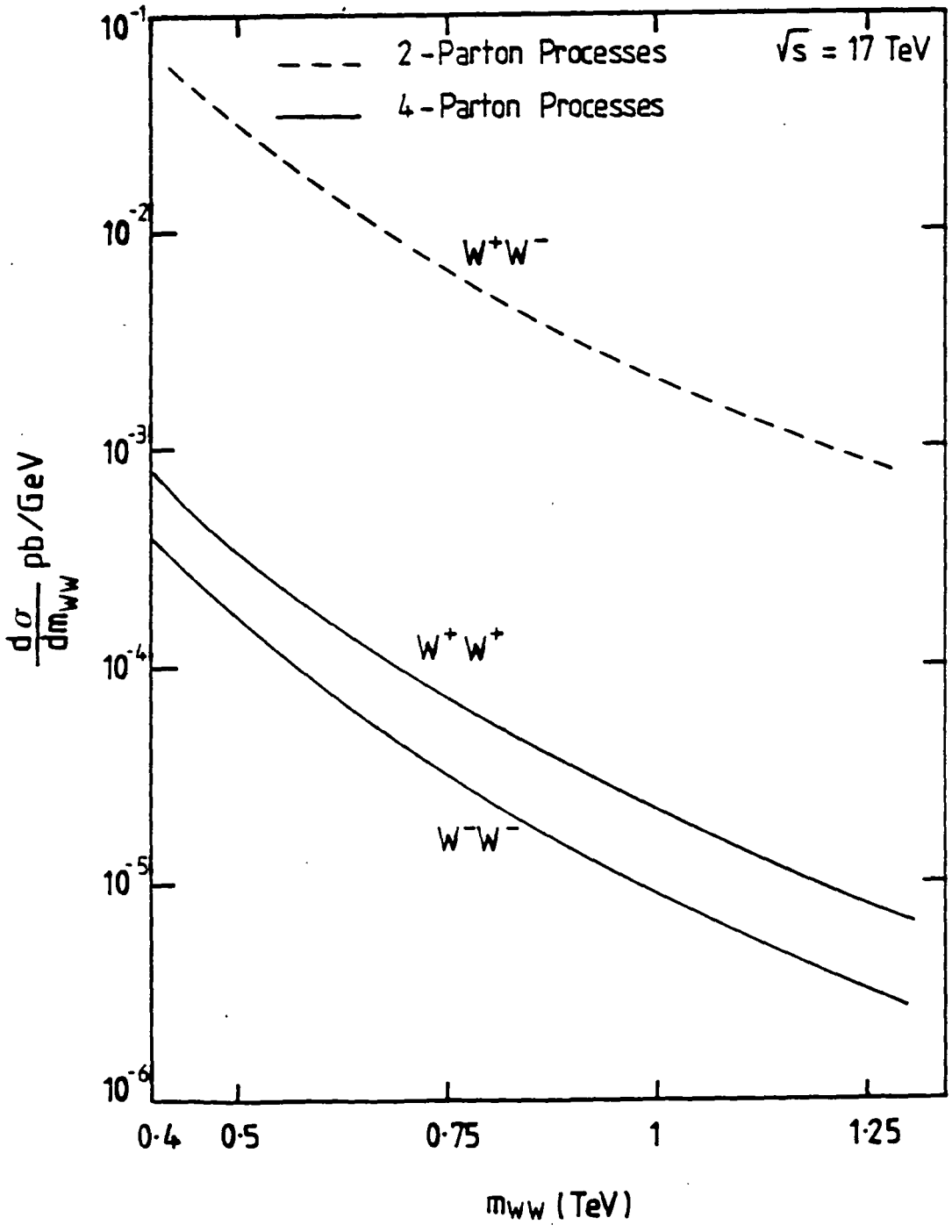

Fig. (4.12) Same as Fig. (4.11) with the exception of $\sqrt{s}$ which is 17 TeV here.

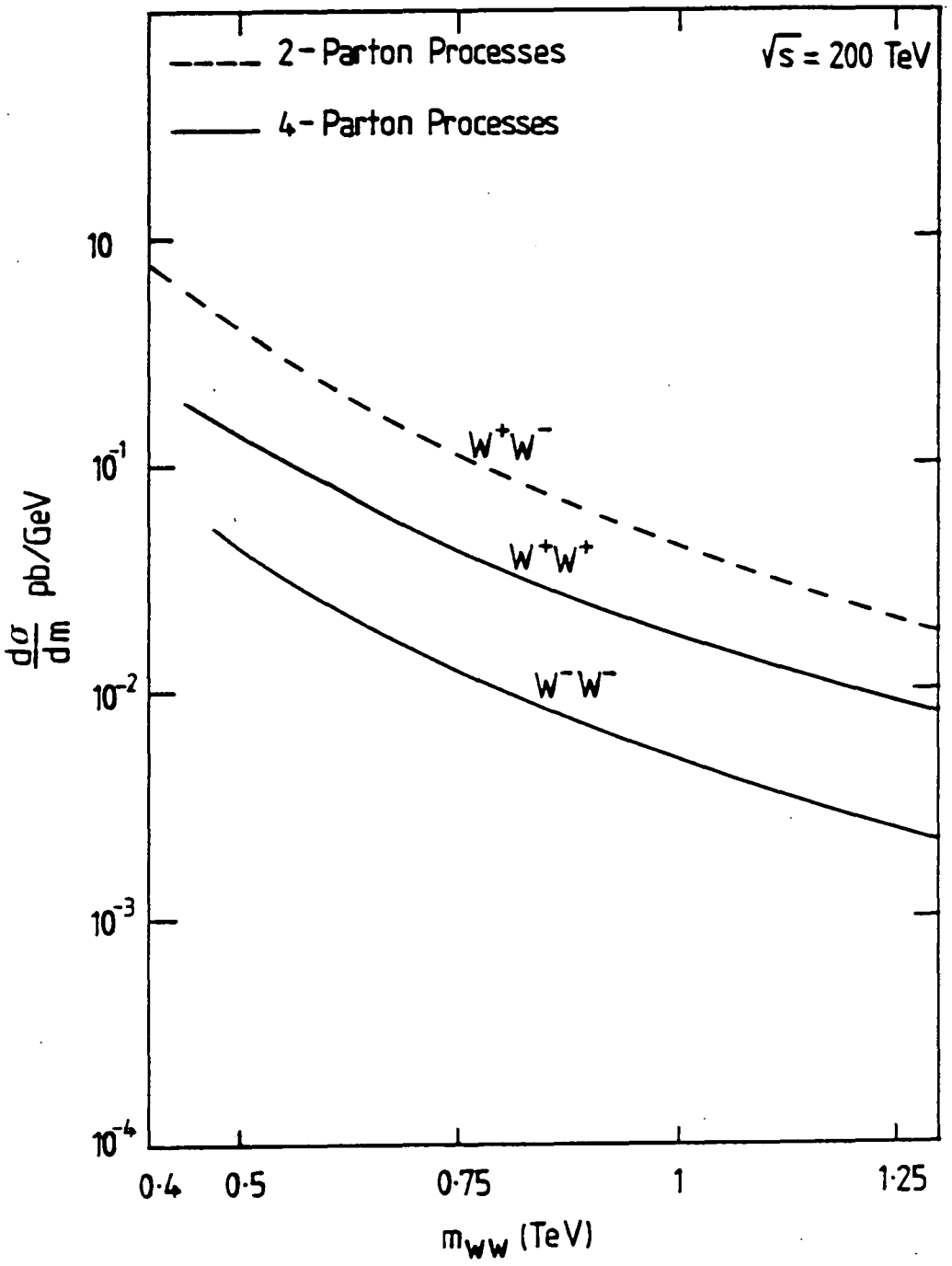

Fig. (4.13) Same as Fig. (4.11) with the exception of $\sqrt{s}$ which is 200 TeV here.

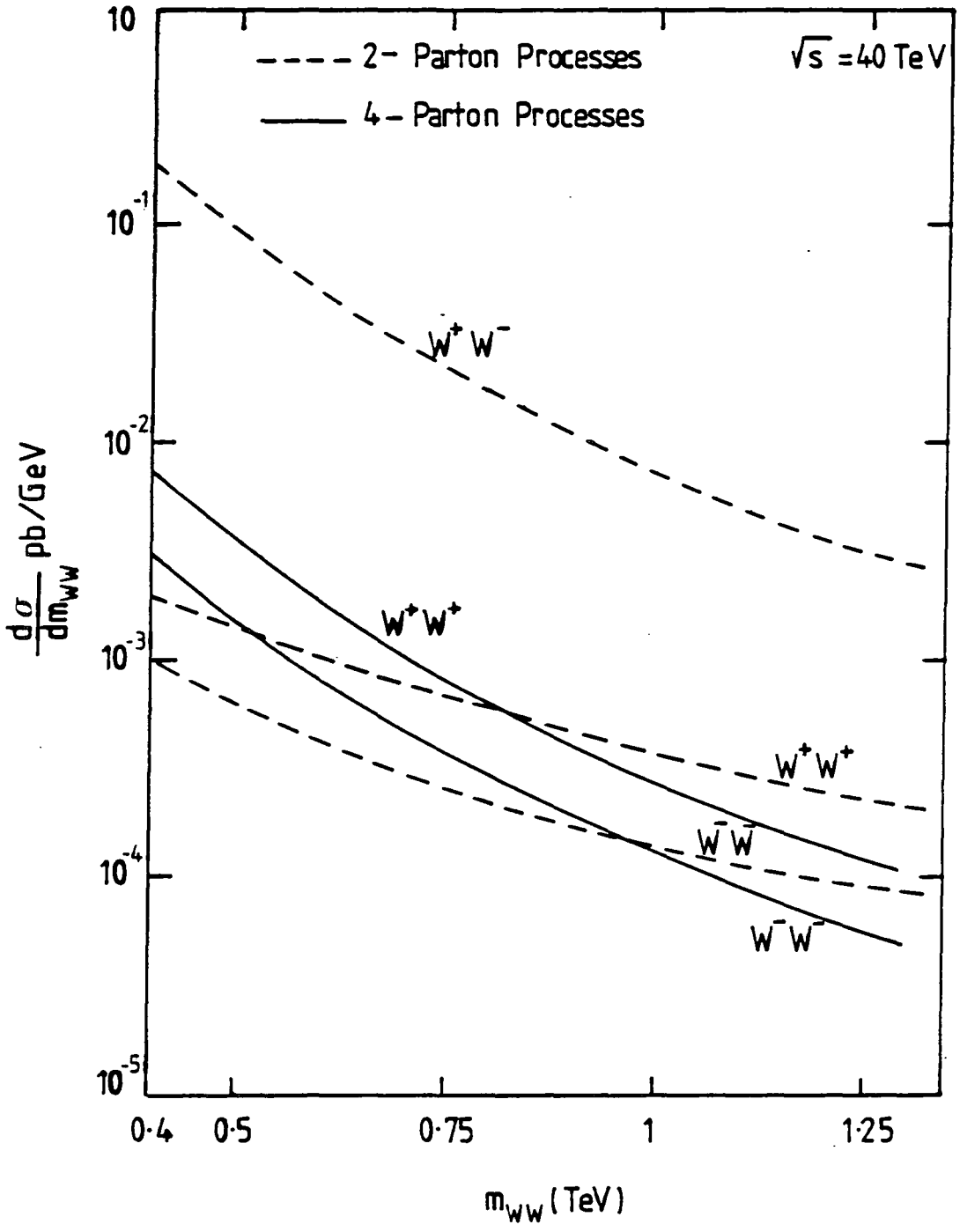

Fig. (4.14) The invariant mass distribution for $pp \to W^+W^+ + X$, $pp \to W^-W^- + X$ and $pp \to W^+W^- + X$ in pb/GeV. Results shown for single and double scattering processes.

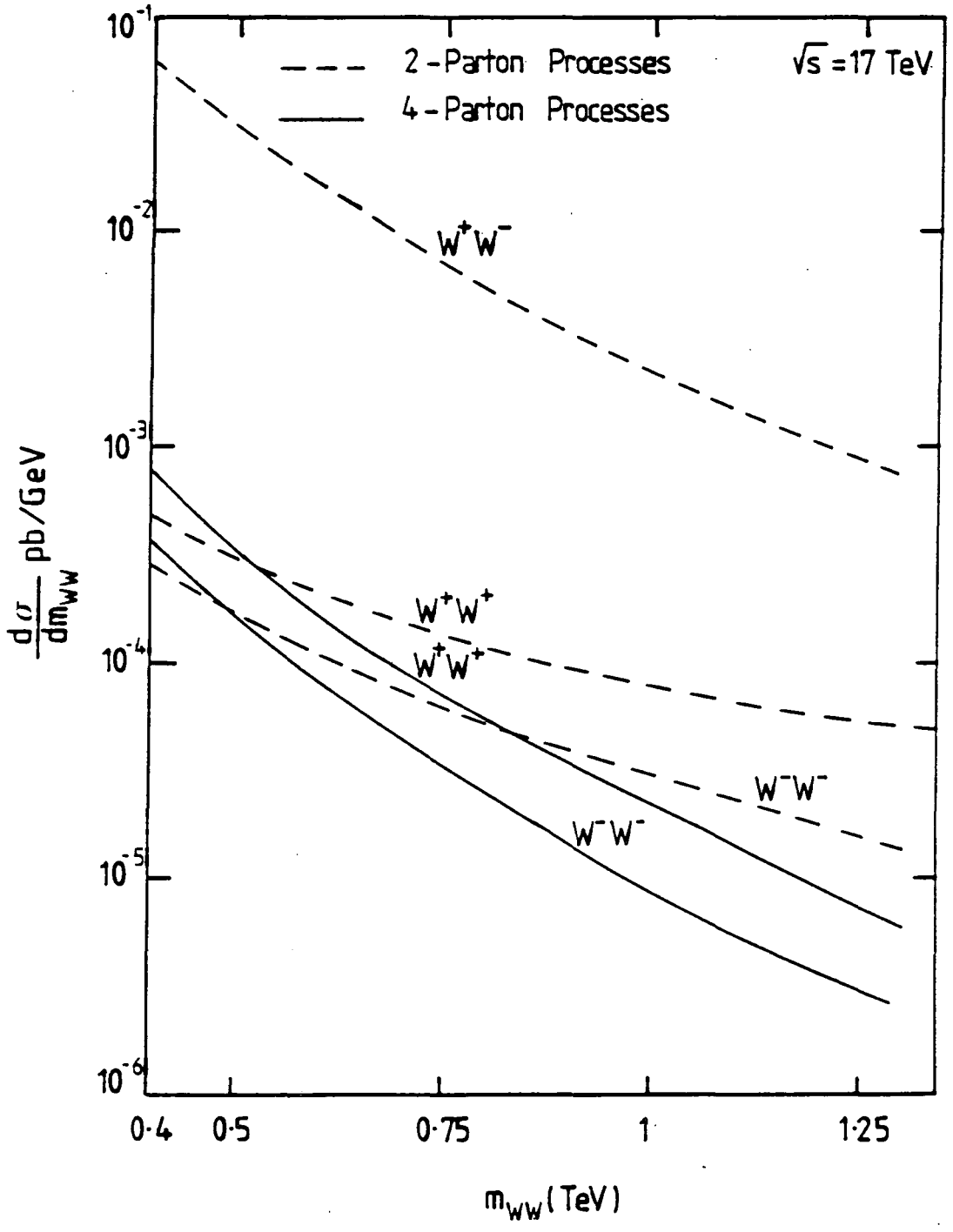

Fig. (4.15) Same as Fig. (4.14) with the exception of $\sqrt{s}$ which is 17 TeV here.

To summarise, we conclude that the $W^{\pm}$ and Z pair production from double scattering mechanism is smaller than the producton from single scattering at small energies, while they are comparible at high values of energy. The like charged W production cross-section and the invariant mass distribution agree better with single scattering process. For W^+W^+ and W^-W^- we find that the cross-sections give a significant number of events at SSC energy, while at LHC the number is smaller by a factor 3-5 but still the number is not negligable.

4.6 Discussion

At the outset of this chapter, we have stressed that a multi-TeV hadron collider should provide the means to test thoroughly the preductions of the standard model, to illuminate the physics of electroweak symmetry breakdown and to explore the unknown. We have calculated and discussed the extrapolation of the hard collisions in pp and $p\bar{p}$ colliders at $\sqrt{s} = 17$, 40 and 200 TeV relevant to the LHC, SSC and ELOISATRON energies respectively. We have calculated the production cross-sections for a variety of hadronic collisions which tests the standard model.

The standard processes that we have dealt in some depth in this chapter include the production of IVB production $W^{\pm}$ and Z , pair production of gauge bosons W^+W^-, W^+W^+, W^-W^- and ZZ. In addition to the single scattering subprocess we have concentrated on and calculated events coming from double scattering mechanism, which is believed to be important at high energies (TeV scales) so it may provide important background rates for new physics.

The way which we have used here is straightforward, in order to evaluate the cross-section numerically we have used the routine Vegas for the integration of the matrix elements over the phase space, which is similar to the usual Monte Carlo generation.

In order to discuss the results it is useful to point out some of the inherent

uncertainties affect which are effecting the final results and they are

1. Structure functions : comparing different structure functions like Duke-Owens [16], EHLQ [3] and finally Martin et. al [7], for the same process, the results are not exactly same which can be accounted due to the uncertainty resulting from the limited knowlege of Λ_{QCD} and the gluon distribution functions.

2. For the choice of Q^2 in $G(x, Q^2)$ and $\alpha_s(Q^2)$, one can look for the dependence of the results on Q.

3. Higher orders in general which is called ' K-factors '. This must be evaluated for the calculation of the total cross section for any process . In general the fully inclusive cross-section should have the form

$$\sigma(p\overline{p} \rightarrow nV + X) = \sigma_0 + \sigma_1\alpha_s(Q^2) + \sigma_2(\alpha_s(Q^2))^2 + ..., \qquad 4.26$$

where V is vector gauge boson, σ_0 is the lowest order cross-section, σ_1 and σ_2 is the corrections from first and second order QCD respectively.

Besides these uncertainties, the results shows a good agreement with some related works [8,9,10], in addition to that we get a comparable results between single parton scattering and two hard parton-parton scattering in parallel.

CHAPTER 5

MULTIPLE GAUGE BOSON PRODUCTION IN HIGH ENERGY PROTON PROTON COLLISIONS

5.1 Intoduction

In the last chapter we evaluated the results of the total cross-section for different hard scattering processes associated with the standard model of weak and electromagnetic interactions. Particularly, we focused on intermediate vector boson (W,Z) and pair gauge boson ($W^+W^-, ZZ, W^+W^+, W^-W^-$) production in pp and $p\bar{p}$ collision. In our calculation we used both two and four parton scattering mechanisms.

In this chapter, we use our calculation to explore the possibility of the production of multiple gauge bosons at the supercolliders using the double parton scattering mechanism, in which two partons of the first hadron collide with two partons of the second. We also try to compare our cross-sections with the cross-sections from single scattering processes at the SSC, in order to test the possibility that the double scattering mechanism dominates to study the production of multiple gauge bosons at hadron supercolliders.

As we mentioned in chapter 4, an important test of the standard electroweak model can be achieved by analyzing the production of weak gauge bosons at hadron colliders [1,2]. Also this production can be considered as the promising channel and may give an important background for Higgs boson detection, which is one of the main subjects of physics studies at future accelerators.

In the near future, the high energy and large luminosity available at supercolliders will allow production of events containing multiple gauge bosons: we consider in this chapter the production of three and four weak gauge bosons (WGBs).

The production of multiple gauge bosons is interesting for several reasons [3]. Firstly, because the total cross-section of multiple WGBs will provide a non-trivial test of the standard model. Secondly, it allows a test of four gauge boson coupling for the first time. Thirdly, the production can also test the existence of the Higgs boson as the most important source for multiple WGBs, where the processes $qq \rightarrow BH$ (where $B \rightarrow W^+, W^-, Z$;$H \rightarrow W^+W^-, ZZ$) and $qq \rightarrow HH$ (where $H \rightarrow W^+W^-$,ZZ). Finally, multiple WGB production may contribute backgrounds to new physics, beyond the standard model.

Section 2 of this chapter contains a description of three gauge boson production at pp supercolliders using the double parton scattering mechanism, with comparision with results from single parton scattering processes. In section 3, we test our calculation of the production of four gauge bosons at pp supercolliders. Finally, in section 4 we conclude with a brief discussion on the observability of the multiple gauge boson processes.

5.2 Triple Weak Gauge Boson Production in High Energy Proton Proton collisions

In this section, we calculate the total cross section for the production of three gauge bosons via the double parton scattering mechanism at pp colliders.

The set of investigated four-parton processes is

$$(qq)_1 + (qq)_2 \rightarrow WWW, WWZ, WZZ, ZZZ \qquad 5.1$$

Two competing mechanisms are responsible for the production of three gauge bosons at hadron colliders. They are shown in figs. 1(a) and 1(b), where the kinematics is defined. The first one produces three gauge bosons via a Drell-Yan type $q\overline{q}$ annihilations in a single collision. The second mechanism is the direct observation of the four parton scattering subprocess for production of three gauge bosons.

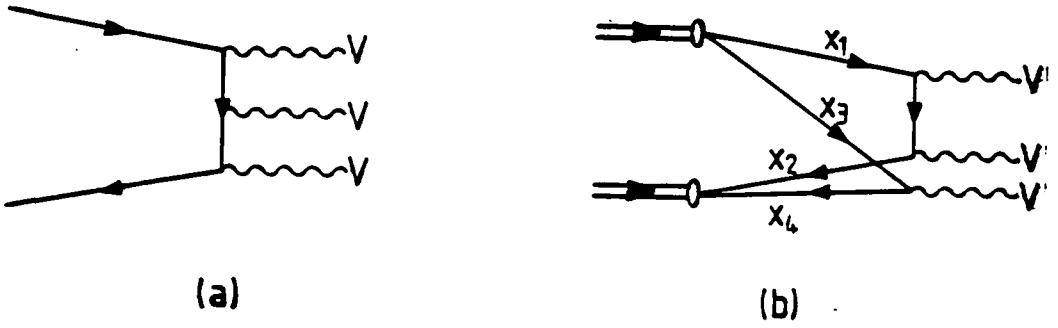

Fig. (5.1) Feynman diagrams for the three gauge boson production. (a). The two-parton production of three gauge bosons. (b). The four-parton production of three gauge bosons.

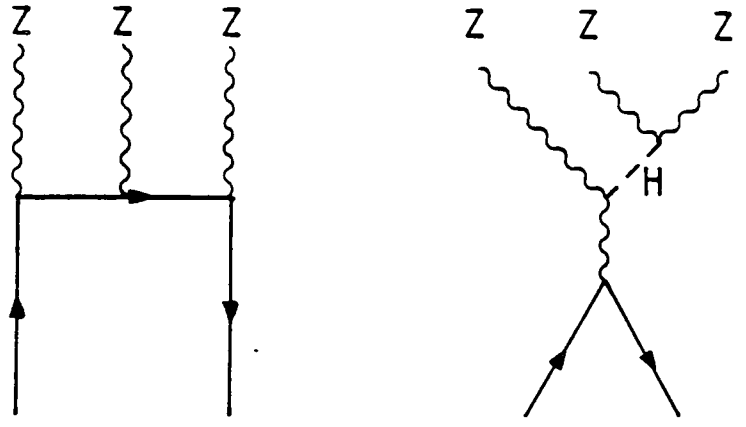

Fig. (5.2) Feynman diagrams for the process $qq \rightarrow ZZZ$.

Recently, Barger and Han [4] have calculated the total cross-section for the production of three gauge bosons at pp supercolliders of fig. 1(b). For three gauge boson production in a single scattering process there are many diagrams that contribute to a given final state. For instance, there are 20 diagrams for WWZ and WZZ, 16 diagrams for WWW and 2 diagrams for ZZZ in any gauge. We present the diagrams for the process $qq \rightarrow ZZZ$ in fig. (5.2).

Their calculations were based on the tree level diagrams for which the initial partons are fermions. Their results are presented in fig. (5.3). The calculated cross-sections at supercollider energy of 40 TeV have the values:

$$\sigma(WWW) \simeq 0.51pb,$$

$$\sigma(WWZ) \simeq 0.43pb,$$

$$\sigma(WZZ) \simeq 0.11pb,$$

$$\sigma(ZZZ) \simeq 0.04pb, \qquad 5.2$$

The actual experimental data are concerned with the possible number of events which can be observed and identified through their final leptonic and hadronic decay modes. This is given through their branching ratio which is the ratio of the decay width of the vector boson into a particular channel to the total width into all possible channels. Thus:

$$B(W \rightarrow l\nu) = \frac{\Gamma(W \rightarrow l\nu)}{\Gamma_{total}} \qquad 5.3$$

Using eqn. (5.3), the weak bosons have the branching ratios are (Assuming $m_W = 80.6GeV, m_Z = 91.9GeV, \sin^2\theta_W = 0.23, m_t = 45GeV$)

$$B(W \rightarrow l\nu) \simeq 0.18, \qquad B(Z \rightarrow l^+l^+) \simeq 0.06,$$

$$B(W \rightarrow q\bar{q}) \simeq 0.18, \qquad B(Z \rightarrow q\bar{q}) \simeq 0.70,$$

$$B(Z \to \nu\overline{\nu}) \simeq 0.20, \qquad 5.4$$

where l denotes e or μ ; the two-quarks final states mainly appear as two jets. The uncertainty in the above branching ratios comes from the uncertainty in the t-quark mass. In the case where the t-quarks are very massive $B(W \to l\nu)$ shifts from 8.8% to 10.8%.

In $pp \to VVV$, the combined branching ratios of the above modes are

$$B(WWW \to l\nu, l\nu, l\nu) \simeq 0.006,$$

$$B(WWZ \to l\nu, l\nu, l^+l^-) \simeq 0.002,$$

$$B(WZZ \to l\nu, l^+l^-, l^+l^-) \simeq 0.0006,$$

$$B(ZZZ \to l^+l^-, l^+l^-, l^+l^-) \simeq 0.0002, \qquad 5.5$$

Multiplying the cross-section by an annual luminosity of $10^4\ pb^{-1}$, we find event rates of

$$N(WWW) \simeq 30 \quad events/year,$$

$$N(WWZ) \simeq 10 \quad events/year$$

As we have discussed in chapter 4, increasing the collider's energy, increases the probability of the collision of fractional parts of hadrons, which means that more partons are loaded in the hadrons and multiple interactions become increasingly important [5].

The total cross-section for the four parton process in eqn. (5.1) can be roughly estimated (neglecting small parton correlations), by the product of the two parton cross-sections $d\sigma_{ij}$ as in the form:

$$\sigma^{DS} = \frac{\sigma^{2\to V}\sigma^{2\to 2V}}{\sigma_{eff}}, \qquad 5.6$$

where σ_{eff} represents the cross-section which estimates the size of a hadron, $\sigma^{2\to V}$ is the total subprocess cross-section for production of single gauge boson and $\sigma^{2\to VV}$ is the total subprocess cross-section for production of a pair of gauge bosons.

The explicit expression for the double parton scattering cross-section can be written with the appropriate two parton momentum distribution as [6-9]:

$$d\sigma = \frac{1}{\sigma_{eff}} \int dx_1 dx_2 dx_3 dx_4 \sum_{i,j,k,l} q_{ij}(x_1, x_3) q_{kl}(x_2, x_4) d\sigma_{12} d\sigma_{34}, \qquad 5.7$$

where the summation in eqn. (5.7) is over all pairs of quarks and antiquarks in both hadrons, which can give rise to appropriate production for processes in eqn. (5.1).

Within the above framework, we have carried out a detailed analysis of the total cross-section for processes of eqn. (5.1), where we have used the appropriate forms for $d\sigma^{2\to V}$ and $d\sigma^{2\to VV}$ from chapter 4.

In fig. (5.3), we present the integrated cross section of eqn. (5.7) for triple gauge boson (WWW,WWZ,WZZ,ZZZ) production as a function of CM energy. The strong cross section rise in double scattering parton processes, with increasing CM energy, is explained by the strong rise of the quark distribution at high energies (low momentum fraction x). Although our results are smaller than the cross section $\sigma(pp \to VVV)$ quoted in ref. [4] at low energies, they show comparable values at high energies.

We used set 1 of the Q^2-dependent gluon distribution of Duke and Owens [10] with $\Lambda_{QCD} = 0.2$ GeV. In our subsequent analysis we choose: $\sigma_{eff} = \pi R^2 = 2.5$ mb [11].

At the SSC CM energy of 40 TeV, the total cross sections for triple gauge boson productions using the double parton scattering mechanism, have the values: :

$$\sigma(WWW) \simeq 0.014pb,$$

$$\sigma(WWZ) \simeq 0.005pb,$$

$$\sigma(WZZ) \simeq 0.003pb,$$

$$\sigma(ZZZ) \simeq 0.002pb \qquad 5.8$$

Multiplying the cross-section by the annual luminosity, we find event rate of

$$N(WWW) \simeq 1 \quad event/year$$

While at the ELOISATRON CM energy of 200 TeV, The total cross-section for triple gauge boson production have the values

$$\sigma(WWW) \simeq 0.25pb,$$

$$\sigma(WWZ) \simeq 0.10pb,$$

$$\sigma(WZZ) \simeq 0.05pb,$$

$$\sigma(ZZZ) \simeq 0.003pb, \qquad 5.9$$

which give the following event rates after multiplying the cross-section by an annual luminosity of $10^4 pb^{-1}$

$$N(WWW) \simeq 15 \quad events/year,$$

$$N(WWZ) \simeq 2 \quad events/year$$

where the leptonic decay modes do not suffer from QCD background, while the hadronic decay mode is difficult to identify because of the large background from $pp \rightarrow VorVV$ + QCD jets or $pp \rightarrow QCDjets$.

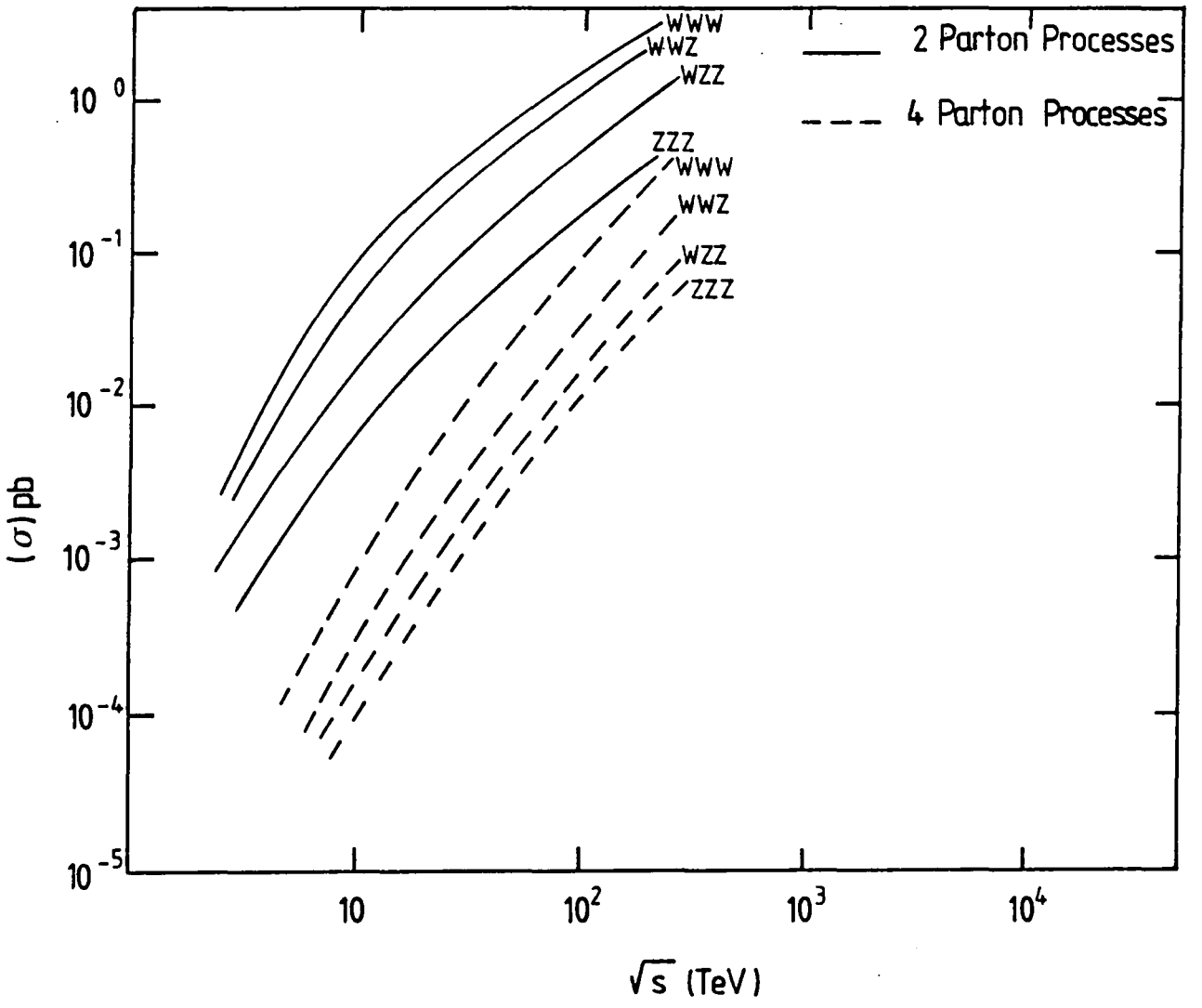

Fig. (5.3) The integrated cross-section for triple gauge boson production as a function of CM energy using the four-parton scattering mechanism (dashed lines). The solid lines are the cross-section for two-parton scattering , as given in ref. (4).

5.3 Four Weak Gauge Boson Production in High Energy Proton Proton Collisions

In this section, we calculate the total cross-section for the production of four gauge bosons (VVVV) at supercolliders.

The set of investigated processes is

$$(qq)_1 + (qq)_2 \rightarrow WWWW, WWZZ, ZZZZ \qquad 5.10$$

As we have discussed in section 2 of this chapter, we use the double parton scattering mechanism in order to calculate the total cross-section for four gauge boson production in pp collisions, as shown in fig. (5.4)

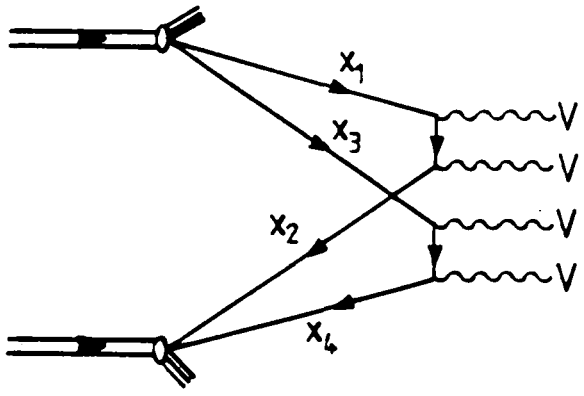

Fig. (5.4) Feynman diagrams for four-parton production of four gauge bosons.

where each single scattering process produces a pair of gauge bosons. The scattering cross-section for fig. (5.4) is:

$$d\sigma = \frac{1}{\sigma_{eff}} \int dx_1 dx_2 dx_3 dx_4 \sum_{i,j,k,l} q_{ij}(x_1, x_3) q_{kl}(x_2, x_4) d\sigma_{12} d\sigma_{34}, \qquad 5.11$$

where $d\sigma_{12}$ and $d\sigma_{34}$ are the subprocess cross-sections for pair gauge boson production. All other kinematics are exactly as in section 2 of this chapter.

In fig. (5.5), we plot the calculated cross-section for four parton processes of eqn. (5.10) versus CM energy, where we have summed over all possible pairs of quarks and antiquarks in both hadrons. Although the total cross-section is small (reaching a value of order 10^{-3} pb), but it still shows the rich phenomena which can be expected at high energies at supercolliders with large luminosities.

At the SSC CM energy of 40 TeV, the total cross-sections for four gauge boson production via double scattering have the values:

$$\begin{aligned} \sigma(WWWW) &\simeq 0.13 \times 10^{-4} pb, \\ \sigma(WWZZ) &\simeq 0.20 \times 10^{-5} pb, \\ \sigma(ZZZZ) &\simeq 0.25 \times 10^{-6} pb \end{aligned} \tag{5.12}$$

While at the LHC CM energy of 16 TeV, the total cross-sections have the values

$$\begin{aligned} \sigma(WWWW) &\simeq 0.16 \times 10^{-5} pb, \\ \sigma(WWZZ) &\simeq 0.24 \times 10^{-6} pb, \\ \sigma(ZZZZ) &\simeq 0.28 \times 10^{-7} pb \end{aligned} \tag{5.13}$$

And at the ELOISATRON CM energy of 200 TeV, the total cross-sections have the values

$$\begin{aligned} \sigma(WWWW) &\simeq 0.16 \times 10^{-3} pb, \\ \sigma(WWZZ) &\simeq 0.30 \times 10^{-4} pb, \\ \sigma(ZZZZ) &\simeq 0.14 \times 10^{-5} pb \end{aligned} \tag{5.14}$$

Because these cross-sections are very small, the expected numbers of events per year is less than one, and so these processes are not (expected to be) observable and probably beyond experimental capability.

We used set 1 of the Q^2-dependent gluon distribution of Martin et. al. [12] with Λ_{QCD}=0.107 GeV, we also used $\sigma_{eff} = \pi R^2$= 2.5 mb [11].

In order to explore our study, we are going to calculate the Higgs boson production. Particularly we are going to concentrate on the Higgs pair production cross-section at hadron colliders via gluon fusion. For completeness we are going to compare the total cross-section for four gauge boson production with the cross section for pair Higgs production and concentrate on the background to the HH search, which is due to $qq \rightarrow VVVV$.

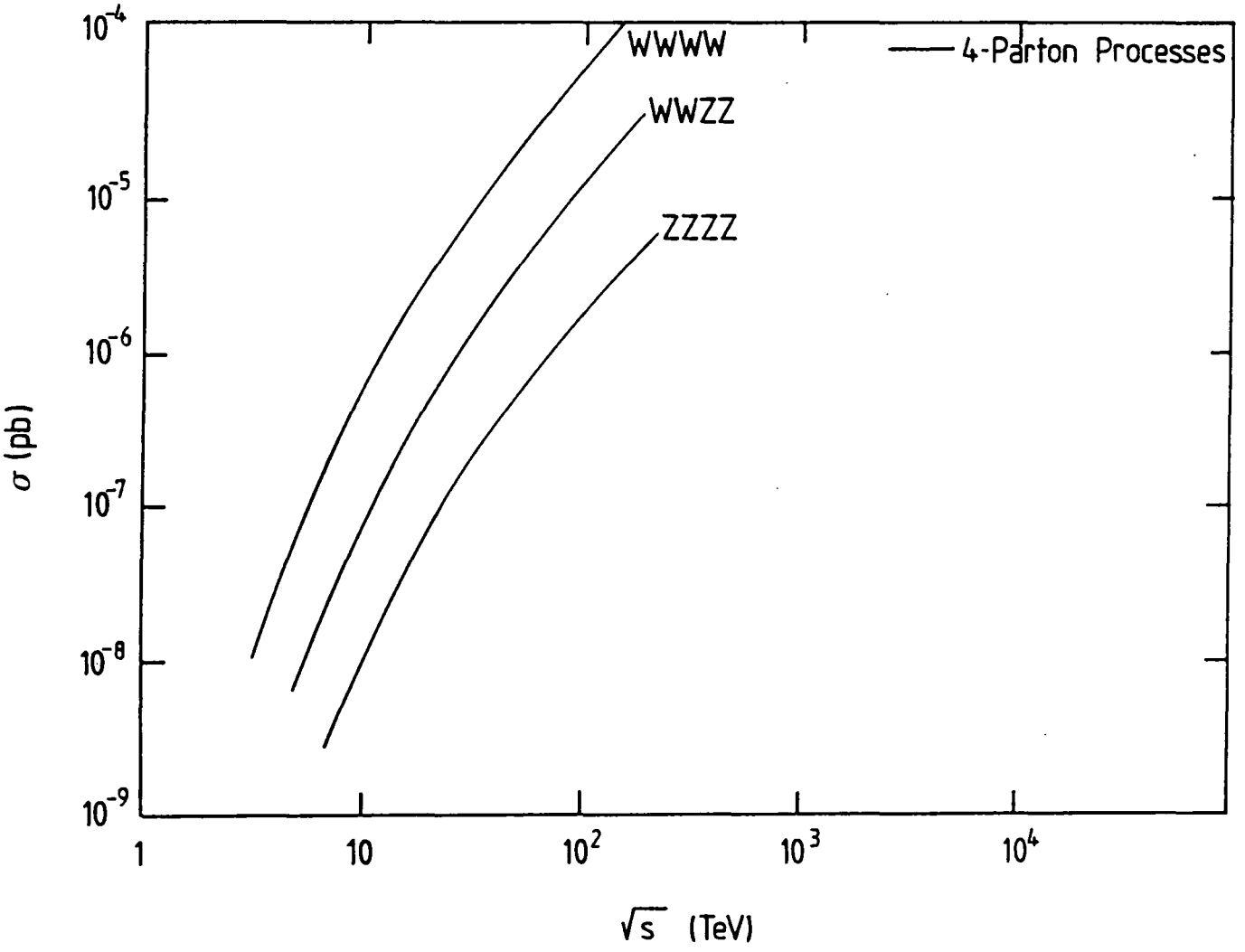

Fig. (5.5) The integrated cross-section for the four gauge boson production as a function of CM energy using four-parton scattering mechanism.

5.4 Discussion

We have calculated multiple (three and four) gauge boson production in pp collisions as a function of CM energy using the double parton scattering mechansim. The values of the cross-section lie in the range 10^{-1}-10^{-3} pb for triple gauge boson and 10^{-4}-10^{-6} pb for quadruple gauge boson production. Although the values are quite small, the process may be observable if large energy is available at supercolliders with large luminosities. Other problems are related with how to turn this cross-section into real observable events, which seems to be difficult because of the large background due to the processes like $pp \rightarrow VorVV+$ 1,2 jets, or $pp \rightarrow QCD \quad jets$. The usual way here is to use cuts to separate gauge boson signals from the V + jets, but this could reduce the value of the cross-section by an order of magnitude.

However, it is also important to remember that there are several sources of uncertainty in the calculation such as the the choice of the structure functions $G(x, Q^2)$, the choice of the kinematic scale which defines the strong coupling $\alpha_s(Q^2)$ and the structure functions and finally the higher order QCD corrections (the K-factor).

CHAPTER 6

HIGGS BOSON

6.1 Introduction

As we have discussed in chapter 1, the Higgs mechanism, through spontaneous symmetry breaking of the fundamental $SU(2) \times U(1)$ electroweak symmetry, is responsible for generating the masses of the vector boson which mediate the weak interactions.

To understand this, we must look at the additional part that has been introduced to the standard model, the SU(2) doublet of scalar fields Φ. The additional scalar fields have a potential of the form [1]:

$$V(\Phi) = -\mu^2\Phi^2 + \lambda\Phi^4$$

$$V(\Phi) = \lambda(\Phi^+\Phi - 1/2v^2)^2, \qquad 6.1$$

where this field acquires a non-vanishing expectation value Φ^2 in the physical vacuum state. The components of this non-vanishing vaccum expectation are combined with the SU(2) gauge particles to create massive vector bosons and the rest create a physical neutral boson (Higgs boson).

Returning to eqn. (6.1), the v term is fixed by the measured parameters of the standard model and provides the W and Z with mass as shown:

$$m_W = \frac{1}{2}gv, \qquad m_Z = \frac{m_W}{\cos\theta_W},$$

while the λ-term, which is related to the physical Higgs mass, is free, hence the Higgs mass is arbitrary in the standard model as shown:

$$\lambda = \frac{m_H^2}{2v^2}$$

Since the discovery of the W and Z gauge bosons in 1983 at CERN, the only particle in the standard model theory that remains to be discovered is the neutral,

spin zero Higgs particle. The main difficulties with the Higgs boson are related to the absence of the theoretical prediction of its mass, and this leads to a number of production and decay modes which explore its detection in a large mass range.

Higgs boson phenomenology has received a large amount of interest in recent years. The hadron collider facilities, such as superconducting supercollider (SSC), are the most suitable tools to search for a Higgs boson. A primary motivation for constructing this machine is to find the Higgs boson or some variety which breaks the underlying symmetry of the electroweak theory.

Section 2 of this chapter contains a description of the Higgs mass and coupling. In section 3, we show the decay width of Higgs boson. In section 4, we show the branching fraction of Higgs boson into fermions and gauge bosons. In section 5, we calculate the cross-section for the production of single and pair Higgs boson via gluon-gluon fusion at hadron colliders. Finally, in section 6 we conclude our results and we also try to compare two Higgs boson production cross-sections with four gauge boson production cross-sections from double scattering mechanism of chapter 5.

6.2 Higgs Search

The discovery of the Higgs boson faces some major problems related to its existence with a large cross-section and its detection through a clear signal.

In order to search for Higgs production, we must look at its coupling with other particles. The Higgs couples very weakly with the fundamental particles like photons, electrons, muons and light quarks. This is because their mass is small. In other words, the Higgs prefers to couple to the heaviest fermion available and it also couples to the W and Z with a standard weak coupling strength. This is shown in fig.(6.1).

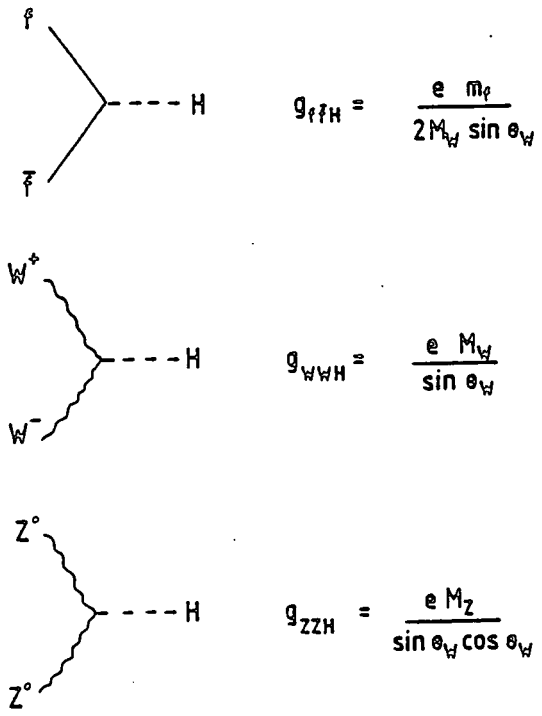

Fig. (6.1) Standard model couplings of the Higgs boson to fermions and W and Z bosons.

Higgs detection is not easy and must be explored over a large range of mass because of the unknown value of its mass. So in order to search for the Higgs, it is useful to divide the mass range into three regions:

1 **Light Higgs Mass** : if the Higgs mass is light, $m_H < m_Z$, then it can radiate from a Z boson. The dominant process is $Z \rightarrow Z^* H$, where Z^* can be detected from $Z^* \rightarrow \nu\overline{\nu}$ decay, using a missing transverse trigger, then H can be detected from $H \rightarrow \tau\overline{\tau}$ or $H \rightarrow b\bar{b}$ decay which appear in the detector as two hadronic jets.

Higgs phenomenology in this mass range can be study at LEP1 machine through the Z decay, where the possible decay are: $Z \rightarrow H l^+ l^-$ and $Z \rightarrow H\gamma$. The corresponding number of events sets the upper limit for Higgs at about 50 GeV at this machine.

With LEP2 machine, the e^+e^- collision energy will reach 200 GeV. The dominant Higgs production processes is the $e^+e^- \rightarrow ZH$. Note that the Z decay into two jets and $H \rightarrow b\bar{b}$. The upper limit for Higgs detection is therefore increased to about 80 GeV.

2 **Intermediate Higgs Mass** : if the Higgs mass is $m_Z < m_H < 2m_W$ then it decays dominantly to a t-quark pair except if $m_t > m_W$ then $H \rightarrow b\bar{b}, \tau\bar{\tau}$... etc.

3 **Heavy Higgs Mass** : if the Higgs mass is $m_H > 2M_W$ or $m_H > 2m_Z$, then its dominant decays are $H \rightarrow W^+W^-$ or $H \rightarrow ZZ$, with branching fraction of ratio 2 to 1 respectively.

6.3 Decay of the Higgs Boson

As we have mentioned in last section the Higgs couples to fermions and W and Z particles, where the coupling is proportional to the particle mass. In other words, the Higgs prefers to couple to the heaviest fermions. In this section we discuss the decay of the Higgs boson into fermions and weak bosons as [1]:

a. Higgs Decays to Fermions

The coupling of Higgs to fermions (leptons or quarks) is given by:

$$\mathcal{L} = -(\sqrt{2}G_F)^{1/2} m_f H \bar{f} f, \tag{6.2}$$

where the decay amplitude is given by

$$\mathcal{M} = (\sqrt{2}G_F)^{1/2} m_f \bar{u}(p_1) u(p_2), \tag{6.3}$$

which yields a partial decay width of

$$\Gamma(H \rightarrow f\bar{f}) = C\frac{G_F m_f^2 m_H}{4\pi\sqrt{2}}[1 - \frac{4m_f^2}{m_H^2}]^{3/2}, \tag{6.4}$$

where C=1 for leptons and 3 for quarks. The dominant decay here will be to the final state of maximum fermion masses.

b. Higgs Decays to Weak Bosons

The coupling of the Higgs to weak bosons (W and Z) is given by:

$$\mathcal{L} = (\sqrt{2}G_F)^{1/2}(2m_W^2 H W_\mu^+ W^{-\mu} + m_Z^2 H Z_\mu Z^\mu), \tag{6.5}$$

where the amplitude for $H \to W^+W^-$ decay is given by:

$$\mathcal{M} = (\sqrt{2}G_F)^{1/2} 2m_W^2 \epsilon_\mu^*(p_1, \lambda_1)\epsilon^\mu(p_2, \lambda_2), \tag{6.6}$$

which yields a partial decay width of

$$\Gamma(H \to W^+W^-) = \frac{G_F m_H^3}{8\pi\sqrt{2}}(1 - \frac{4m_W^2}{m_H^2})^{1/2}(1 - \frac{4m_W^2}{m_H^2} + \frac{12m_W^4}{m_H^4})$$

$$\Gamma(H \to ZZ) = \frac{G_F m_H^3}{16\pi\sqrt{2}}(1 - \frac{4m_Z^2}{m_H^2})^{1/2}(1 - \frac{4m_Z^2}{m_H^2} + \frac{12m_Z^4}{m_H^4}), \tag{6.7}$$

using eqns. (6.4) and (6.7), we calculate the partial decay width of Higgs bosons to fermions and weak bosons.

In fig. (6.2), we show the partial and the total decay width of Higgs boson as a function of Higgs mass (assuming top quark mass $m_t = 40$ GeV).

Figs. (6.3) and (6.4) shows the correspoding decay width at top quark masses of $m_t = 100$ and 160 GeV respectively.

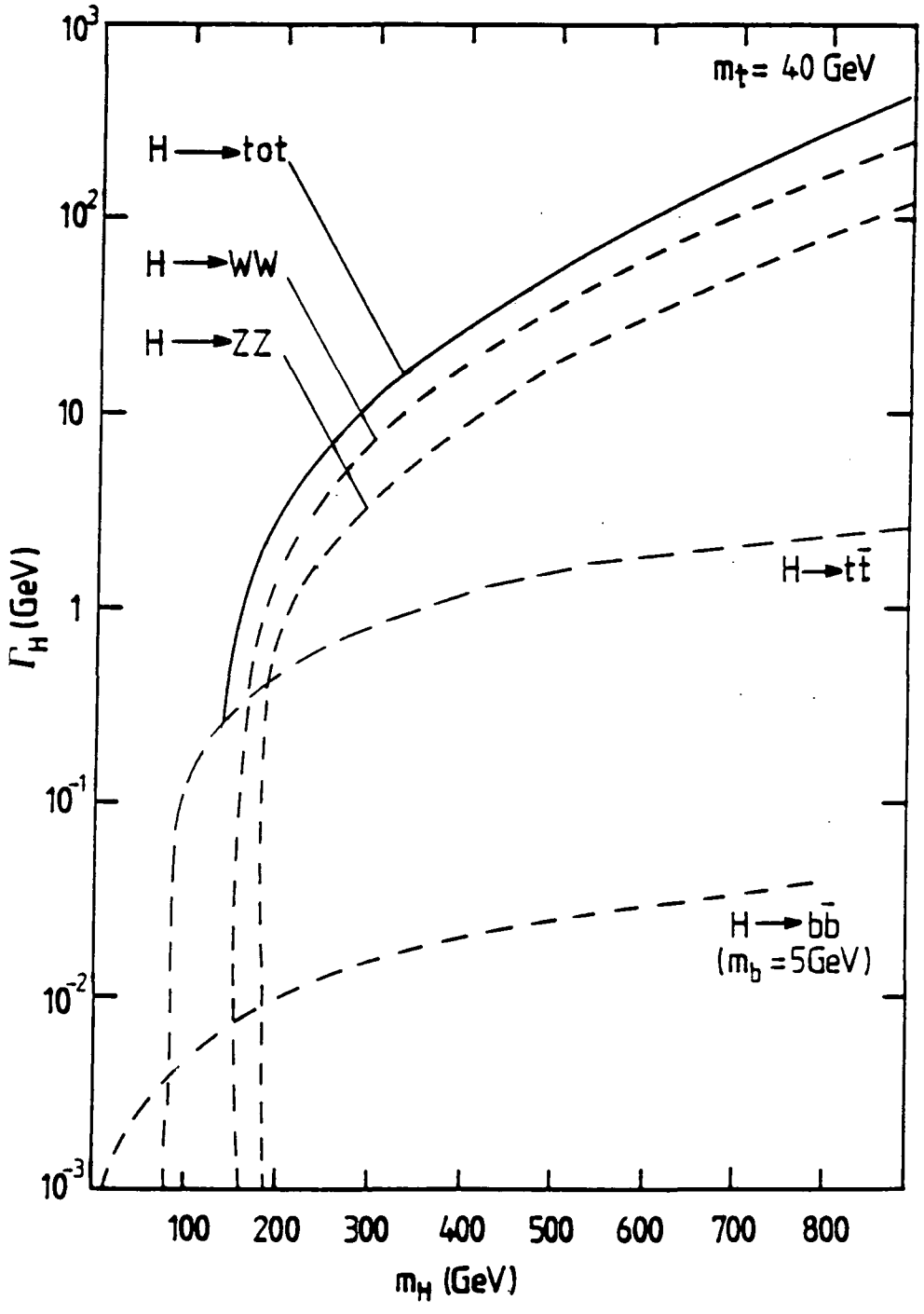

Fig. (6.2) Higgs decay width (dashed lines) into $t\bar{t}$, WW and ZZ pairs as a function of Higgs mass, assuming $m_t = 40$ GeV. Also shown is the total decay width (solid line).

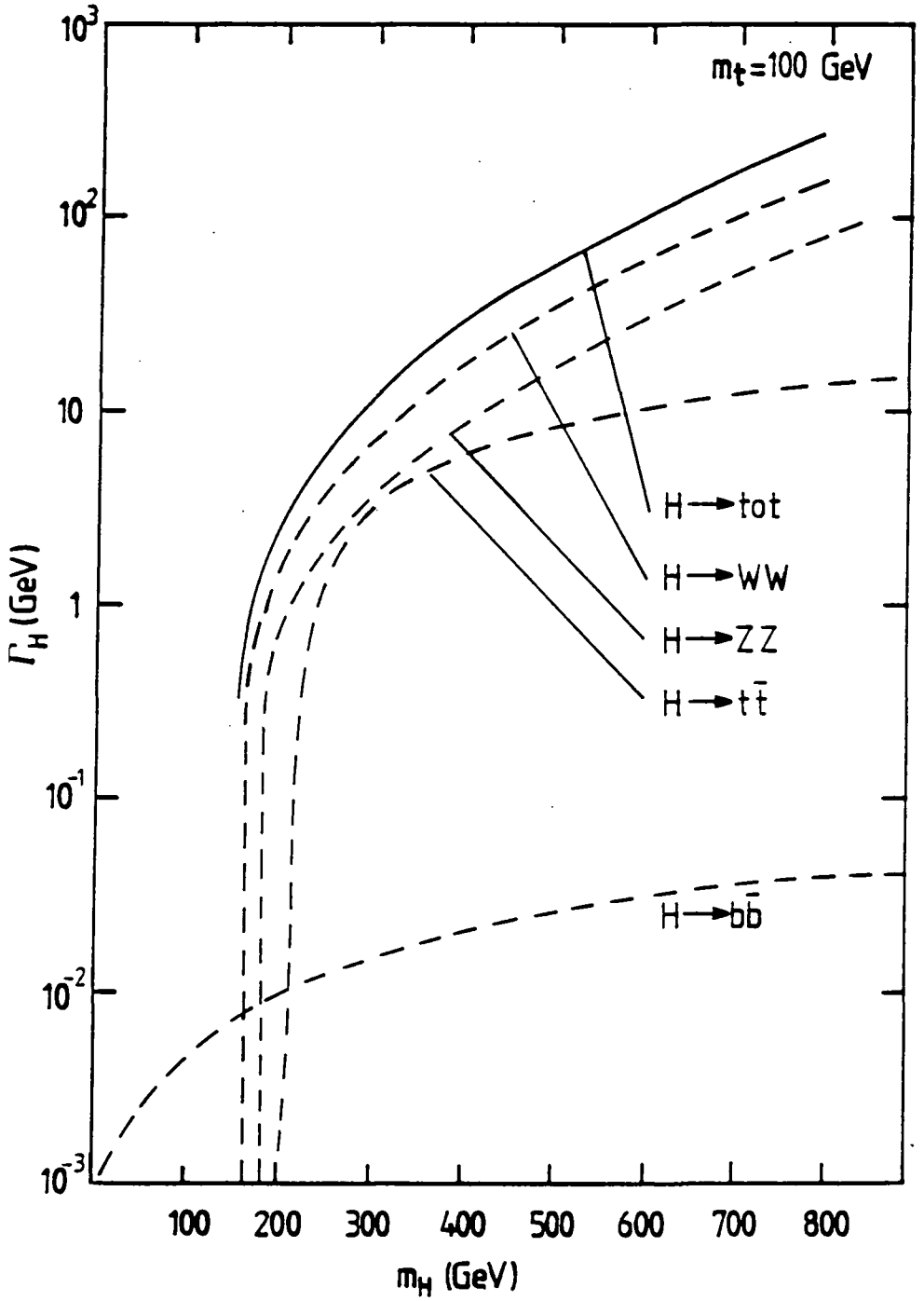

Fig. (6.3) Higgs decay width (dashed lines) into $t\bar{t}$, WW and ZZ pairs as a function of Higgs mass, assuming m_t = 100 GeV. Also shown iss the total decay width (solid line).

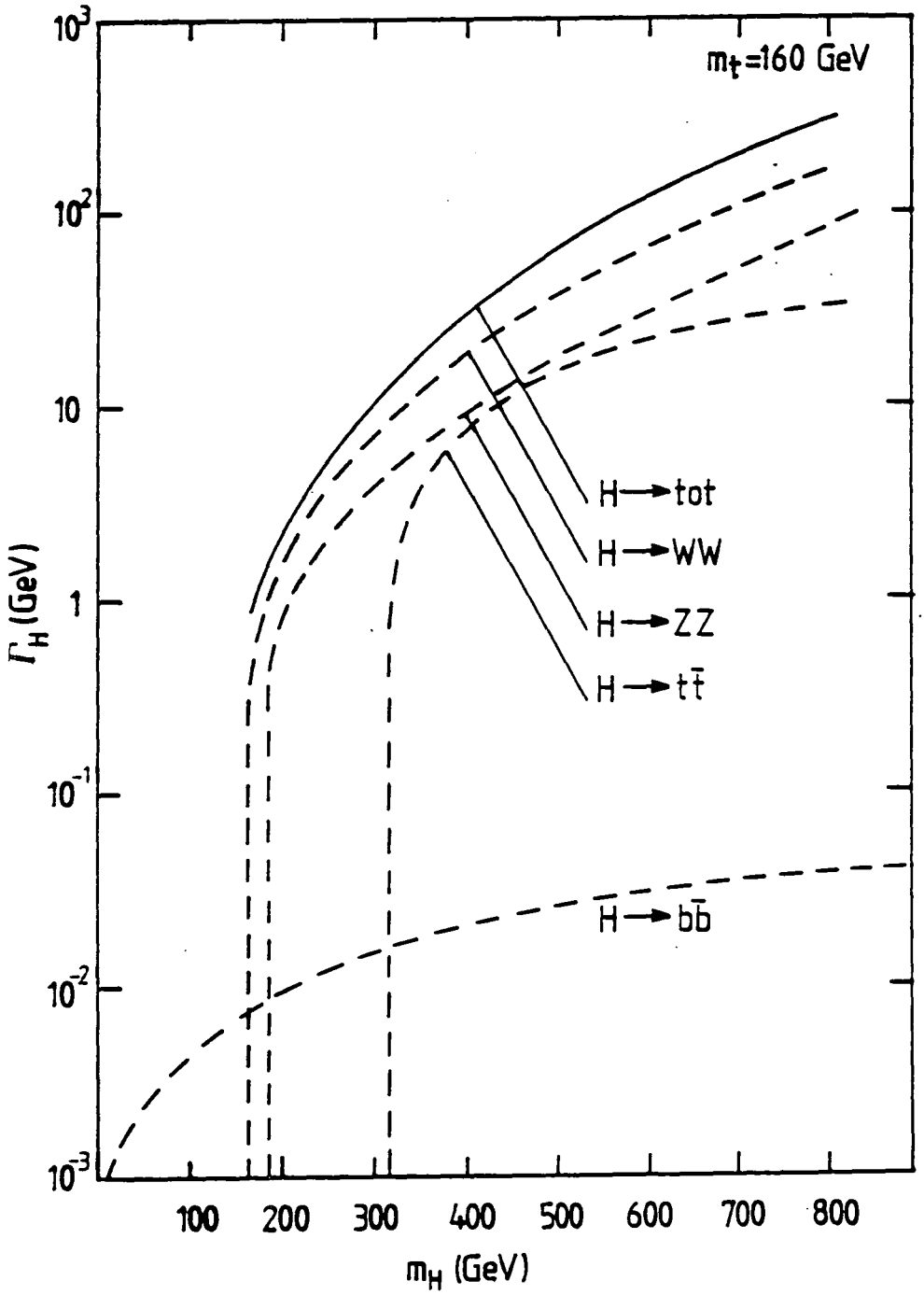

Fig. (6.4) Higgs decay width (dashed lines) into $t\bar{t}$, WW and ZZ pairs as a function of Higgs mass, assuming m_t = 160 GeV. Also shown is the total decay width (solid line).

6.4 Higgs Branching Fractions

With the formulas for the partial decay rates in last section, we can evaluate the branching fractions as a function of Higgs mass into final state quarks, leptons and gauge boson particles.

It is useful to divide Higgs decay in to:

a. $H \rightarrow b\bar{b}$ dominates, if Higgs mass is between $2m_b < m_H < 2m_t$ with branching ratio of $BR(H \rightarrow b\bar{b}) \simeq 1$.

b. $H \rightarrow t\bar{t}$ dominates, if Higgs mass is between $2m_t < m_H < 2m_W$ with branching ratio of $BR(H \rightarrow t\bar{t}) \simeq 1$, and $m_t < m_W$

c. $H \rightarrow W^+W^-$ and Z Z dominate, if $m_H > 2m_W$, unless there is heavy fermion with $m_f > m_W$.

Using the branching ratio formula (ratio of the decay width of the Higgs boson into particular channel to the total width into all possible channels) i.e.

$$B(H \rightarrow VV) = \frac{\Gamma(H \rightarrow VV)}{\Gamma_{total}}$$

We show, in fig. (6.5), the branching fractions of the Higgs boson of the standard model (assuming top quark mass $m_t = 40$ GeV).

Figs. (6.6) and (6.7) are the corresponding branching fractions at top quark masses of $m_t = 100$ and 160 GeV respectively.

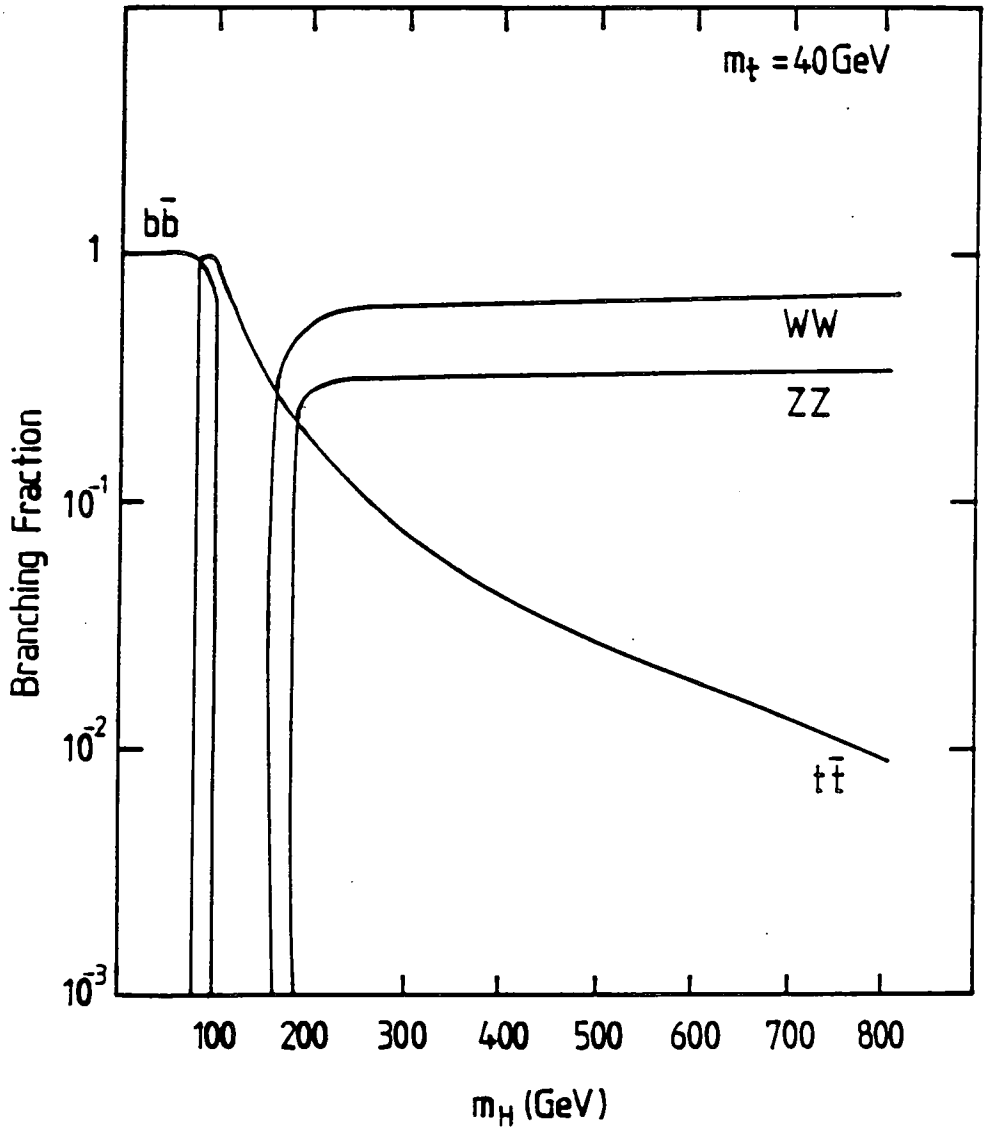

Fig. (6.5) Decay branching fractions of the Higgs decay into $t\bar{t}$, WW and ZZ pairs as a function of the Higgs mass, assuming $m_t = 40$ GeV.

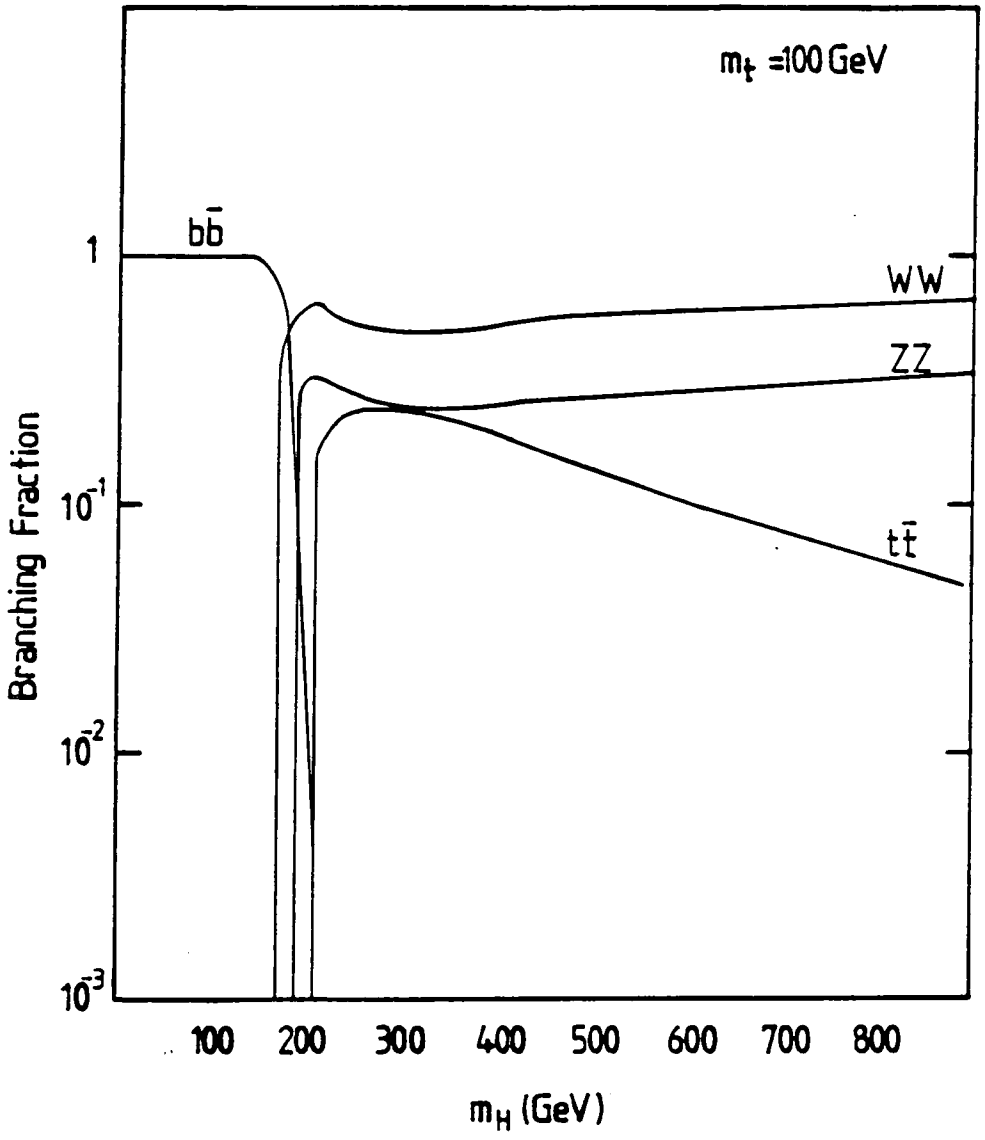

Fig. (6.6) Decay branching fractions of the Higgs decay into $t\bar{t}$, WW and ZZ pairs as a function of the Higgs mass, assuming $m_t = 100$ GeV.

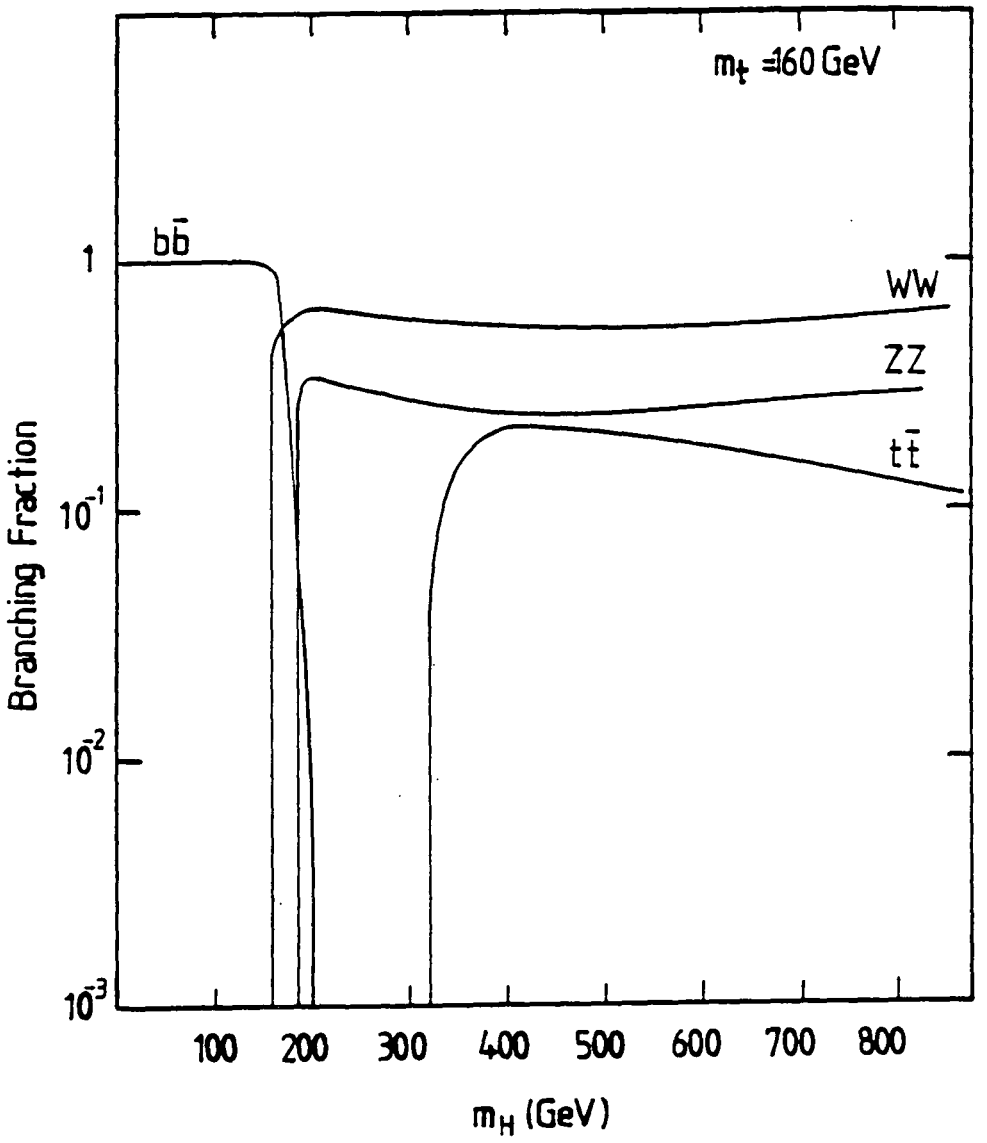

Fig. (6.7) Decay branching fractions of the Higgs decay into $t\bar{t}$, WW and ZZ pairs as a function of the Higgs mass, assuming $m_t = 160$ GeV.

6.5 Higgs Boson Production

6.5.a Production of Single Higgs Boson

In the standard model, a single neutral Higgs particle is the only remaining unknown part of the spontaneous symmetry breaking of the $SU(2) \times U(1)$ gauge symmetry. Unfortunately, although the coupling of Higgs boson to quarks and leptons is predicted, the Higgs mass is not.

We shall consider the possibility of the production of Higgs bosons at hadron colliders. Three different mechanisms are responsible for the production of a single Higgs [2]:

1. The production of Higgs boson through quark-antiquark collisions as in fig. (6.8)

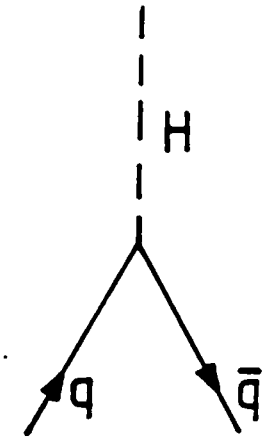

Fig. (6.8) Feynman diagram for the production of Higgs boson in $q\bar{q}$ collisions.

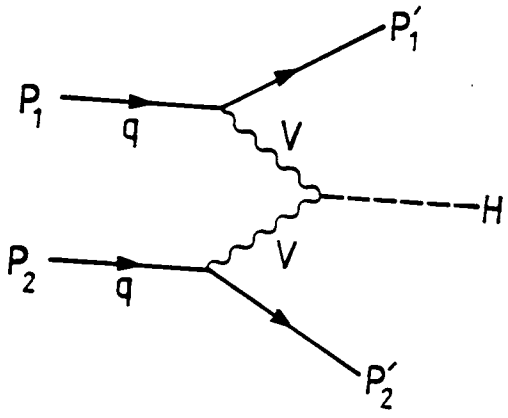

Fig. (6.9) Intermediate-boson fusion mechanism for Higgs boson formation.

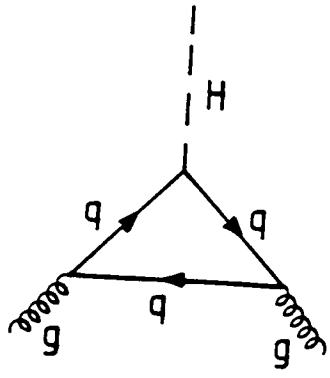

Fig. (6.10) Feynman diagram for the production of a Higgs boson in gluon-gluon fusion.

The integrated cross-section is given by [2]

$$\sigma(p\overline{p} \rightarrow H) = \frac{G_F\pi}{3\sqrt{2}} \sum_i (\frac{m_i^2}{m_H^2})\tau \int_\tau^1 \frac{dx}{x}[f_i(x, m_H^2) f_{\overline{i}}(\frac{\tau}{x}, m_H^2) + f_i(\frac{\tau}{x}, m_H^2) f_{\overline{i}}(x, m_H^2)] \qquad 6.8$$

The total cross-section for this mechanism is very small for two reasons. Firstly, the light quark mass is included in the formula in the factor $\frac{m_i^2}{m_H^2}$ and secondly, the heavy quark contribution is small because of the small parton density in the hadron.

2. The production of Higgs bosons through WW and ZZ fusion: Here quarks in the colliding beam emit virtual W's and Z's which annihilate to form the Higgs boson. These subprocesses are illustrated in fig. (6.9).

   For heavy Higgs boson, $M_H > 300GeV$, this production is important and it dominates because the coupling of Higgs to W and Z is proportional to m_H.

3. The production of Higgs bosons through gluon-gluon fusion: At hadron colliders this mechanism is important and more promising than the above because of the larger luminosity of the gluon-gluon than quark-quark at small x.

   In our calculation, we concentrate on the gluon-gluon mechanism for the production of a single Higgs boson. The total cross section for the reaction $gg \rightarrow H$ shown in fig. (6.10) is given by [2,3]:

$$\sigma(q\overline{q} \rightarrow H) = \frac{G_F\pi}{32\sqrt{2}}[\frac{\alpha_s}{\pi}]^2 |N|^2 \tau \int_\tau^1 \frac{dx}{x} g(x, m_H^2) g(\frac{\tau}{x}, m_H^2), \qquad 6.9$$

where N is the sum of the contributions for heavy quark flavours. When $m_H > m_q$, N is complex and has the form

$$N = \frac{\epsilon}{2}[1 + (\epsilon - 1)\phi(x)], \qquad 6.10$$

with $\epsilon = \frac{4m_i^2}{m_H^2}$ and

$$\phi(x) = -[\sin^-(\frac{1}{\sqrt{\epsilon}})]^2, \quad \epsilon > 1,$$

$$\phi(x) = \frac{1}{4}[\ln(\frac{\xi_+}{\xi_-}) + i\pi]^2, \epsilon < 1, \qquad 6.11$$

where $\xi_\pm = 1 \pm \sqrt{1-\epsilon}$ and m_i is the top quark mass.

In our calculation we have used the gluon-gluon mechanism to calculate the total cross-section for single Higgs boson production. To obtain the predicted cross-section, we integrate eqn. (6.9) with the parton distribution function of ref. [2], which has $\Lambda_{QCD} = .20$ GeV.

Fig. (6.11) shows the numerical evaluation of the exact cross-section of Higgs boson production in pp collision as a function of CM energy, using the gg fusion mechanism. The Higgs mass is taken to be $m_H = 100$, 200 and 400 GeV. The top quark mass is fixed at 30 GeV.

Fig. (6.12) shows the numerical evaluation of the exact cross-section of Higgs boson production in pp collisions as a function of the Higgs mass using the gg fusion mechanism. The top quark mass is taken to be $m_t = 30$, 40, 50, 70 and 80 GeV. At CM energy of 40 TeV.

Fig. (6.13) shows the numerical evaluation of the exact cross-section of Higgs boson production in pp collisions as a function of the Higgs mass using the gg fusion mechanism. The top quark mass is 30 GeV. Curves are for CM energy of 20, 40, 100, and 200 TeV.

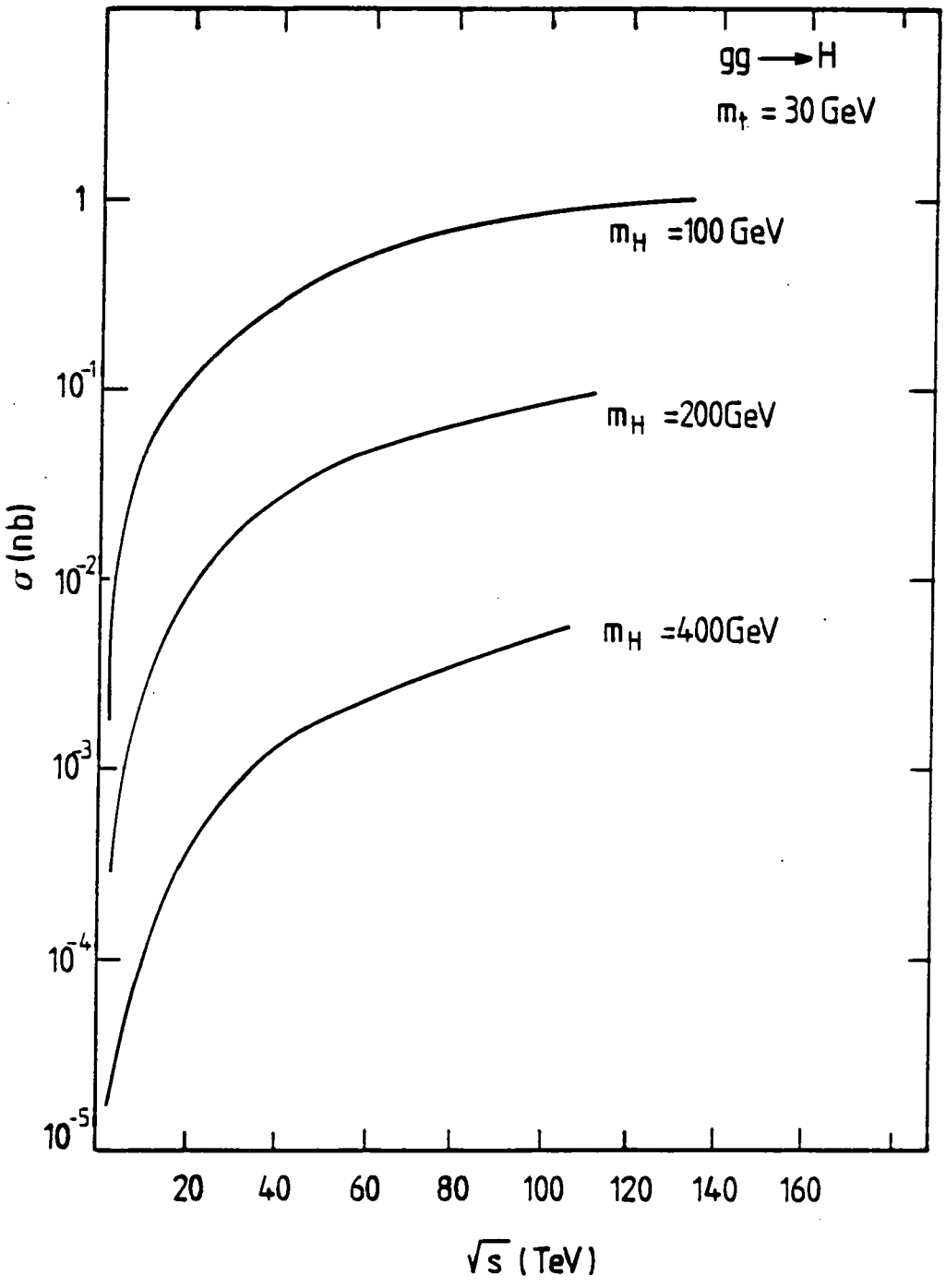

Fig. (6.11) The total cross-section for the production of Higgs boson via gluon-gluon fusion as a function of CM energy of the pp system. The Higgs mass is taken to be 100, 200 and 400 GeV.

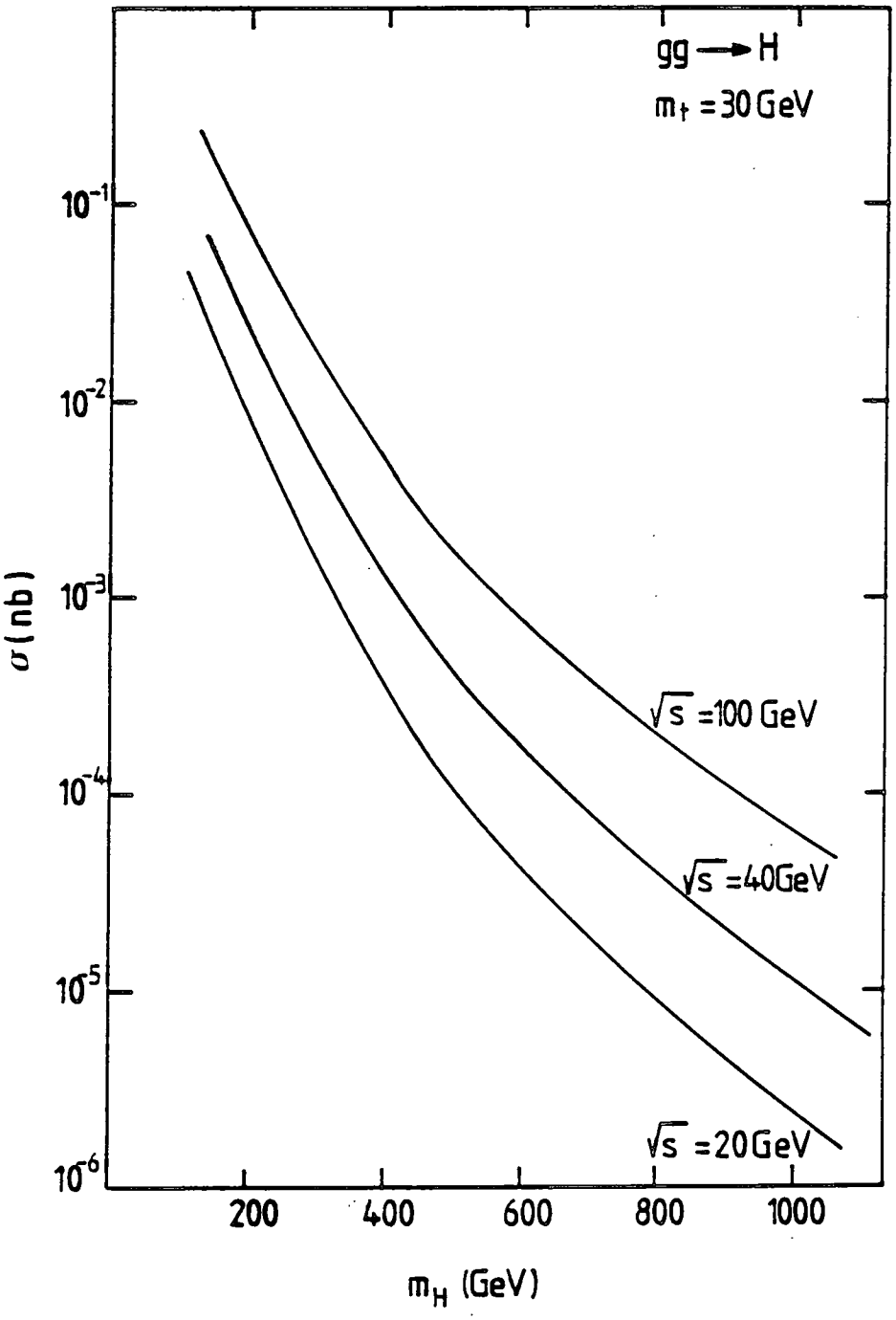

Fig. (6.12) The total cross-section for the production of Higgs boson via gluon-gluon fusion as a function Higgs mass. The top quark mass is fixed at 30 GeV. Curvies for $\sqrt{s}$ = 20, 40 and 100 TeV.

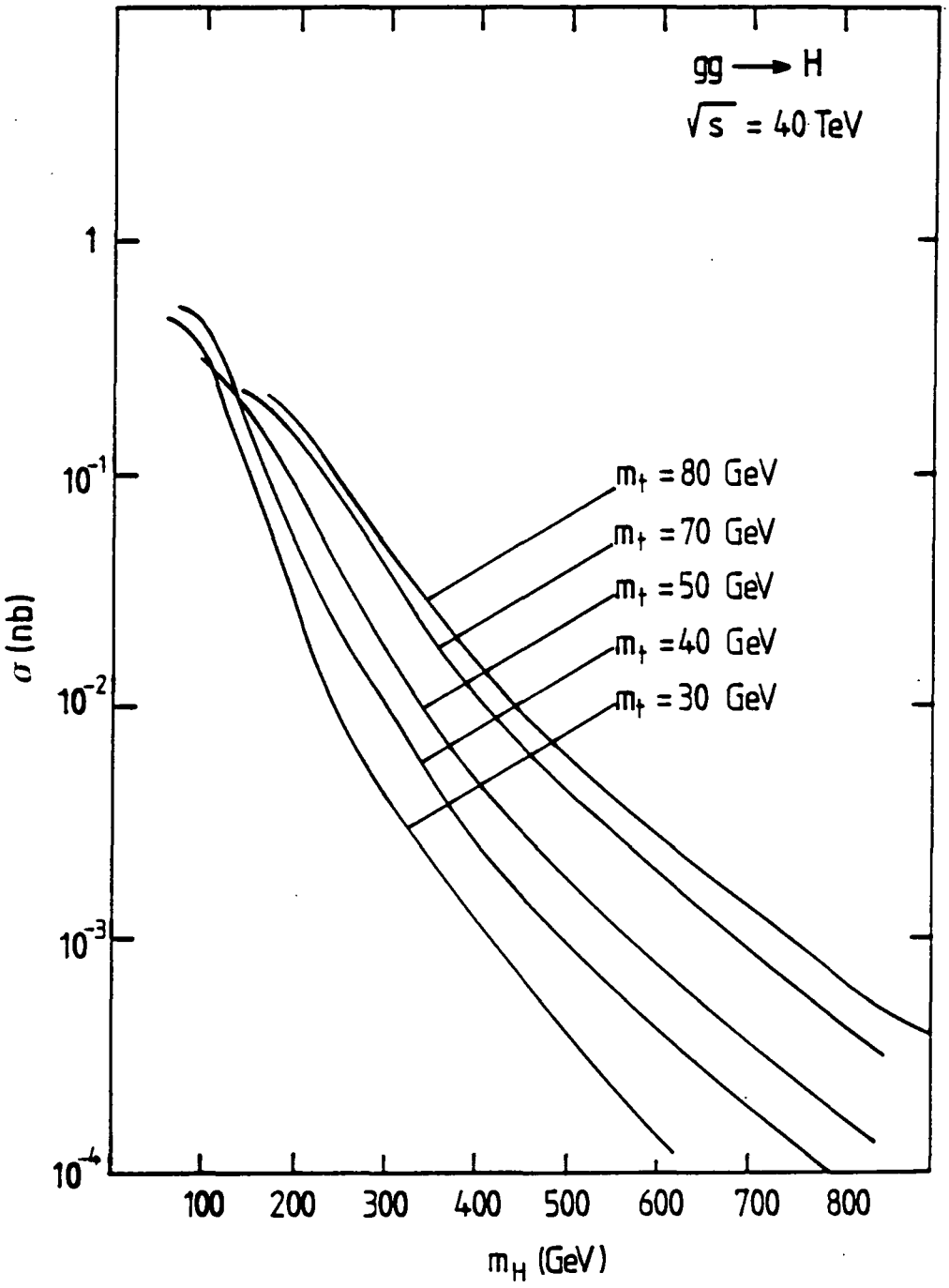

Fig. (6.13) The total cross-section for the production of Higgs boson via gluon-gluon fusion as a function of Higgs mass. The CM energy is fixed at 40 TeV. Curves for top quark mass m_t = 30, 40, 50, 70 and 80 GeV.

6.5.b Higgs Pair Production

In the last section, we mentioned that the existence of Higgs bosons is necessary for the renormalisability of the electroweak theory. Unfortunately, very little is known about it experimentaly. The coupling of the Higgs boson to fermions and gauge bosons is described in terms of gauge coupling and particle masses. Furthermore, the Higgs interacts with itself, with coupling strength proportional to the square of its mass. In order to study the three Higgs self coupling, one has to consider the production of a Higgs boson pair, which involves a cubic self-interaction.

Higgs pair production has been studied by K. Gaemer et. al. [4] for electron-electron annihilation. As they have discussed, more direct information on the Higgs could be obtained by using higher energy reaction, but so far studies of the production cross-section indicate that at presently avaliable energy it is not possible to detect.

At hadron colliders, there are two major production mechanisms for Higgs pair production; gauge boson fusion and gluon-gluon fusion, as shown in fig. (6.14). The contribution from quark-quark fusion can be ignored since Higgs couplings are proportional to the quark mass and the luminosity of heavy quarks is small in hadrons. For top quark-quark fusion, Higgs pair production has been studied [5], and it yields considerably smaller cross-sections. For the gauge boson fusion mechanism, where the quarks in the colliding beam emit virtual W's and Z's which annihilate to form pair Higgs boson, the cross-section is small compared with gluon-gluon fusion.

At hadron colliders, Higgs pair production has been studied by O.J. Eboli et. al. [6], where they have used the gluon-gluon fusion mechanism assuming that the triangle graph gives a lower bound to two Higgs production.

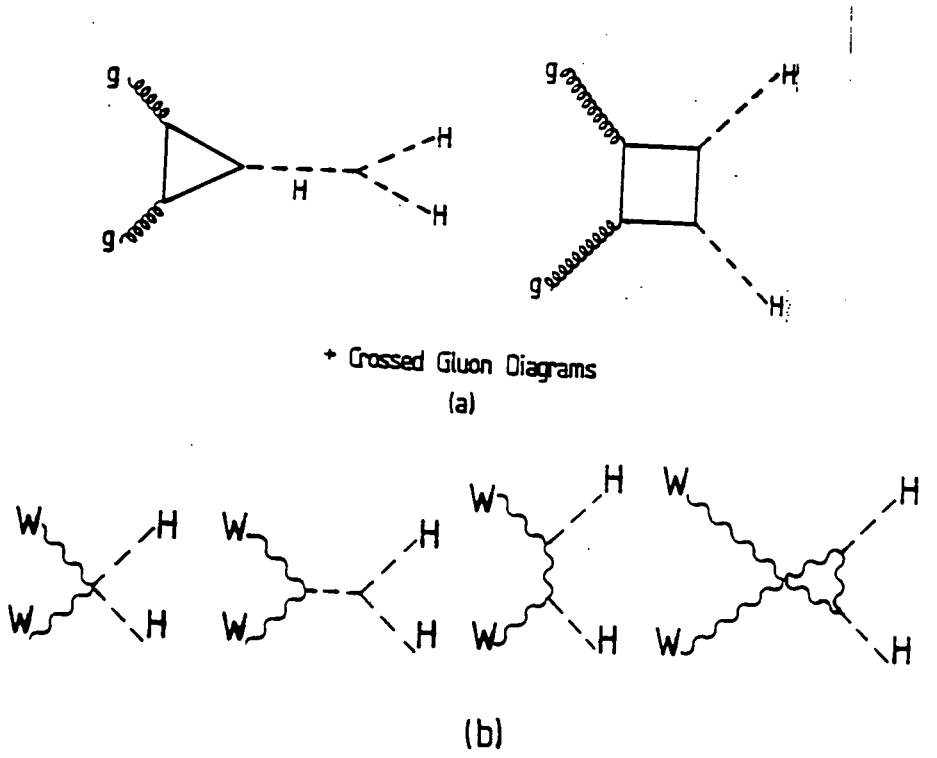

Fig. (6.14) Feynman diagrams contributing to two Higgs boson production (a) via gluon fusion, and (b) via vector boson fusion.

Recently, E.W.N. Glover and J.J Van der Bij [7] have produced a full calculation for the total cross-section of Higgs pair production via gluon-gluon fusion using, both the virtual box graph and the virtual triangle graph. Very recently D. Dicus et. al. [8], have compared the total cross-section for Higgs boson pair production in gluon-gluon fusion for both the total cross-section and the cross-section arising from the triangle diagram. Their calculation shows that at low Higgs mass, $m_H < 250GeV$, the box diagram provides the majority of the cross-section, while the triangle diagram gives the largest source of Higgs pairs at large Higgs mass, $m_H > 250GeV$.

In this section, we extrapolate the calculation of ref. [6] to Higgs pair production via gluon-gluon fusion. We calculate the total cross-section as a function of CM energy and Higgs mass. Following the calculation of ref. [6], the total

cross-section for the subprocess $gg \rightarrow HH$ (assuming the triangle diagram only) is given by:

$$\hat{\sigma}_{gg\rightarrow HH}(\hat{s}) = \frac{9\alpha^2\alpha_s^2}{2048\pi \sin^4\theta_W}(\frac{m_H}{m_W})^4 \frac{\hat{s}\beta}{(\hat{s}-m_H^2)^2}|\sum_q N_q|^2, \qquad 6.12$$

with $\hat{s} = x_1x_2s$, $\beta = (1-4\frac{m_H^2}{\hat{s}})^{1/2}$ and

$$N_q = \frac{1}{2}\epsilon[1+(\epsilon-1)\phi(\epsilon)], \qquad 6.13$$

where

$$\phi(\epsilon) = -[\sin^{-1}(\frac{1}{\sqrt{\epsilon}})]^2, \epsilon > 1$$

$$\phi(\epsilon) = \frac{1}{4}[\log(\frac{(1+\sqrt{1-\epsilon})}{(1-\sqrt{1-\epsilon})}) + i\pi]^2, \epsilon < 1 \qquad 6.14$$

with $\epsilon = \frac{4m_t^2}{\hat{s}}$.

The total cross-section for $pp \rightarrow HH$ is given by

$$\sigma_G(pp \rightarrow HH) = \int dx_1 dx_2 g(x_1)g(x_2)\sigma_{gg\rightarrow HH}(\hat{s}). \qquad 6.15$$

In fig. (6.15), we show the total cross-section for Higgs pair production for pp collision at $\sqrt{s}$= 40 TeV as a function of the Higgs mass for various values of the top quark mass m_t. We used set 1 of the Q^2-dependent parton distributions of Duke and Owens [9] with $\Lambda_{QCD} = 0.2$ GeV. Fig. (6.15) also shows the total cross-section at very high quark mass of, in the limit $m_q \rightarrow \infty$. We use the formula of ref. [7], where they have used the contributions from both box and triangle diagrams. With appropriate approximations the differential cross-section is:

$$\frac{d\hat{\sigma}}{dt} = \frac{\alpha_W^2\alpha_s}{2^{15}\pi m_W^4 \hat{s}^2}(|gauge1|^2 + |gauge2|^2), \qquad 6.16$$

where the leading terms are

$$gauge1(triangle) = \frac{4m_H^2\hat{s}}{\hat{s}-m_H^2},$$

$$gauge1(box) = -\frac{4}{3}\hat{s}, \qquad gauge2(box) = -\frac{11}{45}\hat{s}p_T^2/m_q^2$$

The corresponding cross-sections at $\sqrt{s}$ = 16 TeV and $\sqrt{s}$ = 200 TeV are shown in figs. (6.16, 6.17), respectively. It is clear from these figs. (6.15, 6.16, 6.17), that the value of the cross-section depends sensitivity on the top quark mass, and the cross section falls sharply with increasing Higgs mass.

In fig.(6.18), we show the $gg \rightarrow HH$ cross-section as a function of top quark mass at $\sqrt{s}$ = 40 TeV. Curves are shown for different Higgs masses of m_H= 100, 150, and 250 GeV. From fig. (6.18), it is clear that the cross-section starts increasing with increasing top quark mass, and then it reaches saturation at high value for top quark mass.

The corresponding cross-sections at $\sqrt{s}$ = 16 and 200 TeV are shown in figs. (6.19, 6.20), respectively.

The main dominant decay of Higgs boson pair are through $HH \rightarrow WWWW$ and $HH \rightarrow ZZZZ$, for a Higgs mass greater than $2m_W$ or $2m_Z$. The continuum background for the Higgs boson pair is mostly expected to be four W or Z that are produced via single parton scattering process $qq \rightarrow WWWW, ZZZZ$ or double parton scattering process $(qq)_1 + (qq)_2 \rightarrow WWWW, ZZZZ$.

Fig. (6.21) shows the total cross-section for four gauge boson (WWWW) production . The solid line is due to $gg \rightarrow HH \rightarrow WWWW$ at different Higgs mass while the dashed line indicates the background arising from double scattering process. Fig. (6.22) shows the total cross-section for gauge boson (ZZZZ) production comparing with the background.

The encouraging point is that the Higgs pair signal is larger than the background for small Higgs mass, but for large Higgs mass $m_H > 1$ TeV, the difficulty arises in distinguishing the background from the observed signal, particularly at small energy $\sqrt{s} < 10$ TeV.

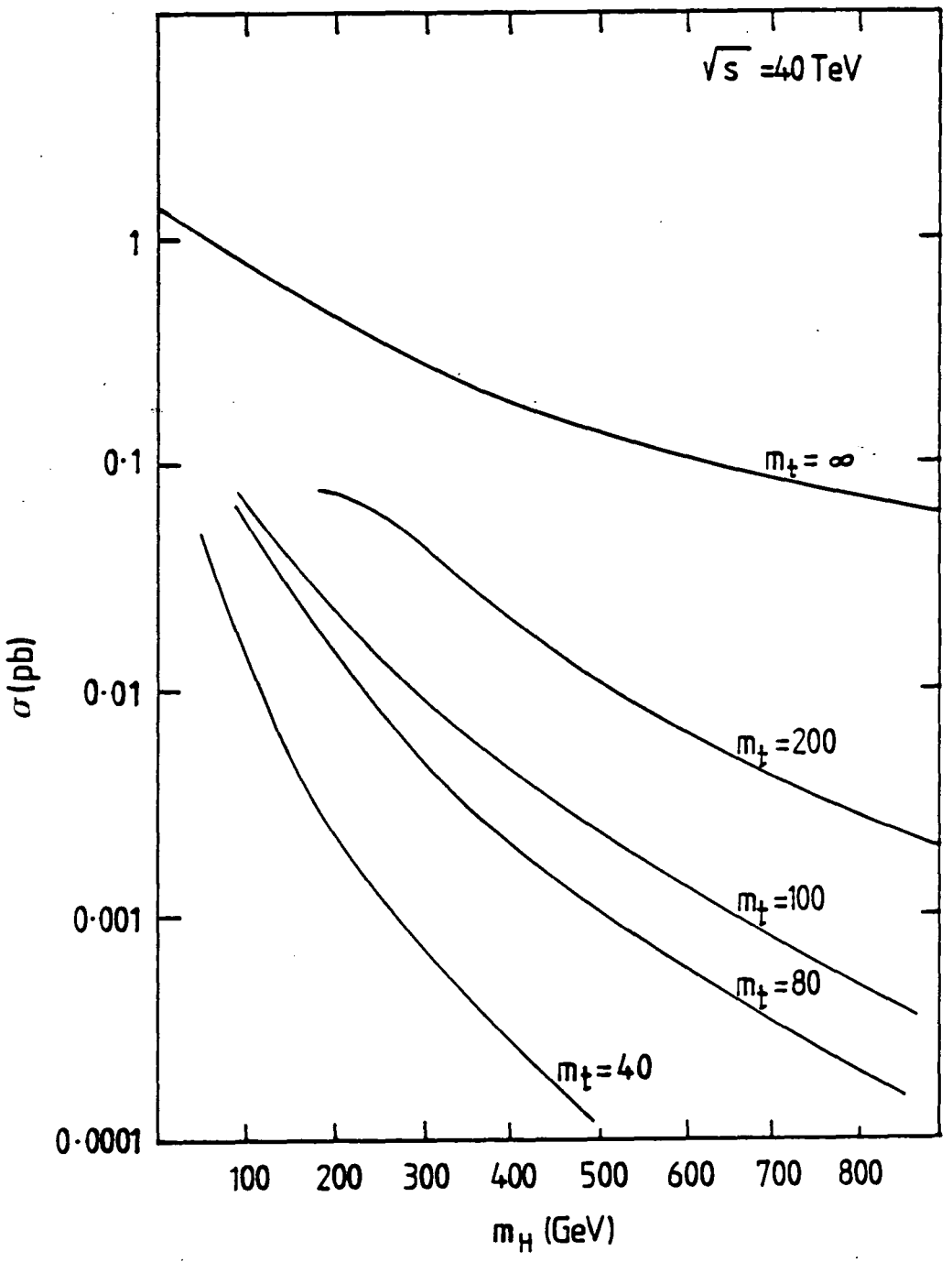

Fig. (6.15) The total $gg \rightarrow HH$ cross-section for pp collisions at $\sqrt{s} =$ 40 TeV as a function of Higgs mass.

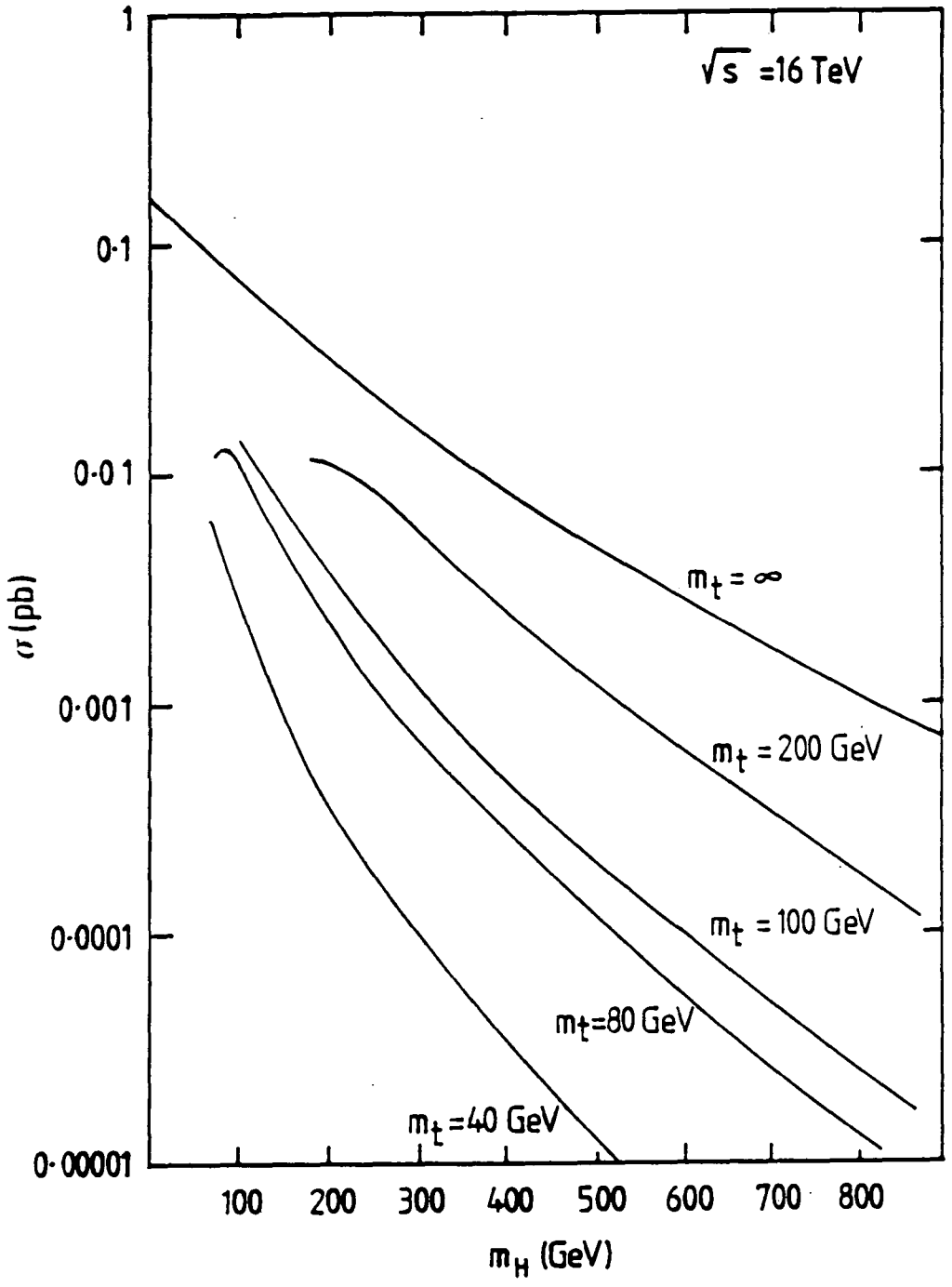

Fig. (6.16) The total $gg \rightarrow HH$ cross-section for pp collisions at $\sqrt{s} =$ 16 TeV as a function of Higgs mass.

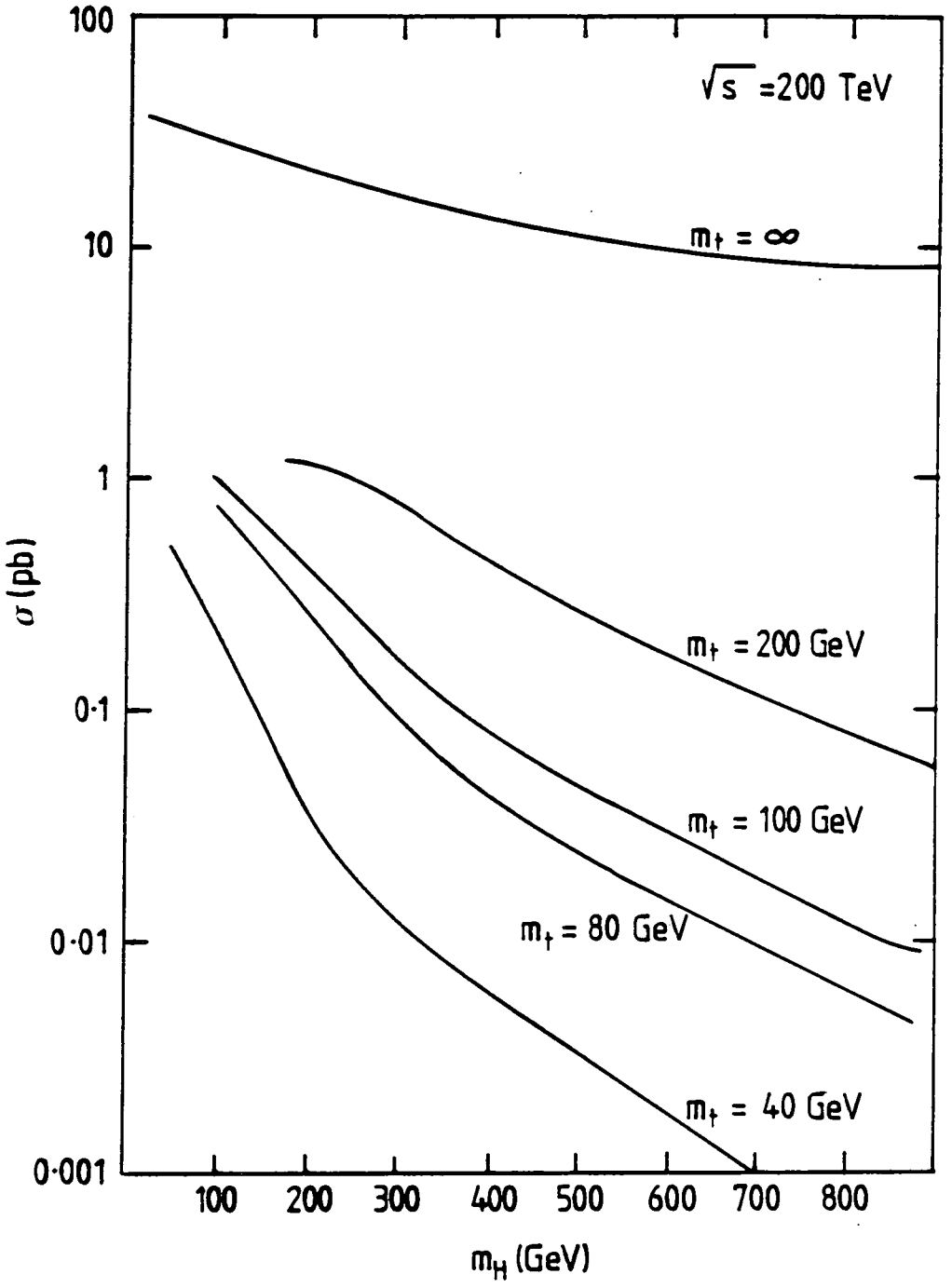

Fig. (6.17) The total $gg \to HH$ cross-section for pp collisions at $\sqrt{s} =$ 200 TeV as a function of Higgs mass.

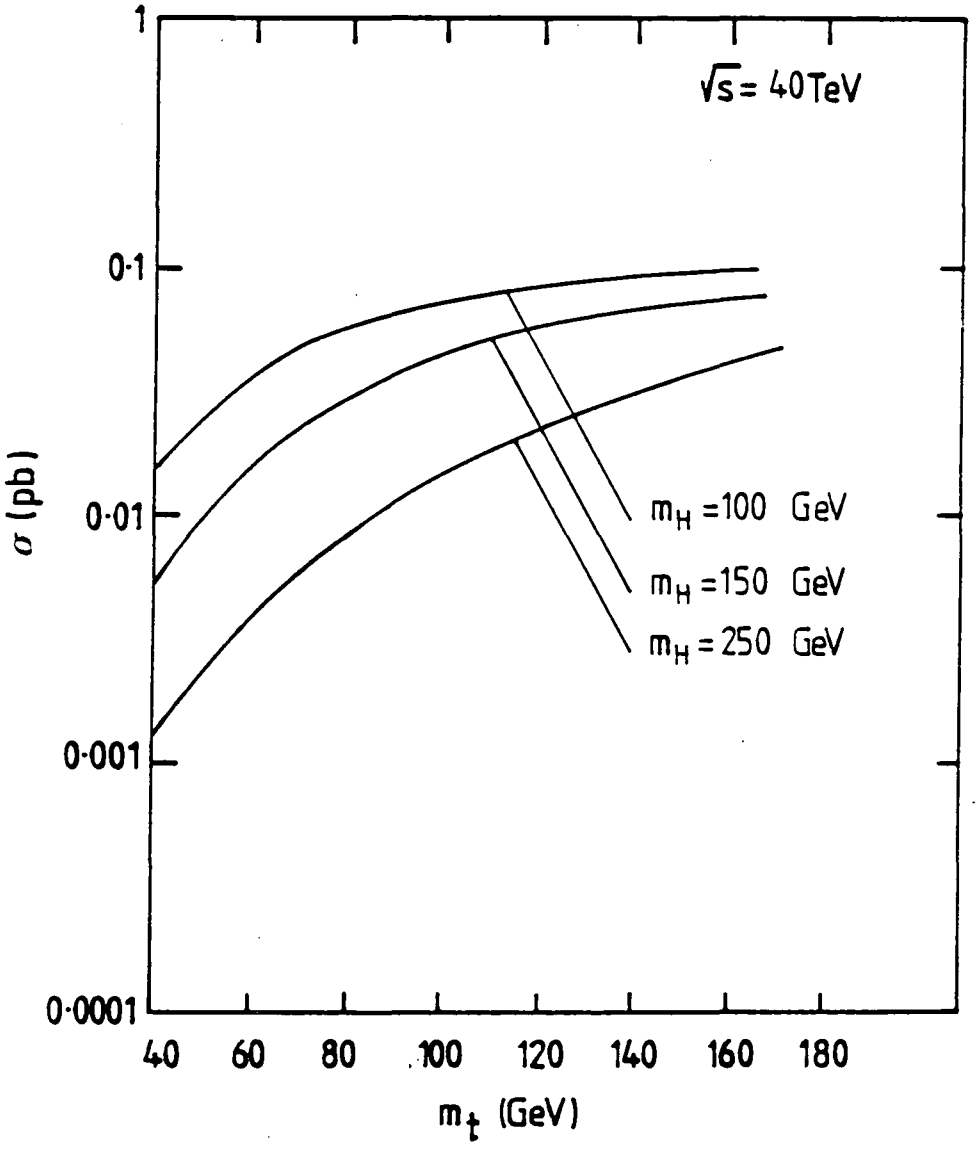

Fig. (6.18) The total $gg \to HH$ cross-section for pp collisions at $\sqrt{s} =$ 40 TeV as a function of top quark mass m_t.

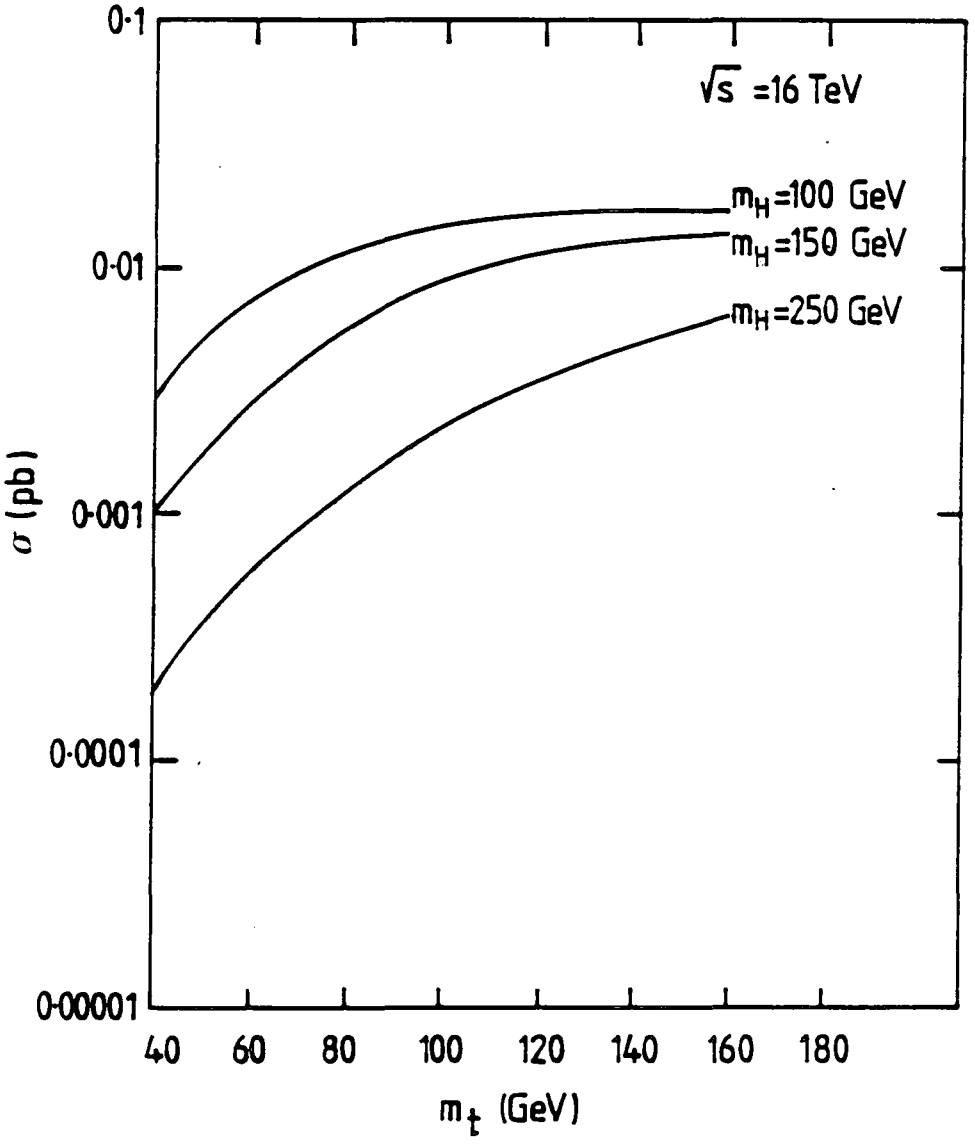

Fig. (6.19) The total $gg \to HH$ cross-section for pp collisions at $\sqrt{s} =$ 16 TeV as a function of top quark mass m_t.

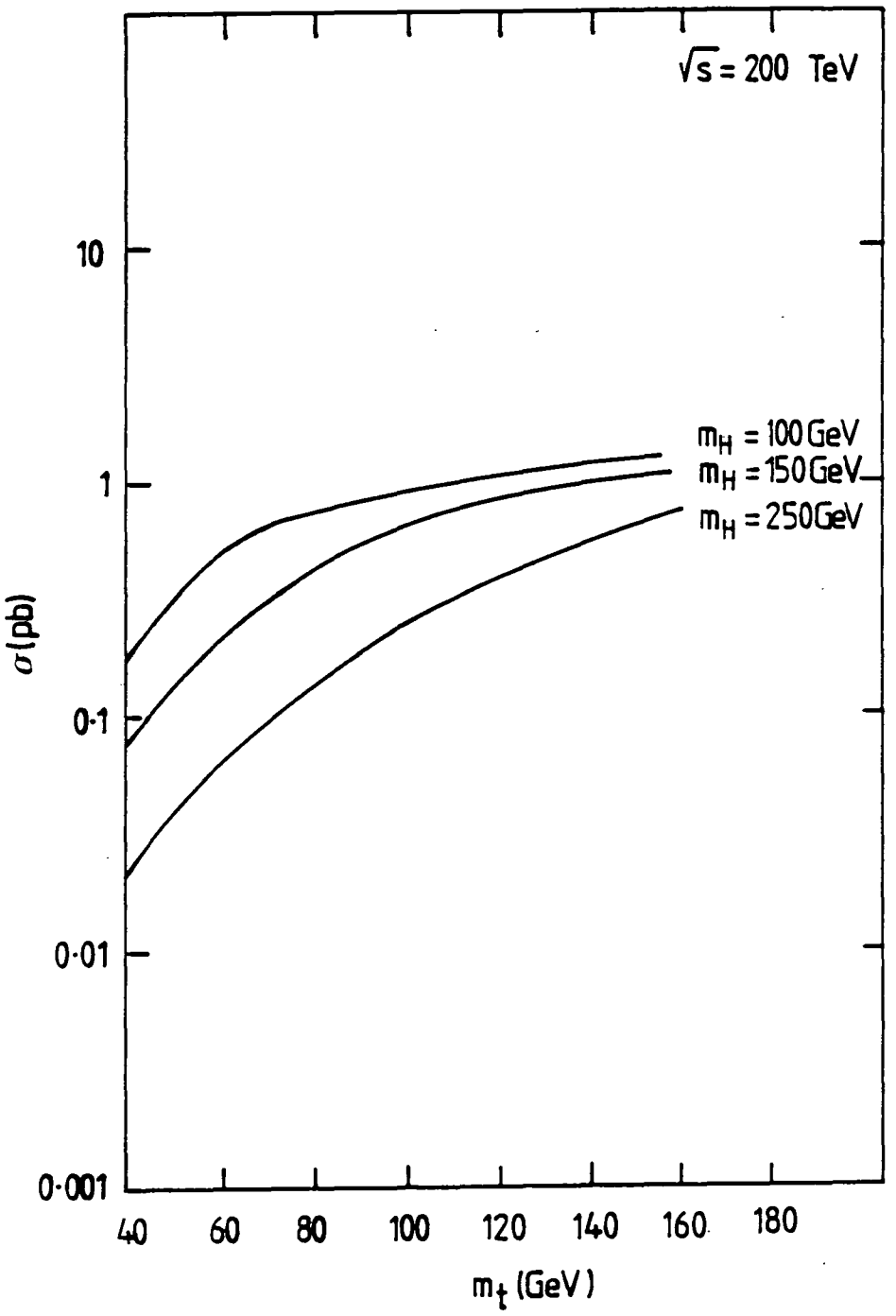

Fig. (6.20) The total $gg \rightarrow HH$ cross-section for pp collisions at $\sqrt{s} =$ 200 TeV as a function of top quark mass m_t.

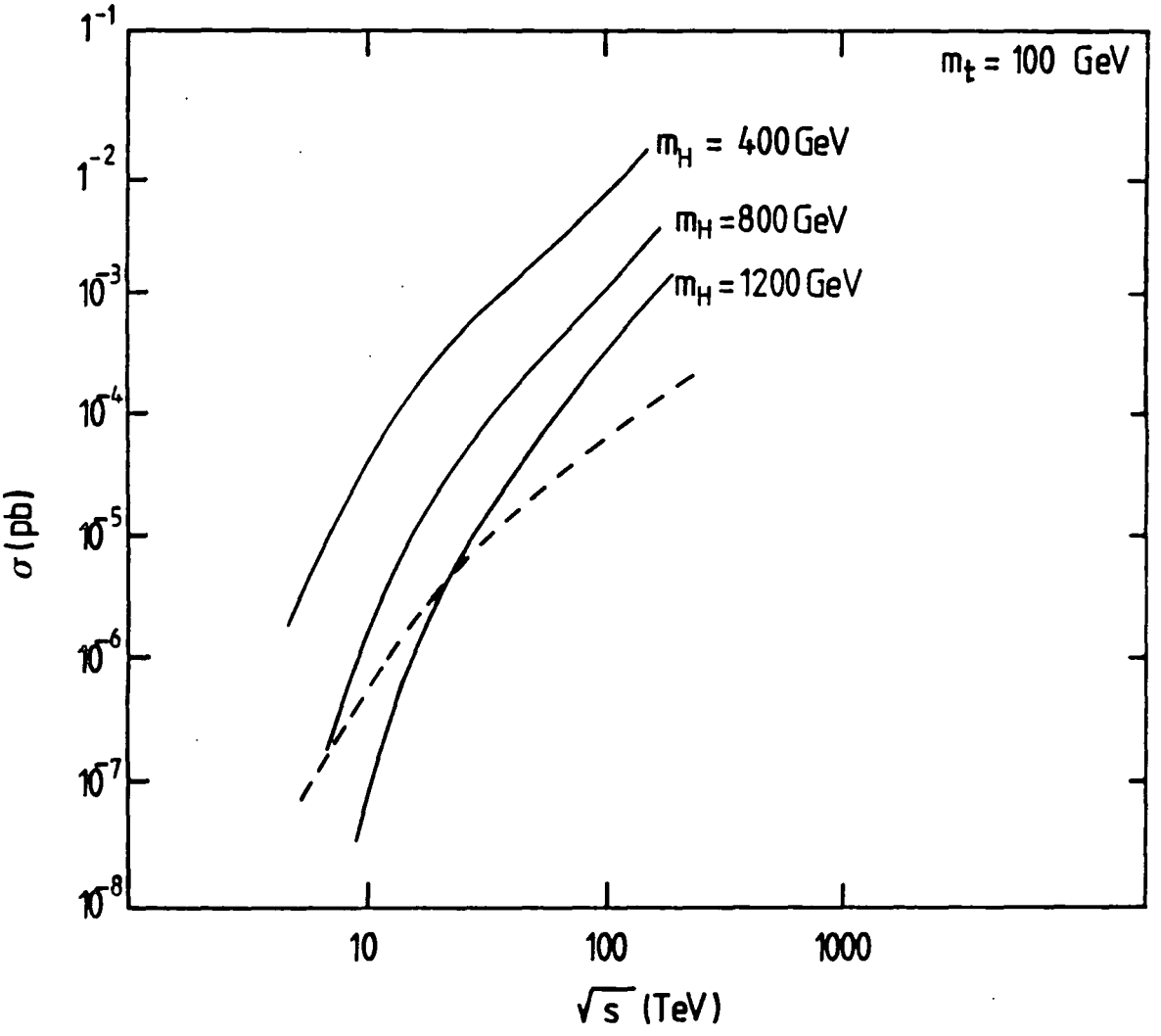

Fig. (6.21) The total cross-section for four gauge boson (WWWW) production as a function of CM energy. The solid line is due to $gg \rightarrow HH \rightarrow WWWW$ at different Higgs mass (with branching fraction), while the dashed line represents the background from four gauge boson production (WWWW) via double scattering process.

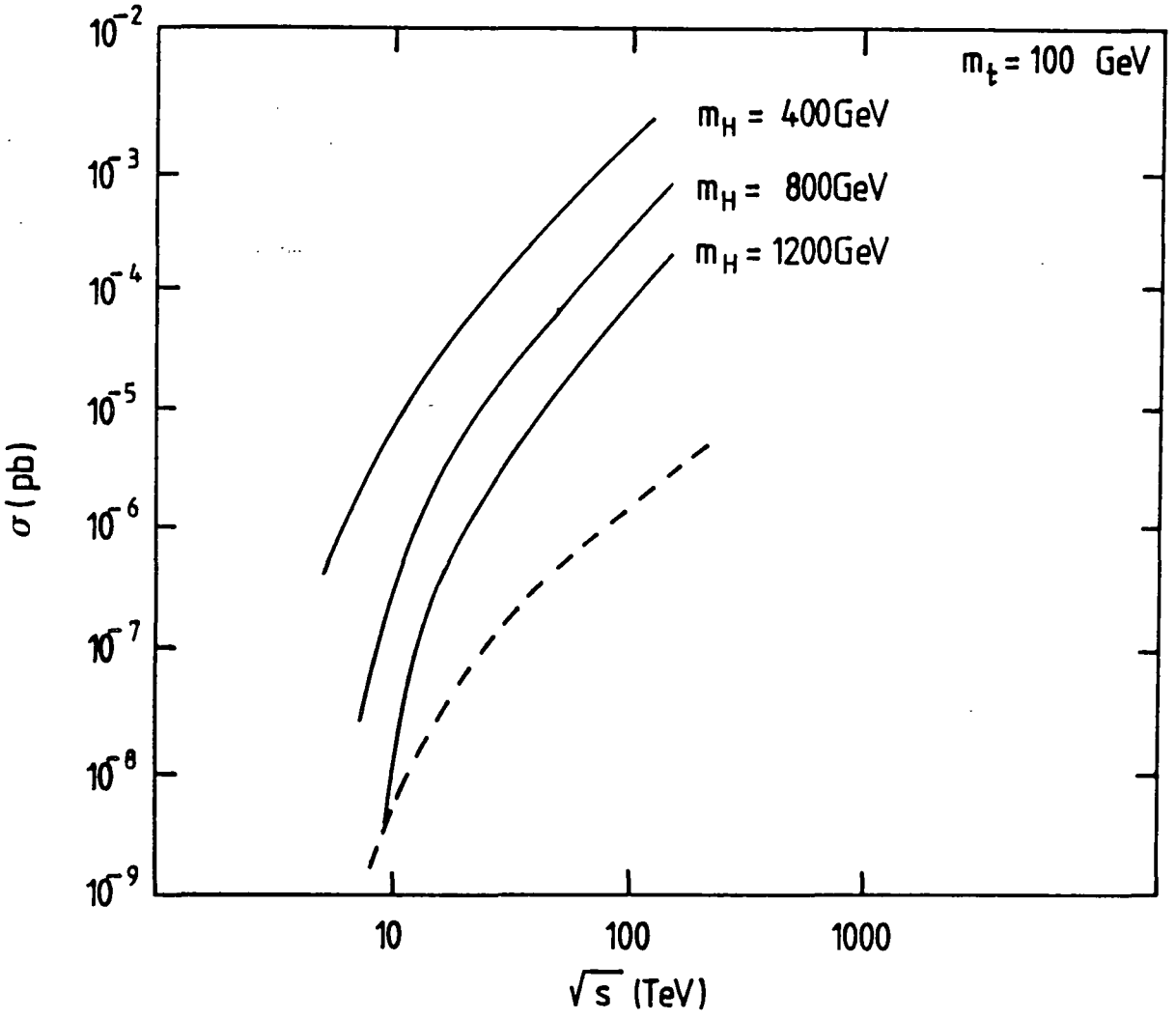

Fig. (6.22) The total cross-section for four gauge boson (ZZZZ) production as a function of CM energy. The solid line is due to $gg \rightarrow HH \rightarrow ZZZZ$ at different Higgs mass (with branching fraction), while the dashed line represents the background from four gauge boson production (ZZZZ) via double scattering process.

6.6 Discussion

The Higgs mechanism provides an excellent way of breaking the $SU(2) \times U(1)$ electroweak symmetry. Although, experimentally very little is known about the mechanism which breaks $SU(2) \times U(1)$, the investigation of this symmetry breaking is one of the main task of present and future accelerators.

The next generation of high energy proton proton colliders admits the possibilitis of production and detection of Higgs particles. At present time nothing is known about Higgs mass. The problem of producing and detecting the Higgs particles has been studied in connection with the new colliders at the SSC and LHC.

In this chapter we have studied the production of single and pair Higgs bosons without other particles in the final state at hadron colliders. As it can be seen from results of section 3, the most promising way to look at hadron colliders is through single Higgs cross-section since its cross-section is one or more orders of magnitude larger than for production of Higgs pair.

For single Higgs production we have calculated the cross-section in gluon-gluo n fusion mechanism at pp collision as a function of Higgs mass at 40 TeV and also as a function of energy at different Higgs masses. Although the cross- sections are large, but the dominant decay mode which is $H \rightarrow t\bar{t}, b\bar{b}$ is suffering from large QCD background like from ($gg \rightarrow t\bar{t}, b\bar{b}$). For the case of a large Higgs mass the cross- section is small but the decay modes are free from QCD background because the most dominant decay of Higgs is to gauge boson pairs.

For Higgs pair production we have calculated the cross-section for g g $\rightarrow$ H H in pp collision concentrating on the contributions from triangle diagram only which gives the largest source of Higgs boson pair at large Higgs masses. The cross-section is probabily unobservable and lies in the range $10^{-2} - 10^{-4}$ pb for Higgs mass $200 < m_H < 400$ GeV and top quark mass of $m_t > 40$ GeV for

pp collision at $\sqrt{s} = 40$ TeV, this corresponds to 100-1 HH events per year at the SSC. For $m_H > 2m_W$, the pair Higgs decay into gauge bosons, the rate of production is very small unless the top quark mass is very heavy which reflects that the observation of Higgs boson at the SSC is rather difficult.

In contrast at ELOISATRON (200 TeV) the total cross-section lies in the range $10^{-2} - 1$ pb for Higgs mass $200 < m_H < 400$ GeV and top quark mass of $m_t > 40$ GeV for pp collision, which corresponds to many more events $10^2 - 10^4$ each year.

The contribution from the third generation of fermions with high masses (if they exist) will increase the cross-section, this is due to the large coupling of Higgs to the heavy quarks.

Once the Higgs is found, the study of the trilinear coupling through pair Higgs boson production can verify whether the Higgs is elementary as it is expected in the standard model, or whether it is composite.

We have also calculated the partial decay width of Higgs boson for kinematically allowed decays. Here the dominant decay of the Higgs boson is into fermions and weak gauge bosons. The decay into pairs of intermediate bosons is dominant for high Higgs mass. Using partial decay width rate formulas, we have evaluated the branching fraction ratio as a function of Higgs mass into final states of quarks and gauge boson particles.

Also we have tried to compare the total cross-section of Higgs pair production as a signal to the background which is mostly from four gauge bosons production. We have used the total cross-section for four gauge bosons from double scattering mechanism which is assumed to be smaller than the cross-section from single scattering for the same process. The figs. (6.21, 6.22) show that the signals can be identified easily from the background for ranges of Higgs mass $100 < m_H < 800$ GeV, but the difficulty arises in distinguishing the background from the observed

signal for large range of Higgs mass $m_H > 1$ TeV with top mass of 40 GeV. However, there are several sources of uncertainty which effect the calculation such as the uncertainties in the gluon structure functions, the choice of the scale which defines the strong coupling $\alpha_s(Q^2)$ and the structure functions and the higher order corrections.

CHAPTER 7

SUMMARY

The standard model, the gauge theory describing the strong, weak and electromagnetic interactions of quarks and leptons, has been remarkably successful in describing a broad spectrum of high energy data. With the advent of the CERN $p\bar{p}$ collider, the model has been tested at high energy and its correct prediction of the masses of the W and Z bosons has been verified.

The production of two weak gauge bosons in a $p\bar{p}$ collision is predicted within the framework of the standard model and the Drell-Yan processes. They can be identified through a leptonic decay of one of the gauge bosons and two jets from the other. The predicted cross-section of this process is smaller than the cross-section to which the observed events rates correspond i.e. the cross-section for W pair production is $\sigma_{WW}BR \simeq 0.02$ pb at a CM energy of 630 GeV.

The present thesis is devoted to the study of some of the most important processes associated with the standard model. In particular we have concentrated on (1) the calculation of the first order perturbative QCD corrections to photon and Z pair production in hadron collisions, (2) the production rate of multiple weak gauge boson through single and double scattering mechanisms and (3) Higgs boson phenomenology.

We have started with some detailed calculations of the first order perturbative QCD corrections to photon and Z pair production in hadron collisions in chapters 2 and 3 respectively. The exact calculation of higher order QCD corrections is very complicated. The corrections contain many terms and it is hard to find singularities, which would allow us to estimate the overall size of the QCD corrections. The precise magnitude of these corrections depend on the renormalisation scheme and on the definition of the parton distribution functions beyond the leading order

approximation in perturbation theory.

The calculation were performed with real gluon emission (hard collinear gluon emission and soft gluon emission) and include the interference of the lowest order diagrams with the virtual graphs (self-energy, vertex and box diagrams). The calculated corrections contain divergences represented in the method of dimensional regularisation by $O(\frac{1}{\epsilon})$ and $O(\frac{1}{\epsilon^2})$ poles. The $O(\frac{1}{\epsilon^2})$ poles are eliminated when we were combined real and virtual corrections. The remaining $O(\frac{1}{\epsilon})$ divergences are absorbed into the quark momentum distribution functions beyond leading order so that they contain all the higher and lower order terms. Since the appearance of such singularity in the quark distribution functions has a universal structure and is independent of the process, the usual way to remove it is by the standard subtraction procedure with a similar term from another process like deep inelastic scattering (DIS).

Due to the large number of terms involved, it was not possible to calculate all of them, and in some cases we have concentrated on the singular terms only. For this reason it was not possible to work out exactly the numerical values of the QCD corrections for the processes in chapter 2 and chapter 3.

Then, we have investigated the production rate of multiple weak gauge bosons in hadron collisions using both single and double parton scattering mechanisms. It is known that with increasing collider energies there is a need to consider more complicated parton scattering which means that more partons are loaded in the hadrons and multiple parton interactions become increasingly important.

The goal of our study was to look in some depth at the production rate of multiple weak gauge bosons via the double scattering parton mechanism, which is very important because it will provide a crucial test of the standard electroweak model at high energies (TeV scale), and will test for the existence of the Higgs boson, besides to that it may contribute a significant background to new physics

beyond the standard model.

In chapters 4 and 5, we have used the double parton scattering mechanism to calculate the production rate of weak gauge boson pairs, triple gauge bosons and four gauge bosons in hadron collisions. Although the results showed small values for the cross-section from double scattering compared with the single scattering for the same process, they showed a large numbers of observable events at high energies such that these processes may be observed if high energies and large luminosities are being used. Our calculations, however, cannot be exactly precise especially in view of the large uncertainities associated with the gluon structure functions, the scale of α_s and the higher order QCD corrections which would affect such calculations. We have to add the reminder here, that an accurate value for σ_{eff} (the hadronic cross-section which estimates the size of a hadron in double scattering mechanism) is also needed and this means that more accurate information on hadron structure is very important. Aside from all these uncertainties, our results were seen to be in agreement with similar results obtained from recent calculations.

Finally, we have examined the Higgs boson phenomenology, which now forms a substantial part of the physics program at the next generation of high energy colliders. We have concentrated on the study of single and pair production of Higgs bosons at hadron colliders via gluon-gluon fusion processes. It is clear from the results that the most promising approach is through single Higgs production rather than Higgs pair production since its cross-section is one or more order of magnitude greater. Also we have shed light on the Higgs decay width and branching ratio. Finally, we have compared Higgs pair production cross-sections $\sigma_{HH}BR$ with the cross-sections for four W and Z weak gauge bosons production obtained via double scattering parton mechanism, which contribute to the background.

The conclusions of this thesis can be briefly summarised in a few points:

1. Higher-order perturbative QCD corrections are important and give significant change to the lowest order especially for the next generation of hadron colliders where the gluon effects play an important role at high energies (TeV scale). The exact calculation for the first order QCD correction to Z pair production in hadron collisions is very important as a background for Higgs boson detection since the main dominant decay of Higgs boson is $H \rightarrow W^+W^-$ or $H \rightarrow ZZ$. The most important processes which one should look at are $q\bar{q} \rightarrow ZZg$, $qg \rightarrow ZZg$ and $\bar{q}g \rightarrow ZZ\bar{q}$.
2. For the next generation of hadron colliders, the double scattering parton mechanism is extremely important and may give significant evidence for testing the standard model at high energies (TeV scale). Also multiparton scattering is expected as a potential background for new physics beyond the standard model.
3. Higgs boson phenomenology is extremely important and need further study since it is the only particle which is left undiscovered in the standard model. Unfortunately nothing is known about the Higgs mass, but the next generation of supercolliders are the most suitable tools to search for the discovery of the Higgs boson.

REFERENCES

Chapter 1

Introduction

[1] For the introduction to the idea of particle physics see:

a F. Halzen and A.D. Martin, *Quarks and Leptons*, John Wiley and Sons, New York, 1984

b D.H. Perkins, *Intoduction to High Energy Physics*, Addison-Wesley, Reading, Massachusetts, 1982

c L.B. Okun, *Leptons and Quarks*, North-Holland, Amsterdam, 1982

d J.E. Dodd, *The Idea of Particle Physics*, Camdridge University Press, Cambridge, 1984

e I.J.R. Aithcison and A.J.G. Hey,*Gauge Theories in Particle Physics*, Adam Hilger, Bristol, 1982

f P. Watkins, *Story of the W and Z*, Cambridge Univ. Press, Cambridge, 1986

g F.E. Close, *An Introduction to Quarks and Partons*, Academic Press, London, 1979

h P.D.B. Collins and A.D. Martin, *Hadron Interactions*, Adam Hilger, Bristol, 1984

[2] M. Gell-Mann and Y. Ne'eman, *The Eightfold Ways*, Benjamin, N.Y., 1964; J.J.J. Kokkedee, *The Quark Model*, Benjamin, Reading, Massachusetts, 1969

[3] F.E. Close,'The Quark Parton Model', Rep. Prog. Phys.,**42** (1979), 1285; J. Bjorken, Phys. Rev., **179** (1969), 1547; C.G. Callan and D.J. Gross,Phys. Rev., **22** (1969), 156; J. Bjorken and E.A. Pashos, Phys. Rev., **185** (1969), 1975; R.P. Feynman, *Photon-Hadron Interactions*, Benjamin, New York, 1972

[4] F.J. Yndurain, *Quantum Chromodynamics*, Springer-Verlag, New York, 1983; M.R. Pennington, Rep. Prog. Phys., **46**(1983), 393; D.M. Scott,'Topics of

Modern Phenomenology', Lectures Delivered at the School for Young High Energy Physicists, Rutherford Appleton Lab., Sept. 1984; E. Rey ,'Perturbative Quantum Chromodynamics', DESY 79/88

[5] P.W. Higgs, Phys. Rev. Lett., **12** (1964), 132; Phys. Rev., **145** (1966), 1156; D. Bailin, *Weak Interactions*, Adam Hilger LTD, Bristol, 1982

[6] UA1 Collaboration, G. Armison et. al., Phys. Lett. **122B** (1983), 103; **129B** (1983), 273

[7] S. L. Glashow, Nucl. Phys., **22** (1961), 579; S. Weinberg, Phys. Rev., **19** (1961), 1264; Sea also A. Salam, 'Elementary Particle Theory', editer N. Svartholm (Almqvist and Wiksell), Stockholm, 1968

[8] W.J. Stirling,'Short diatance QCD', Proc. 1987 Int. Symposium on Lepton and photon Interactions at High Energies, Humburg, Germany, 1987, eds W. Barfel and R. Ruckl, 1987;'Topics Of Modern Phenomenology', Lectures Delivered at the School for Young High Energy Physicists, Rutherford Appleton Lab., Sept. 1987

[9] L. Ametller, N. Paver and D. Treleani, Phys. Lett., **169B** (1986), 289; B. Hampert and R. Odorico, Phys. Lett., **154B** (1985), 211; B. Humpert, Phys. Lett., **135B** (1984), 179; N. Paver and D. Treleani, Phys. Lett., **146B** (1984), 252; F. Halzen, P. Hoyer and W.J. Stirling, Phys. Lett, **188B** (1987), 375

[10] T. Mullar,'Production Properties of the Intermediate Vector Bosons W and Z at the CERN $p\overline{p}$ Colliders', CERN-EP/88-48

[11] W.J. Stirling, Durham DPT/88/38 preprint 1988

[12] N.G. Antoniou, E.N. Argyres, A.P. Contogouris and S.D.D. Vlassopulos, Phys. lett., **128B** (1983), 257

[13] S.G. Gorishny, A.L. Kataev and S.A. Larin, Phys. Lett., **212B** (1988), 238

[14] R.K. Ellis and J.C. Sexton, Nucl. Phys., **B269** (1983), 257

[15] T. Matsuura, S.C. van der March and W.L. van Neerven, Leiden Univ.

preprint 88-422 (1988)

[16] J. Ellis, G. Gelmini and H. Howalski, Proceeding of the ECFA-CERN workshop, CERN, Geneva, 1984; E.D. Ellis, NSF-ITP-88-55, lectures presented at the 1987 theoretical advanced study institute, st. John's College, Santa Fe, NM, July 1987

[17] V.D. Barger and R.J.N. Phillips, *Collider Physics*, Frontiers in Physics, 1987

Chapter 2

First order perturbative QCD corrections to photon pair production in hadron collisions

[1] G. Altarelli, Phys. Reports, **81** (1981), 1

[2] P. Aurenche , and J. Lindfors, Nucl. Phys., **B185** (1981), 274; **B185** (1981), 301

[3] G. Altarelli, R.K. Ellis and G. Martinelli, Nucl. Phys., **B157** (1979), 461; **B143** (1978), 521

[4] F. Khalafi, Z. Phys., **C14** (1982), 135; **C11** (1981), 251

[5] C.J. Gilmour, DAMTP, **19** (1984)

[6] W.J. Marciano, Phys. Rev., **D12** (1975), 3861; G. Gastmans and R. Meuldermans, Nucl. Phys., **B63** (1973), 277; G. Gastmans, J. Verwaest and R. Meuldermans, Nucl. Phys., **B105** (1976), 454

[7] J.C. Taylor, ' Fundamentals of QCD', Lectures in the 1982 CERN School of Physics, Cambridge, 1982, CERN Report, 83-05 (1983)

[8] P.V. Landshof, ' Applications of QCD', Lectures in the 1982 CERN School of Physics, Cambridge, 1982, CERN Report, 83-05 (1983)

[9] P. Ramond, *Field Theory*, A Modern Primer, Benjamin, ark, Reading, Massachusetts, 1981; G.'t Hooft and M. Veltman, Reprint of CERN Yellow Report 73-96 ; Nucl. Phys., **B44** (1972), 189

[10] A.C. Hearn, *REDUCE*, Users Manual, Utah (1987)

[11] I.S. Gradshteyn and I.M. Ryzhik, *Table of Integrals*, Series and Products, New York, Academic Press (1980)

[12] *Handbook of Mathematical Functions*, eds. M. Abramowitz and I.A. Stegun, Dover Publications, INC., New York

[13] F.A. Berends, Z. Kunset and R. Gastmans, Nucl. Phys., **B182** (1981), 397; Phys. Lett., **92B** (1980), 186

[14] UA1 Collaboration, C. Albajar et. al., Phys. Lett., **209B** (1988), 385

[15] UA2 Collaboration, R. Ansari et. al., Z. Phys., **41** (1988), 395

Chapter 3

First order perturbative QCD corrections to weak boson pair production in hadron collisions

[1] S. L. Glashow, Nucl. Phys., **22** (1961), 579; S. Weinberg, Phys. Rev., **19** (1961), 1264; Sea also A. Salam, 'Elementary Particle Theory', editer N. Svartholm (Almqvist and Wiksell), Stockholm, 1968

[2] UA1 Collaboration, G. Armison et. al., Phys. Lett., **122B** (1983), 103; **129B** (1983), 273; UA2 Collaboration, M. Banner et. al., Phys. Lett., **122B** (1983), 476

[3] R.N. Cahn, S.D. Ellis, R. Kleiss, and W.J. Stirling, Phys. Rev., **D35** (1987), 1626

[4] R.W. Brown and K.O. Mikaelian, Phys. Rev., **D19** (1979), 922; R.W. Brown, D. Sahdev, and K.O. Mikaelian, Phys. Rev., **D20** (1979), 1164; E. Eichten, I. Hinchliffe, K. Lane, and C. Quigg, Rev. of Mod. Phys., **56** (1984), 579

[5] A.C. Hearn, *REDUCE*, Users Manual, Utah (1987)

[6] P. Ramond, *Field Theory*, A Modern Primer, Benjamin, orina Reading, Massachusetts, 1981; G. 't Hooft and M. Veltman, Report of CERN Yellow Report,

73-96; Nucl. Phys., **B44** (1972), 189

[7] *Handbook of Mathematical Functions*, eds. M. Abramowitz and I.A. Stegun, Dover Publications, INC., New York

[8] I.S. Gradshteyn and I.M. Ryzhik, *Table of Integrals*, Series and Products, New York, Academic Press, (1980)

[9] A. Devoto and D.W. Duke, *Table of Integrals and Formulae for Feynman Diagram Culculations*, Florida state Univ., Florida, 1983

[10] F.A, Berends, Z. Kunszt and R. Gastmans, Nucl. Phys., **B182** (1981), 397; Phys. Lett., **92B** (1980), 186; I. Kang, Oxford Univ. Preprint, TP-50/82, 1982

Chapter 4

Hard scattering processes

[1] D. Froidevaax and P. Jenni, CERN preprint EP/88/111; T. Mullar, CERN preprint EP/88/48; W.J. Stirling, DTP/89/28, talk presented at Symposium on Particle Identification at High Luminosity Hadron Colliders, Fermilab, April 1989

[2] J. Ellis and G. Gelmini and H. Kawalski, Proceedings of the ECFA-CERN workshop, CERN, Geneva, 1984

[3] E. Eichten, I. Hinchliffe, K. Lane and C. Quigg, Reviw of modern phys., **56** (1984), 579

[4] W.J. Stirling, Lecture notes delivered at the summer school for young high energy physicist, Rutherford Appleton Laboratory, sept. 1987; D.M. Scott, Lecture notes delivered at the summer school for young high energy physicist, Rutherford Appleton Laboratory, sept. 1984

[5] The European Muon Collaboration, Aubert et. al., Nucl. Phys. **B259** (1985), 189; **B272** (1986), 158; **B293** (1987), 740; D. Bollini et. al., Phys.

Lett., **104B** (1983), 403; Charm Collaboration, F. Bergsma et. al., Phys. Lett., **123B** (1983), 269; D. Allasia et. al., Z. Phys., **C28** (1985), 321

[6] CDF Collaboration, F. Abe et. al., Phys. Rev. Lett., **62** (1989), 1005

[7] A.D. Martin, R.G. Roberts and W.J. Stirling, Phys. Rev., **D37** (1988), 1161

[8] R.W. Brown and K.O. Mikaelien, Phys. Rev., **D19** (1979), 922; R.W. Brown, D. Sahdev and K.O. Mikaelien, Phys. Rev., **D20** (1979),1164

[9] B. Humpert, Phys. Lett., **131B** (1983), 461

[10] B. Humpert, Phys. Lett., **131B** (1983), 461; N. Paver and D. Treleani, Phys. Lett., **146B** (1984), 252; B. Humpert and R. Odorico, Phys. Lett., **154B** (1985), 211; N. Paver and D. Treleani, Nuovo Cimento, **70A** (1982), 215; **73A** (1983), 392

[11] W.J.Stirling, "short distance QCD", Proc. 1987 Int. Symposium on Lepton and Photon interactions at High energies, Humberg, Germany, eds. W.Bartel and R.Ruckl, 1987

[12] J. Kuti and V.F. Wisskopf, Phys. Rev., **D4** (1971), 3418; C. Goebel, D.M. Scott and F. Halzen, Phys. Rev., **D22** (1980), 2789

[13] E.W.N. Glover and J.J. Van der Bij, CERN-TH-5247/1988

[14] J.F. Gunion, J. Kalinowski and A. Tofighi-Niaki, Phys. Rev. Lett., **57** (1986), 2351

[15] D.A. Dicus and R. Vega, UCD-88/35

[16] D.W. Duke and J.F. Owens, Phys. Rev., **D30** (1984), 49

Chapter 5

Multiple gauge boson production in high energy proton proton collisions

[1] R.W.Brown and K.O.Mikaelian, Phys. Rev., **D19** (1979), 922; R.W.Brown, D.Sahdev and K.O.Mikaelian, Phys. Rev., **D20** (1979), 1164

[2] E. Eichten, I. Hinchliffe, K. Lane and C. Quigg, Rev. of Modern Phys., **56** (1985), 579 ; **58** (1984), 1065

[3]. M. Golden and S.R. Sharpe, Nucl. Phys., **B261** (1985), 217

[4] V. Barger and T. Han, Phys. Lett., **212B** (1988), 117

[5] AFS Collaboration, T.Akesson et. al., Z. Phys., **C34** (1987), 293

[6] N.Paver and D.Treleani, Nuovo Cimento, **70A** (1982) 215; **73A** (1983) 392; B.Humpert, Phys. Lett., **131B** (1983) 461

[7] N.Paver and D.Treleani, Phys. Lett., **146B** (1984) 252; B.Humpert and R.Odorico, Phys. Lett., **154B** (1985) 211

[8] L.Ametller, N.Paver and D.Treleani, Phys. Lett., **169B** (1986) 289

[9] C.Goebel, D.Scott and F.Halzen, Phys. Rev., **D22** (1980), 2789

[10] D.W.Duke and J.F.Owens, Phys. Rev., **D30** (1984), 49

[11] W.J.Stirling, "short distance QCD", Proc. 1987 Int. Symposium on Lepton and Photon interactions at High energies, Humberg, Germany, eds. W.Bartel and R.Ruckl, 1987

[12] A.D. Martin, R.G. Roberts and W.J. Stirling, Phys. Rev., **D37** (1988), 1161

Chapter 6

Higgs boson

[1] V.d. Barger and R.J.N. Philips, *Collider Physics*, Frontiers in Physics, 1987; sea also: W.J. Stirling, Topics in Modern Phenomenology, Lecture Notes-HEP summer school, Rutherford Appleton Laborotary, 1987

[2] E. Eichten, I. Hinchliffe, K. Lane and C. Quigg, Rev. of Modern Phys., **56** (1985), 579 ; **58** (1984), 1065

[3] R.N. Cahn and S. Dawson, Phys. Lett., **136B** (1984), 196

[4] K.J.F. Gaemers and F. Hoogeveen, Z. Phys., **C26** (1984) 249

[5] K.J. Kallianpur, Univ. of Wisconsion report MAD/PH/371, (1987)

[6] O.J.P. Eboli, G.C. Marques, S.F. Novaes and A.A. Natale, Phys. Lett., **197B** (1987), 269

[7] E.W.N. Glover and J.J.Van der Bij, Nucl. Phys., **B309** (1988), 282

[8] D.A. Dicus, C. Kao and S.S.D. Willenbrock, Phys. Lett., **203B** (1988), 457

[9] D.W. Duke and J.F. Owens, Phys. Rev., **D30** (1984), 49